



HAL
open science

Conception d'antennes spirales large bande à alimentation coplanaire pour des applications radar sur dirigeable

Karim Louertani

► **To cite this version:**

Karim Louertani. Conception d'antennes spirales large bande à alimentation coplanaire pour des applications radar sur dirigeable. Electronique. Université Pierre et Marie Curie - Paris VI, 2010. Français. NNT : 2010PA066302 . tel-00815267

HAL Id: tel-00815267

<https://theses.hal.science/tel-00815267>

Submitted on 18 Apr 2013

HAL is a multi-disciplinary open access archive for the deposit and dissemination of scientific research documents, whether they are published or not. The documents may come from teaching and research institutions in France or abroad, or from public or private research centers.

L'archive ouverte pluridisciplinaire **HAL**, est destinée au dépôt et à la diffusion de documents scientifiques de niveau recherche, publiés ou non, émanant des établissements d'enseignement et de recherche français ou étrangers, des laboratoires publics ou privés.

**THÈSE DE DOCTORAT
DE L'UNIVERSITÉ PIERRE ET MARIE CURIE
PARIS 6**

**Spécialité :
ÉLECTRONIQUE**

**Pour obtenir le grade de :
DOCTEUR DE L'UNIVERSITÉ PIERRE ET MARIE CURIE**

**Présentée par :
Karim LOUERTANI**

**CONCEPTION D'ANTENNES SPIRALES LARGE BANDE A
ALIMENTATION COPLANAIRE POUR DES APPLICATIONS
RADAR SUR DIRIGEABLE**

Devant le jury composé de :

Pr. Raphaël GILLARD, INSA de Rennes	Rapporteur
Dr. Xavier BEGAUD, TELECOM ParisTech	Rapporteur
Pr. Aziz BENLARBI-DELAÏ, Université Pierre et Marie Curie	Examineur
Dr. Nicolas RIBIÈRE-THARAUD, Encadrant DRE-L2S	Examineur
Dr. Régis GUINVARC'H, Encadrant SONDRÀ	Examineur
Pr. Marc HÉLIER, Université Pierre et Marie Curie	Directeur de thèse
M. Marc LESTURGIE, Directeur SONDRÀ	Invité

Résumé étendu

Introduction

Souvent utilisé en tant que plate-forme publicitaire dans le ciel, le dirigeable est ici considéré en tant que plate-forme d'accueil d'un réseau d'antennes pour des applications radar (voir figure 1). On considère plus particulièrement les dirigeables hautes altitudes (High Altitude Airship) qui évoluent à une altitude supérieure à 20 km au-dessus du sol. À cette altitude, l'effet du vent est réduit, ce qui augmente la stabilité de sa position.



Figure 1: *High Altitude Airship*

L'utilisation d'un tel dirigeable comme plate-forme d'un réseau d'antennes permet de bénéficier d'une large surface pour monter les antennes. Cependant, du fait de la nature de la plate-forme, de fortes contraintes sur le poids et le volume des antennes doivent être prises en compte pour le choix du réseau.

Ce réseau sera utilisé pour des applications radar telles que la détection sous couvert forestier, la surveillance ou encore la polarimétrie radar. Ces applications imposent des caractéristiques particulières aux éléments du réseau. Le réseau doit notamment fonctionner en bande P, entre 400 MHz et 600 MHz et doit pouvoir fournir une double polarisation.

Toutes ces contraintes et ces besoins ont été pris en compte pour choisir l'élément du réseau. Ce travail a été effectué lors d'une précédente thèse réalisée par F. Chauvet [1]. Au cours de cette thèse, la faisabilité d'un réseau d'antenne conformé sur le dirigeable a été validée. L'élément choisi pour constituer le réseau est l'antenne spirale d'Archimède.

Chapitre 1 : Antennes spirales d'Archimède et solutions coplanaires

Le premier chapitre détaille le fonctionnement de l'antenne spirale d'Archimède et souligne l'inconvénient d'une alimentation centrale en vue de son intégration sur le dirigeable. L'état de l'art des solutions d'antennes spirales alimentées par l'extérieur est également présenté ainsi que leurs avantages et inconvénients.

Antenne spirale d'Archimède

L'antenne spirale d'Archimède (voir figure 2(a)) fait partie de la famille des antennes indépendantes de la fréquence. Elle présente ainsi de très bonnes performances large bande. En effet, lorsque la géométrie de l'antenne est auto-complémentaire i.e. la largeur des pistes est égale à l'espace entre les pistes, l'impédance d'entrée de l'antenne est égale à 200Ω sur une large plage de fréquence. Les bornes haute et basse de cette plage de fréquence sont directement reliées à la géométrie de l'antenne. La limite basse est inversement proportionnelle au diamètre D de l'antenne tandis que la limite haute est inversement proportionnelle au petit diamètre d . Pour des impératifs de mesure, la plage de fréquence souhaitée est multipliée par 2 (de 0.8 GHz à 1.2 GHz). Le diamètre de l'antenne est donc divisé également par 2. Toutes les antennes étudiées par la suite sont construites avec un diamètre externe de 12 cm.

L'alimentation de cette antenne se fait en son centre par un signal symétrique i.e. les deux bras de l'antenne sont alimentés en opposition de phase. En combinant une alimentation symétrique à une géométrie symétrique, on obtient une distribution du courant sur la surface de l'antenne qui est symétrique par rapport au centre de la spirale (voir figure 2(b)). En tout point de l'antenne, la valeur du courant est identique à celle au point symétrique par rapport au centre.

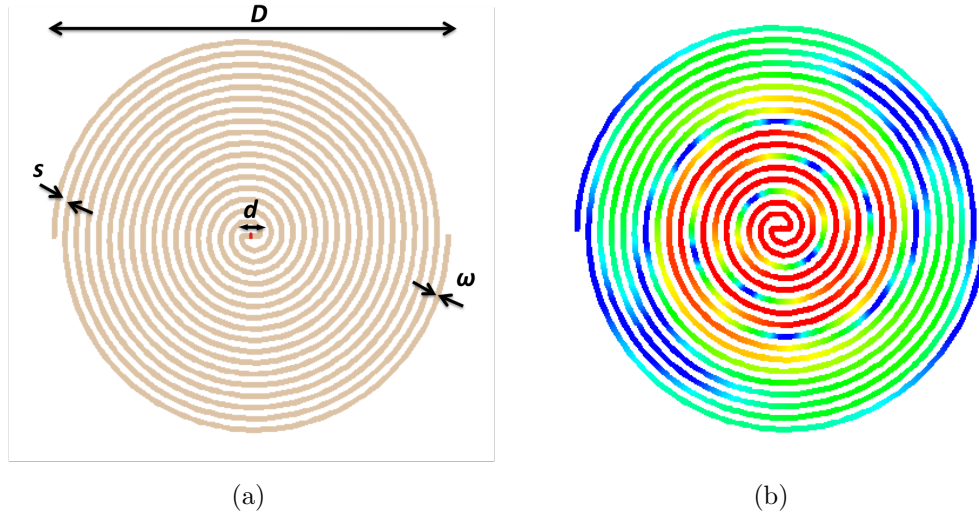


Figure 2: Antenne spirale d'Archimède : (a) géométrie et (b) distribution du courant à 1.1 GHz

Cette distribution de courant sur une surface plane produit un rayonnement symétrique par rapport au plan et à l'axe de propagation de l'antenne (voir figure 3). L'antenne rayonne suivant deux lobes principaux dans deux directions opposées et perpendiculaires à la spirale. La distribution du courant évolue en fonction de la fréquence, produisant ainsi la rotation du diagramme de rayonnement autour de l'axe de propagation de l'antenne. Cependant, grâce aux différentes symétries, la forme du diagramme de rayonnement du champ électrique est identique en fonction de la fréquence (voir figure 3(b)). Deux polarisations croisées sont rayonnées, une polarisation circulaire droite (RHCP) d'un côté et une polarisation circulaire gauche (LHCP) de l'autre. Pour étudier la polarisation, on s'intéresse à l'axial ratio (AR) qui est le rapport axial du champ électrique. Un AR égal à 0.7 correspond à une réjection de la polarisation croisée de -15 dB. On considère ainsi que, lorsque l'AR est supérieur à 0.7, la polarisation rayonnée est circulaire droite ou gauche. D'après la figure 4, qui représente la polarisation en fonction de la fréquence, la valeur de l'AR reste supérieure à 0.7 à partir de 1 GHz. Ainsi, même si l'antenne commence à rayonner à partir de 800 MHz, la spirale n'est utilisable qu'à partir de 1 GHz.

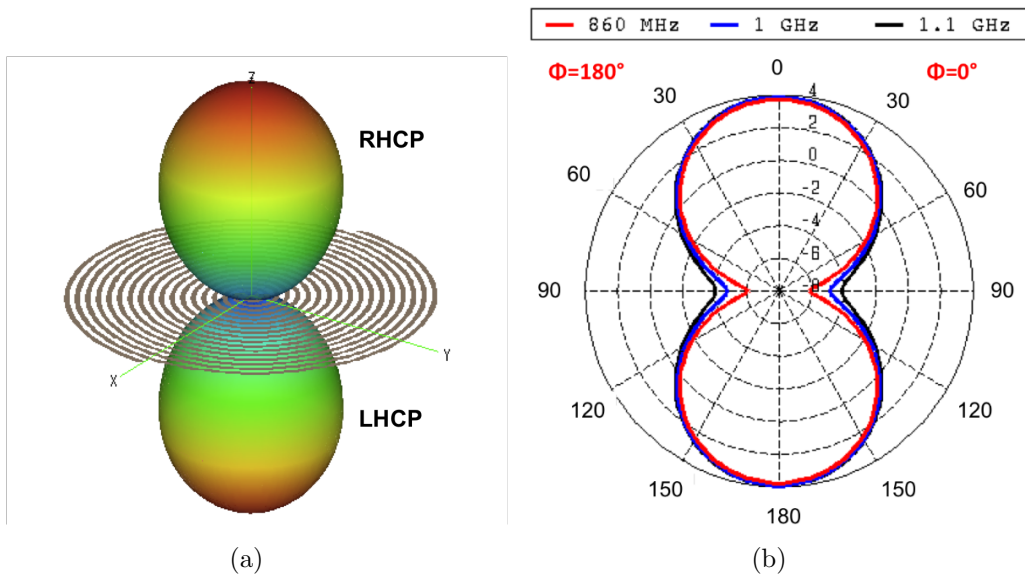


Figure 3: Antenne spirale d'Archimède : (a) vue 3D du diagramme de rayonnement du champ électrique et (b) coupe en élévation à 860 MHz, 1000 MHz et 1100 MHz

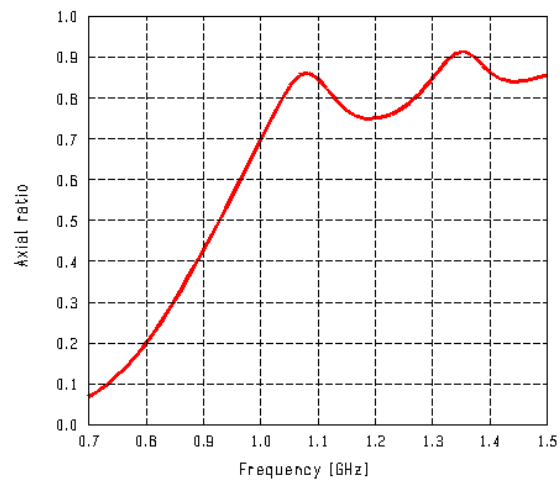


Figure 4: Antenne spirale d'Archimède : rapport axial en fonction de la fréquence à la position $\theta = 0^\circ$ et $\phi = 0^\circ$

En plus de ces performances large bande et le rayonnement d'une double polarisation croisée, la spirale d'Archimède est un élément plat et peu encombrant, ce qui la rend intéressante pour des applications aéroportées. Cependant, l'alimentation se fait au centre par un câble coaxial dans le plan perpendiculaire à l'antenne (voir figure 5). Cette configuration n'est pas envisageable dans le cas d'un réseau d'antennes monté sur un dirigeable. Il ne sera pas possible d'accéder au centre des spirales une fois les antennes conformées sur l'enveloppe externe de la plate-forme. Ce travail de thèse a pour but d'étudier l'alimentation de la spirale et de fournir une solution d'alimentation coplanaire qui permettra l'intégration du réseau sur le dirigeable.

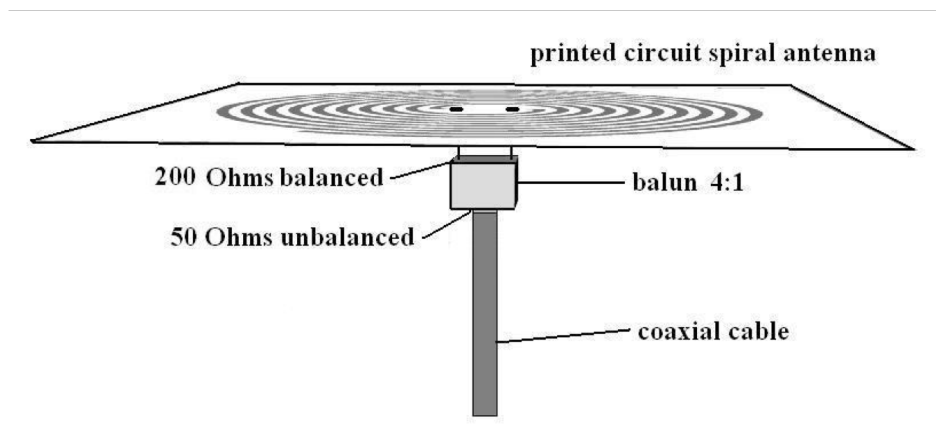


Figure 5: Antenne spirale d'Archimède : schéma d'alimentation

Etat de l'art des solutions à alimentation coplanaire

Plusieurs études ont été menées pour décaler l'alimentation à l'extérieur de la spirale. Quelques solutions d'antennes spirale à alimentation coplanaire tirées de la littérature sont présentées à la figure 6. Toutes ces antennes sont alimentées par l'extérieur. Cependant la spirale présentée par D. J. Muller et K. Sarabandi [2] (voir figure 6(a)) produit un diagramme de rayonnement non symétrique. De plus, la plage de fréquence de fonctionnement de l'antenne est multipliée par un facteur 2 comparée à une antenne spirale alimentée au centre, à diamètre égal. L'antenne de E. Gschwendtner et W. Wiesbeck [3] (voir figure 6(b)) présente les mêmes inconvénients sur les fréquences de fonctionnement et le diagramme de rayonnement. Dans les deux cas, le diagramme de rayonnement n'est pas symétrique par rapport à l'axe de

l'antenne. Ces antennes ne sont donc pas préconisées pour des applications en réseau. La structure présentée par C. W. Jung [4] (voir figure 6(c)) permet une alimentation au centre et à l'extérieur. Dans les trois cas, ni la géométrie ni la distribution du courant ne sont symétriques. Il en résulte que le diagramme de rayonnement ne correspond plus à celui de la spirale alimentée au centre.

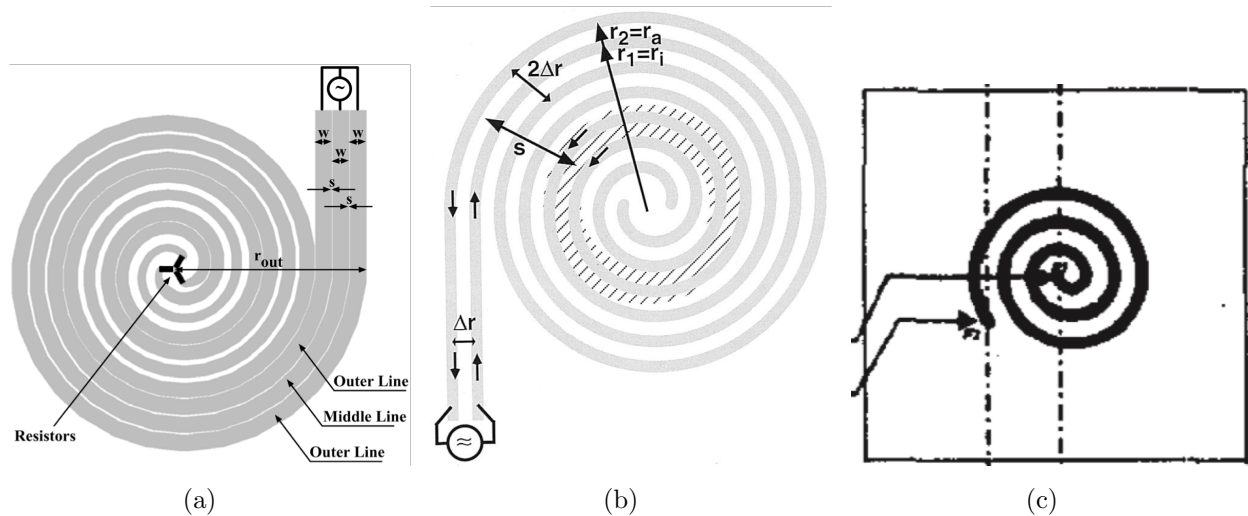


Figure 6: Solutions d'antennes spirales à alimentation coplanaire

Chapitre 2 : Premières solutions d'antennes spirales à alimentation externe

Ce chapitre présente deux solutions d'antennes spirales à alimentation coplanaire. Dans les deux cas, les antennes ont été créées en respectant les principes de symétrie au niveau de la géométrie et de l'alimentation.

Antenne spirale à 2×2 bras à charges résistives

Le principe de cette antenne est de conserver la géométrie symétrique de la spirale d'Archimède en ajoutant deux sources d'alimentations pour obtenir une distribution de courant symétrique (voir figure 7). Chaque source fournit un signal symétrique aux deux bras connectés. Pour

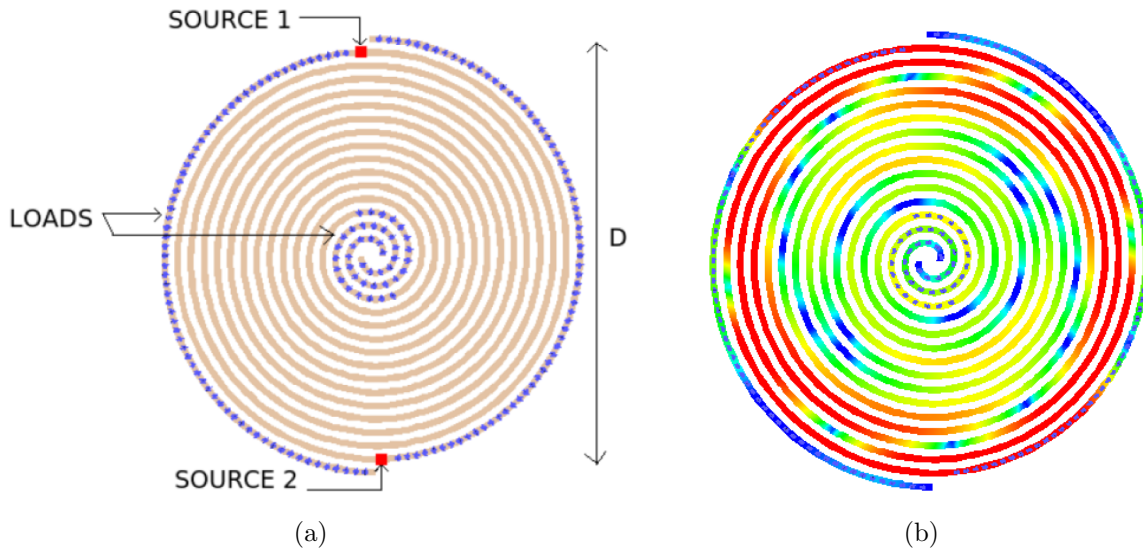


Figure 7: Antenne spirale à 2×2 bras : (a) géométrie et (b) distribution du courant à 1.1 GHz

éviter les réflexions à l'extrémité des bras, qui ont pour effet de dégrader les performances de l'antenne, des résistances sont placées tout au long des bras externes et au centre. Ainsi, l'onde incidente est particulièrement atténuée au centre pour les fréquences les plus basses, ce qui réduit le rayonnement d'une polarisation croisée dû aux ondes réfléchies. L'AR est donc amélioré (voir figure 2.4(a)) et une polarisation circulaire est rayonnée à partir de 880 MHz. Grâce aux charges résistives placées sur l'antenne, la bande de fréquences est élargie de 120 MHz comparée à celle de l'antenne spirale alimentée au centre. Cependant, l'utilisation de charges résistives sur l'antenne introduit des pertes. Ainsi, la puissance totale rayonnée est réduite, ce qui affecte l'efficacité de l'antenne (voir figure 2.4(b)). Aux basses fréquences, la puissance est principalement dissipée par les charges au centre et sur les bras périphériques tandis que la dissipation de l'énergie aux hautes fréquences est uniquement due aux charges périphériques. Il existe donc un compromis entre l'AR et l'efficacité pour obtenir de meilleures performances.

Cette antenne présente des performances intéressantes, principalement au niveau de la polarisation rayonnée. De plus, l'alimentation se fait dans le plan de l'antenne, ce qui facilite son intégration sur le dirigeable. Néanmoins, l'utilisation de charges résistives nuit à l'efficacité de l'antenne.

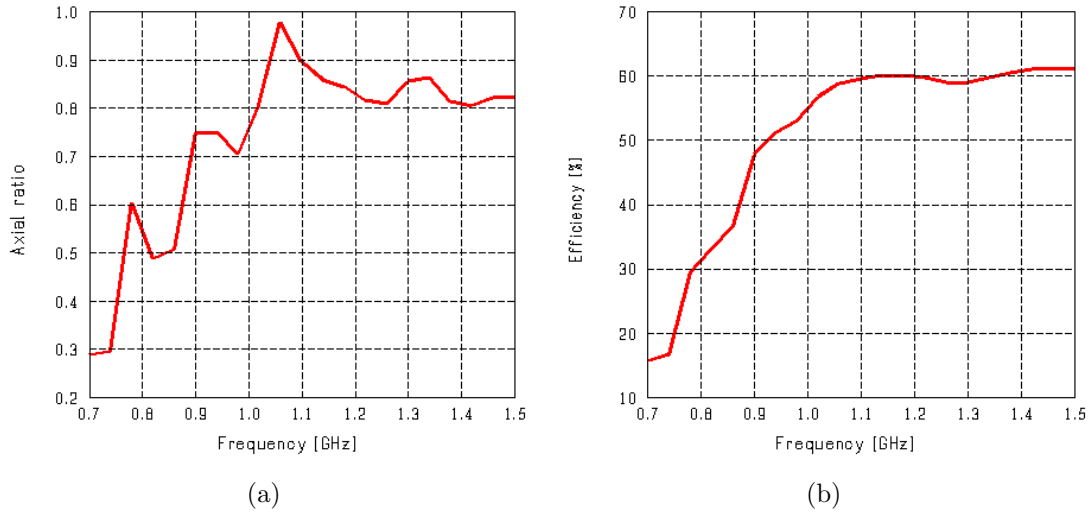


Figure 8: Antenne spirale à 2×2 bras : (a) rapport axial et (b) efficacité en fonction de la fréquence à $\theta = 0^\circ$ et $\phi = 0^\circ$

Antenne spirale à 2×2 bras

Pour éviter l'utilisation de charges résistives sur l'antenne, les deux bras connectés à chaque source ont été enroulés ensemble pour former cette antenne spirale (voir figure 2.5(a)). L'alimentation fournit un signal symétrique de sorte à conserver une distribution du courant symétrique par rapport au centre sur la surface de l'antenne (voir figure 2.5(b)).

Lorsque l'antenne est adaptée sur une impédance caractéristique de 200Ω , la plage de fréquence est élargie d'environ 150 MHz, comparée à la spirale classique (voir figure 10(a)). En effet, le coefficient de réflexion est inférieur à -10 dB à partir de 650 MHz, excepté entre 770 MHz et 830 MHz où la valeur est inférieure à -8 dB. Cette spirale accroît donc la largeur de bande, cependant la polarisation rayonnée est elliptique sur la majeure partie de cette plage de fréquence (voir figure 10(b)). Pour valider les résultats obtenus par la simulation, un prototype a été créé et mesuré en chambre anéchoïque (voir figure 11). Deux baluns sont utilisés pour adapter l'impédance caractéristique à 200Ω et symétriser l'alimentation. L'adaptation d'impédance n'est pas correctement réalisée par les baluns et l'impédance d'entrée de l'antenne mesurée n'est pas conforme à la simulation. Toutefois, l'alimentation est correctement symétrisée et les résultats présentés à la figure 12 montrent que la forme du diagramme de rayonnement est similaire à celle de l'antenne spirale d'Archimède et que les résultats de mesures concordent avec les simulations.

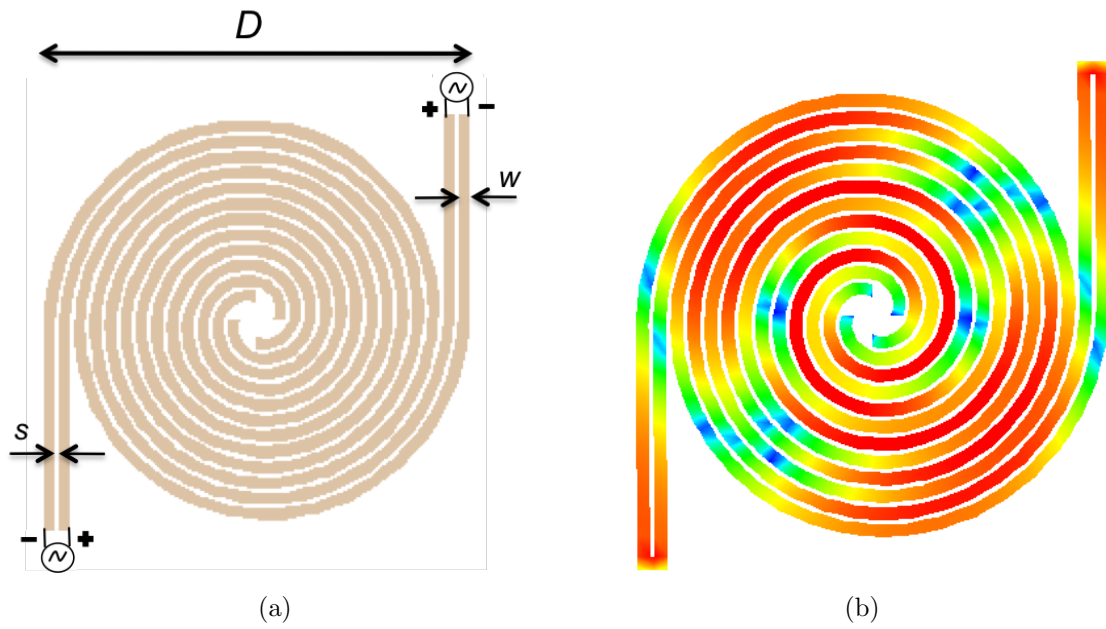


Figure 9: Antenne spirale à 2×2 bras : (a) géométrie et (b) distribution du courant à 1.1 GHz

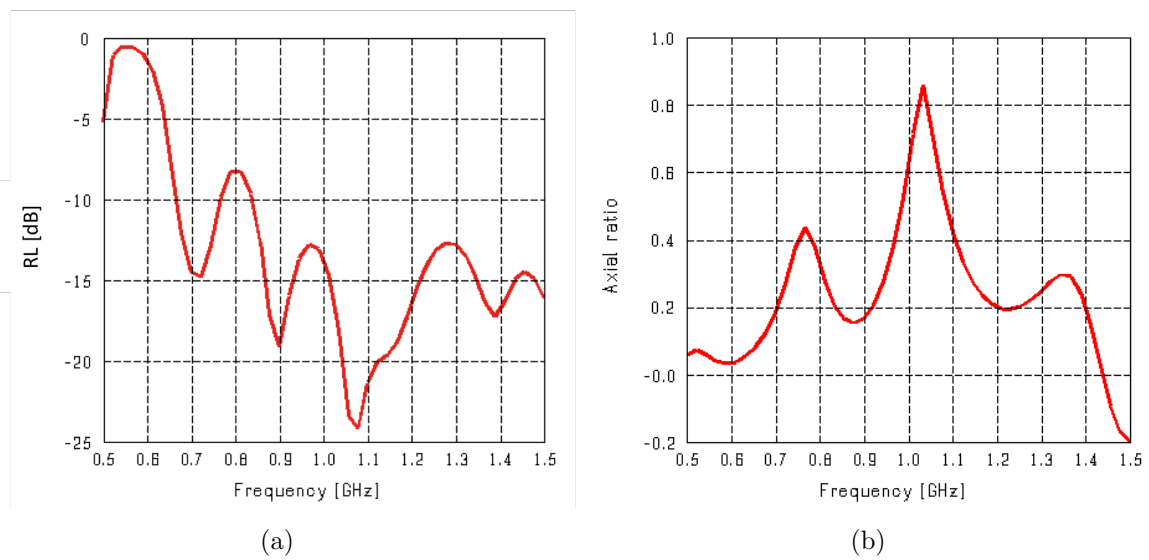
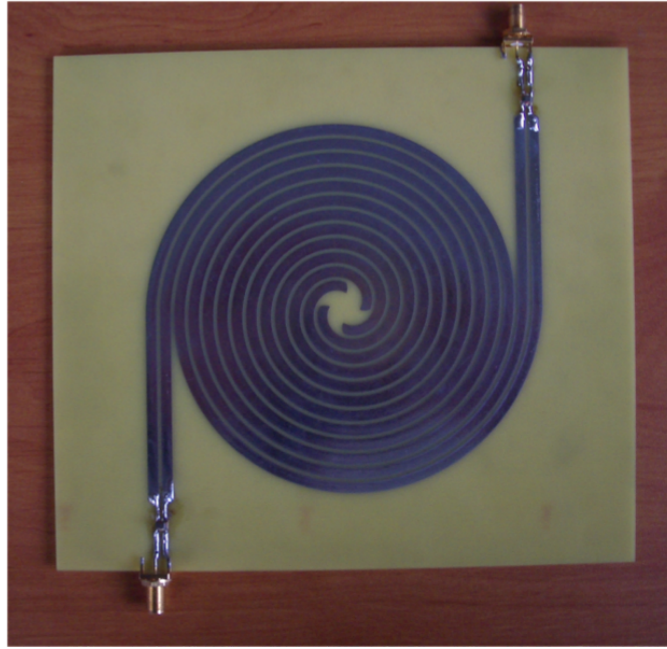
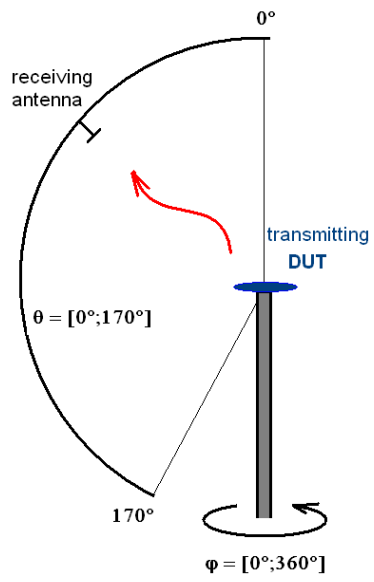


Figure 10: Antenne spirale à 2×2 bras : (a) coefficient de réflexion et (b) rapport axial à $\theta=0^\circ$ et $\phi=0^\circ$ en fonction de la fréquence



(a)



(b)



(c)

Figure 11: Antenne spirale à 2×2 bras : (a) prototype, (b) schéma et (c) photographie de la chambre anéchoïque à SUPELEC

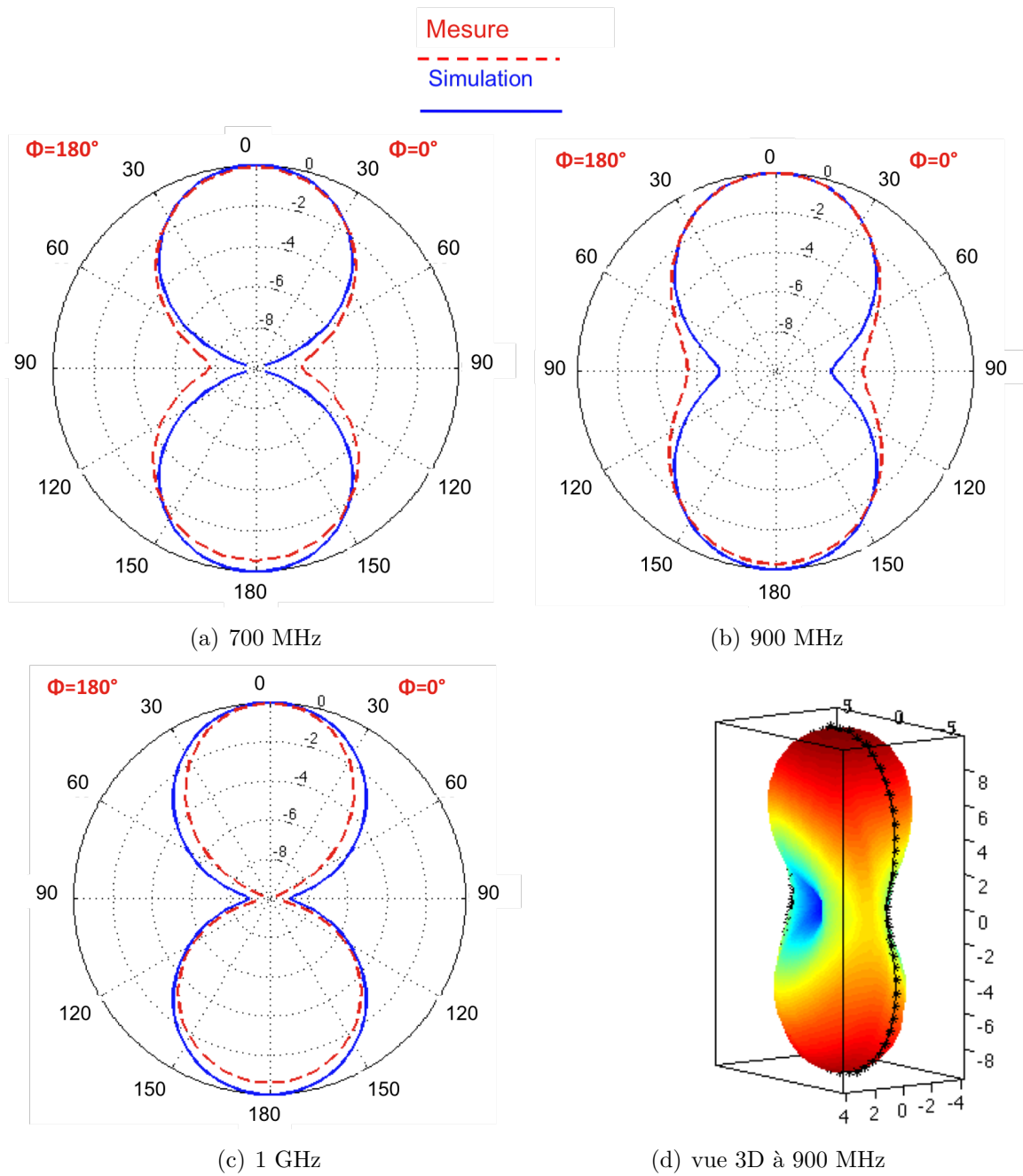


Figure 12: Antenne spirale à 2×2 bras : (a) comparaison des coupes en élévation du diagramme de rayonnement du champ électrique simulé et mesuré à 700 MHz, 900 MHz et 1 GHz avec une vue 3D du diagramme mesuré à 900 MHz

Chapitre 3 : De la théorie des réseaux à géométrie circulaire aux antennes multi-sources

Le chapitre 3 introduit un point de vue différent sur les antennes spirales alimentées par l'extérieur. En effet, les antennes alimentées par plusieurs sources peuvent être perçues comme un petit réseau composé de plusieurs éléments. Afin d'améliorer les performances des antennes, une étude sur les réseaux à géométrie circulaire combinée à des techniques de rotations séquentielles a été menée.

Le principe des réseaux à géométrie circulaire est résumé par la figure 13. Les éléments, identiques, sont disposés le long d'un cercle et chaque élément résulte d'une rotation par rapport au centre du cercle. De plus, une différence de phase égale à $\frac{2\pi}{N}$, N étant le nombre d'éléments, est appliquée entre deux antennes successives. Ainsi, dans cet exemple de 3 éléments, le décalage de phase des antennes est respectivement de 0° , 120° et 240° .

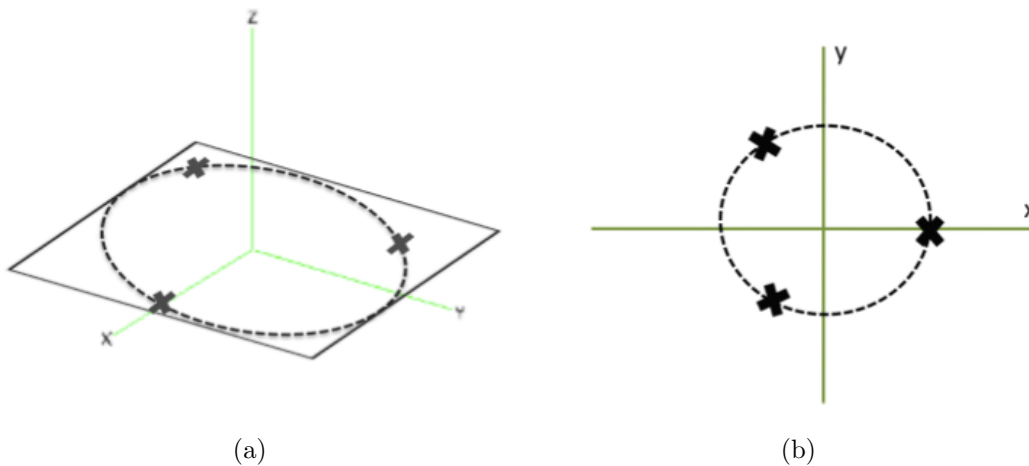


Figure 13: (a) vue 3D et (b) vue de dessus de la géométrie du réseau

En adoptant cette configuration de réseau, on montre que, pour un réseau d'au moins 3 éléments, la polarisation rayonnée est parfaitement circulaire dans l'axe quelle que soit la polarisation des éléments. Il est donc possible de générer une polarisation circulaire sur une large ouverture angulaire lorsque les antennes sont placées sur un cercle avec un jeu de phase approprié.

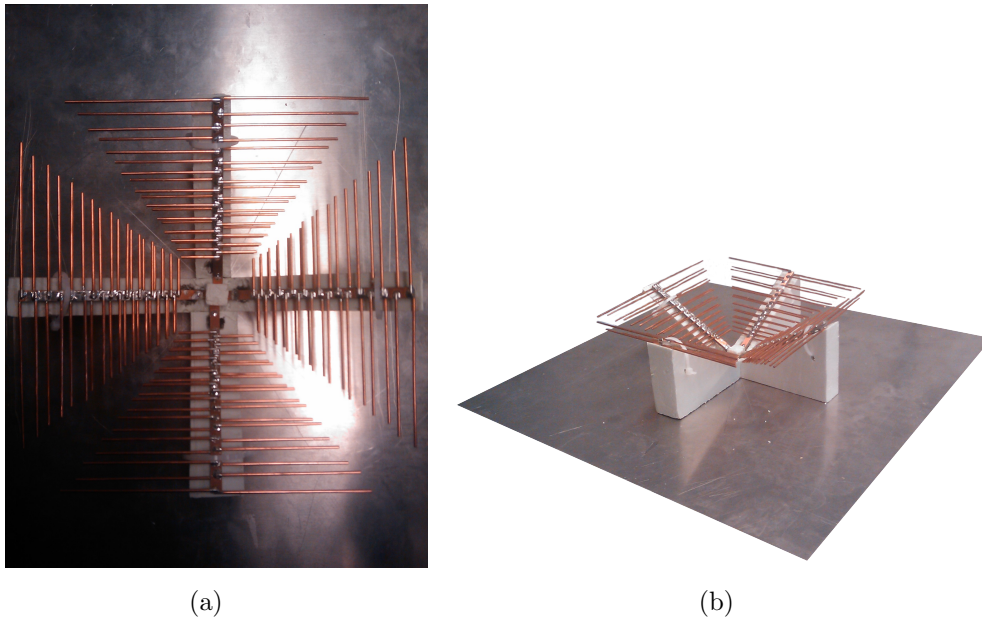


Figure 14: Réseau d'antennes LPDA : (a) vue de dessus et (b) vue 3D

Cette théorie a été validée par la simulation d'un réseau de 3 dipôles ainsi que par la simulation et la mesure d'un réseau de 4 antennes log-periodiques (log periodic dipole antenna, LPDA) (voir figure 14). Les résultats obtenus montrent bien qu'une polarisation circulaire pure ($AR = 1$) est rayonnée à $\theta = 0^\circ$ et une bonne polarisation circulaire ($AR \geq 0.7$) est obtenue sur une large plage angulaire (voir figure 15). De plus, l'étude de l'influence du nombre d'éléments sur la polarisation du réseau montre que la plage angulaire comprenant une polarisation circulaire, augmente avec le nombre d'éléments. Cependant, à partir d'un certain nombre d'éléments, des lobes de réseau se forment. Il est donc nécessaire de trouver un compromis entre la plage angulaire et le nombre d'éléments.

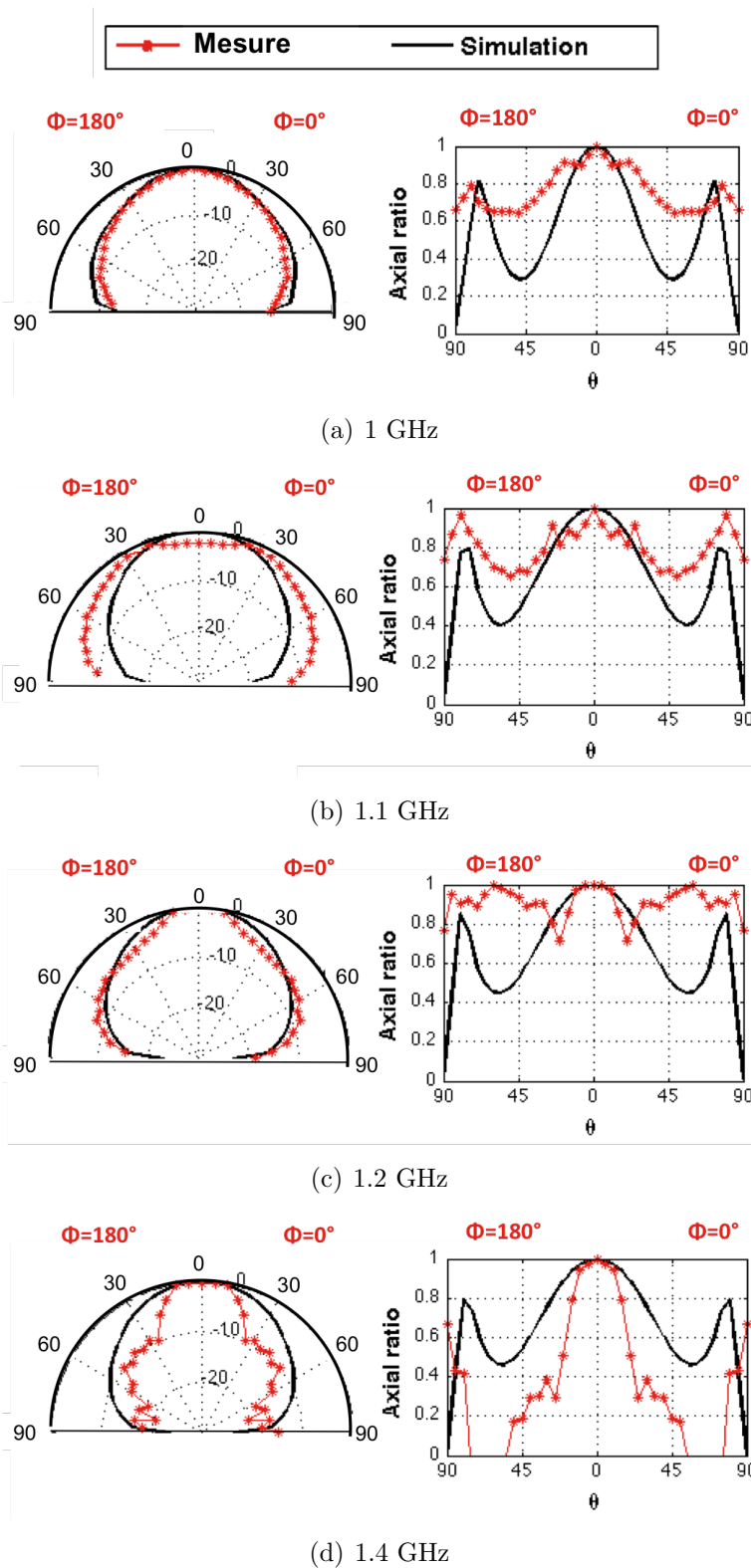


Figure 15: Réseau d'antennes LPDA : (gauche) comparaison de la coupe en élévation simulée et mesurée du gain normalisé et (droite) du rapport axial à 1GHz (a), 1.1GHz (b), 1.2GHz (c) and 1.4GHz (d)

Chapitre 4 : Application de la théorie des réseaux à géométrie circulaire aux antenne spirales

Ce chapitre est consacré à l'étude de deux antennes spirales alimentées par l'extérieur et réalisées en appliquant la théorie présentée au précédent chapitre. La première antenne est alimentée par 3 sources dans le même plan (voir figure 16). On peut donc considérer que cette antenne est un petit réseau composé de 3 éléments. Chaque élément est issu d'une rotation d'un angle de $\frac{2\pi}{3}$ de l'élément qui le précède par rapport au centre. En respectant cette configuration, la distribution du courant sur l'antenne est symétrique par rotation. A chaque point de la spirale, la valeur du courant est identique aux points symétriques par rotations de 120° et 240° . Le rayonnement du champ électrique est donc symétrique par rapport au plan de l'antenne et est similaire à celui de l'antenne spirale alimentée au centre. Trois baluns sont utilisés et les mêmes inconvénients observés pour l'antenne à 2×2 bras sont présents au niveau de l'alimentation.

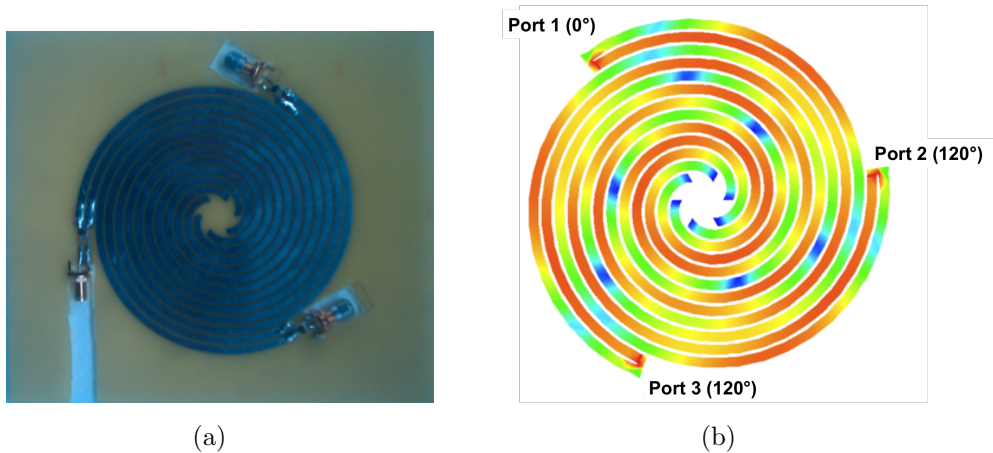


Figure 16: Antenne spirale à 3×2 bras : (a) prototype et (b) distribution du courant à 750 MHz

En accord avec la théorie des réseaux à géométrie circulaire, la simulation de l'AR de cette antenne montre bien une polarisation circulaire pure, rayonnée à $\theta = 0^\circ$ et une bonne polarisation circulaire sur une plage angulaire de $\pm 20^\circ$ (voir figure 17). Avec trois sources d'alimentation, l'antenne est reconfigurable en polarisation circulaire droite ou gauche en fonction du jeu de phase appliqué aux 3 accès (voir figure 18 et tableau 1). Les résultats de mesure du champ électrique concordent bien avec la simulation (voir figure 19).

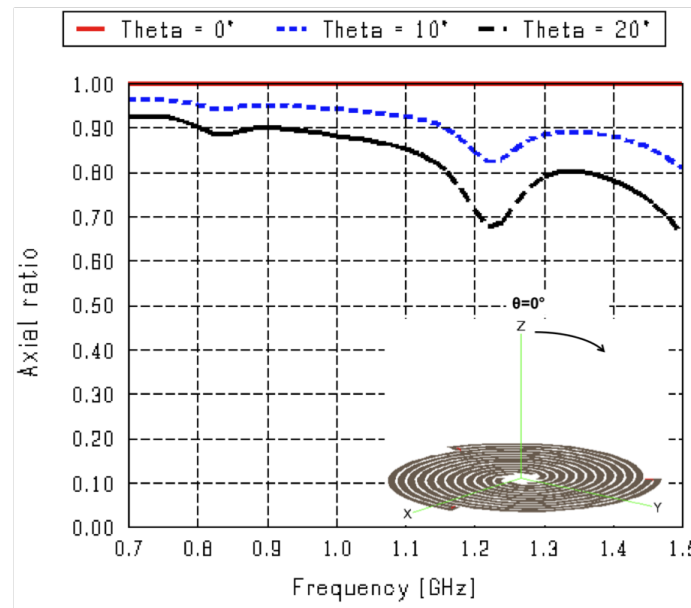


Figure 17: Antenne spirale à 3×2 bras : rapport axial en fonction de la fréquence à $\theta = 0^\circ$, 10° et 20°

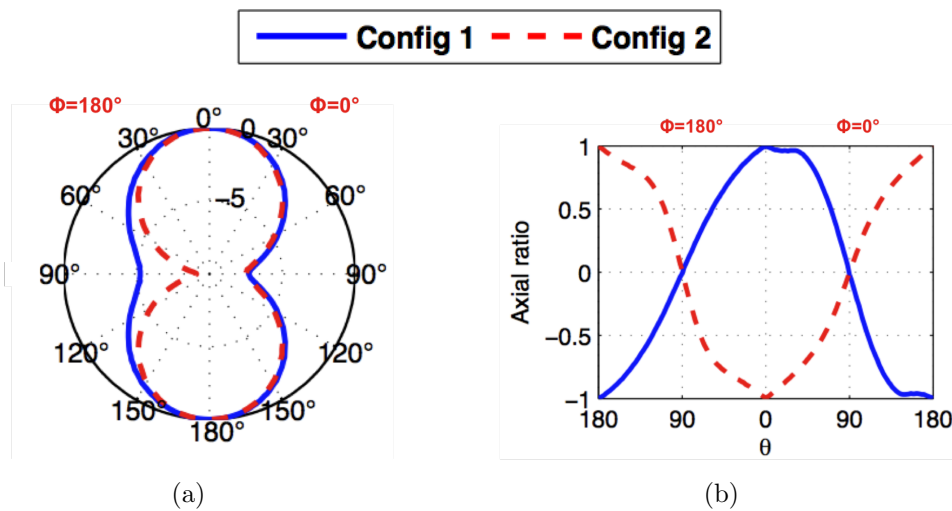
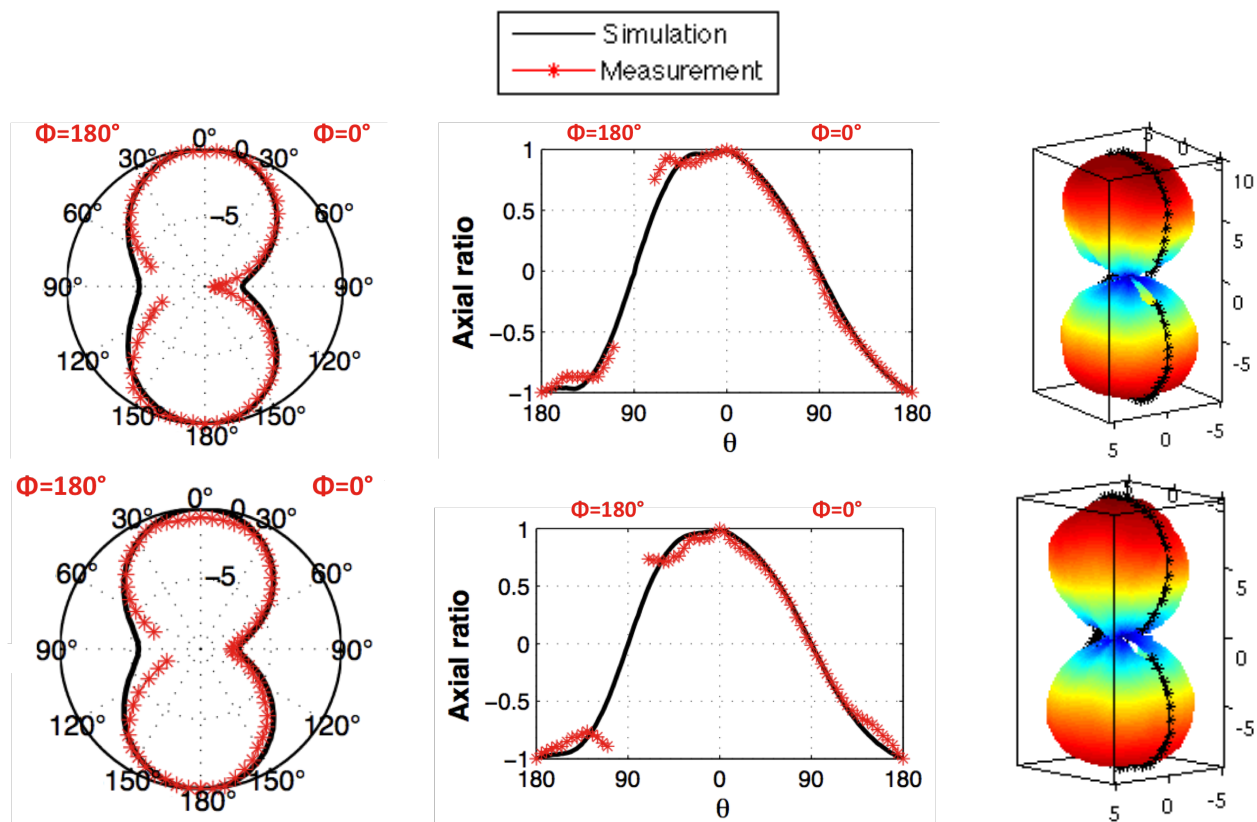


Figure 18: Antenne spirale à 3×2 bras : (a) simulation de la coupe en élévation du gain normalisé et (b) du rapport axial à 1 GHz

Table 1: Polarisation en fonction des phases appliquées aux sources à $\theta=0^\circ$

	Port 1	Port 2	Port 3	Polarisation
Configuration 1	0°	120°	240°	Circulaire droite
Configuration 2	0°	240°	120°	Circulaire gauche

**Figure 19:** Antenne spirale à 3×2 bras : (gauche) comparaison de la coupe en élévation simulée et mesurée du gain normalisé, (milieu) du rapport axial et (droite) une vue 3D du diagramme mesuré à 1 GHz (haut) et 1.04 GHz (bas)

L'antenne à 3×2 bras offre des performances intéressantes en terme de polarisation. De plus, l'antenne est reconfigurable selon deux polarisations circulaires. Cependant, l'utilisation des baluns pour symétriser l'alimentation et réaliser une adaptation d'impédance dégrade le coefficient de réflexion de l'antenne. Afin de résoudre les inconvénients liés à l'utilisation de baluns, une nouvelle antenne spirale à alimentation externe a été développée (voir figure 20). Il s'agit d'une antenne à fentes alimentée par 4 sources fournissant un signal différentiel déphasées respectivement de 0° , 90° , 180° et 270° . Ainsi, la forme de la spirale a été découpée dans un carré de cuivre.

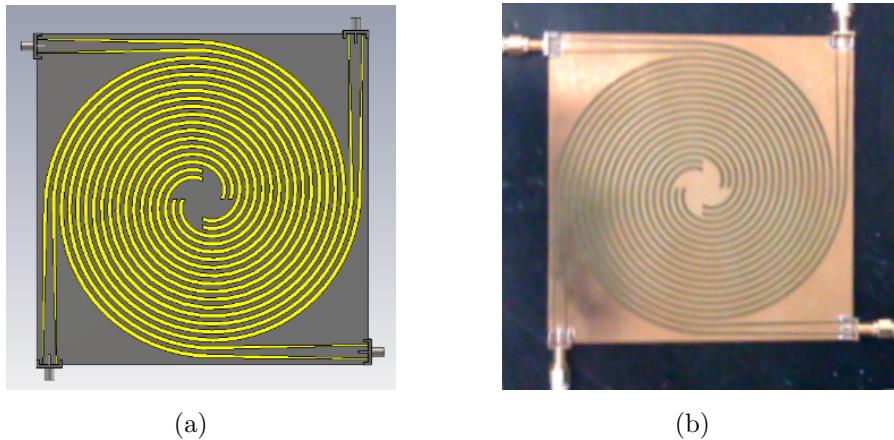


Figure 20: Antenne spirale à 4×2 bras : (a) modélisation et (b) prototype

Chaque ligne connectée aux sources, réalise une transition de l'impédance de la spirale aux 50Ω du câble coaxial. Il n'est donc plus nécessaire de faire appel à des baluns pour adapter l'antenne. Le coefficient de réflexion mesuré concorde très bien avec le résultat de simulation (voir figure 21) et montre que la bande de l'antenne est comprise entre 1.25 GHz et 2 GHz. Le coefficient de réflexion peut encore être amélioré en utilisant des charges résistives au centre de l'antenne pour éviter les réflexions aux basses fréquences.

La polarisation rayonnée est circulaire sur la plage angulaire comprise entre $\pm 40^\circ$ (voir figure 22). De plus, la polarisation est reconfigurable en linéaire horizontale/verticale ou en circulaire droite ou gauche (voir figure 4.12 et tableau 2). Les résultats de mesure, obtenus en chambre anéchoïque, correspondent à la simulation (voir figure 24). En plus d'être facilement alimentée par un câble coaxial, cette antenne permet de rayonner une polarisation circulaire sur une large plage de fréquences avec un diagramme de rayonnement similaire à celui de l'antenne spirale d'Archimède. De plus, grâce à son alimentation externe, l'antenne peut être aisément intégrée sur l'enveloppe externe du dirigeable.

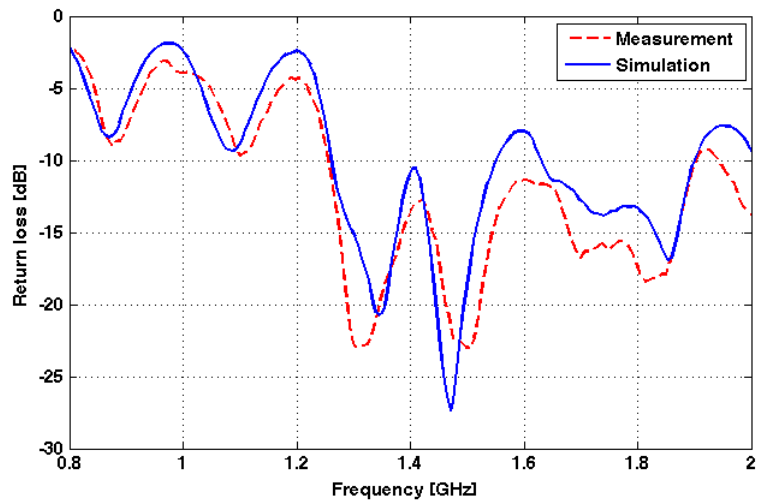


Figure 21: Antenne spirale à 4×2 bras : comparaison des coefficients de réflexion simulé et mesuré en fonction de la fréquence pour $Z_c = 50 \Omega$

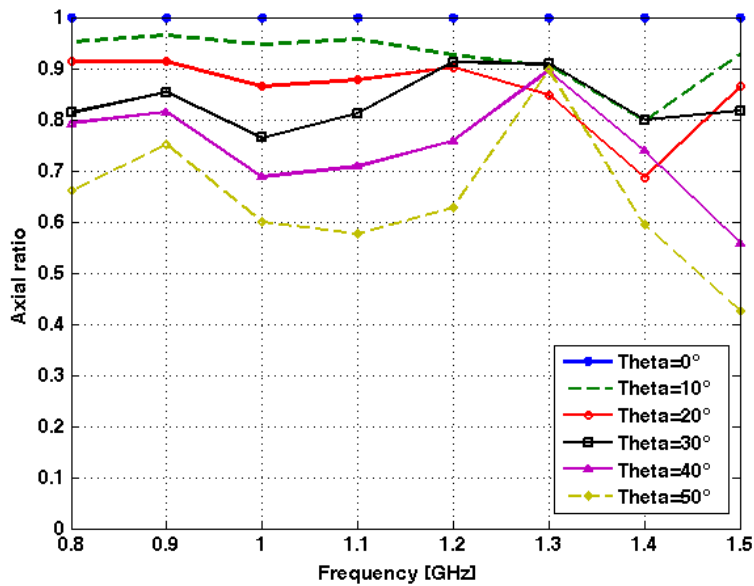


Figure 22: Antenne spirale à 4×2 bras : rapport axial en fonction de la fréquence pour $\theta = 0^\circ$ à 50°

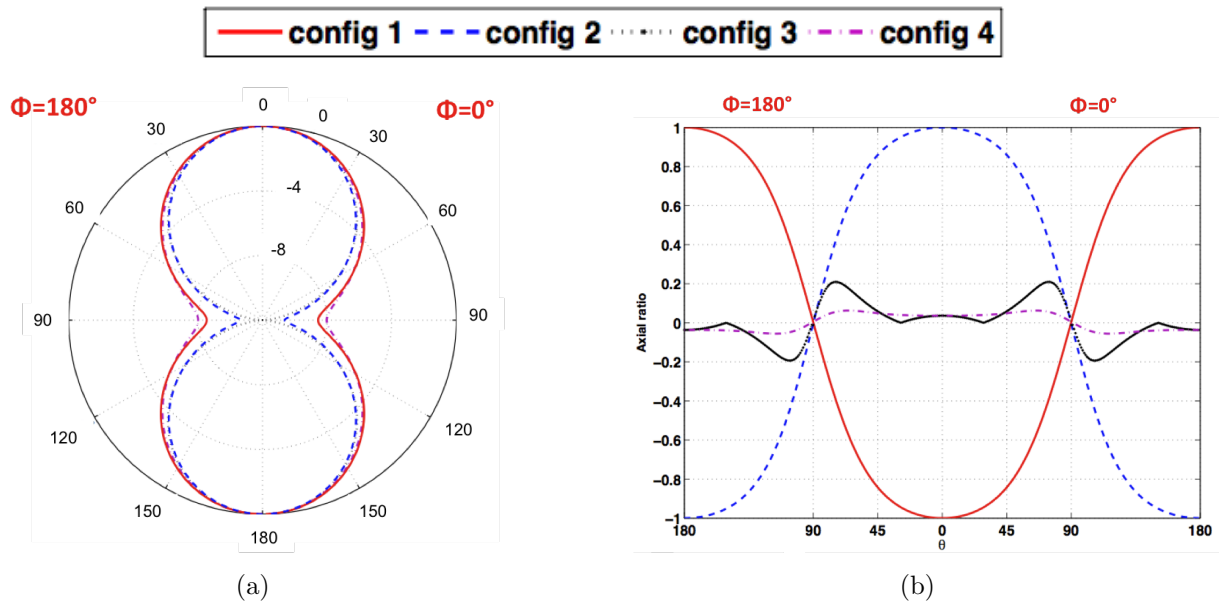


Figure 23: Antenne spirale à 4×2 bras : (a) coupe en élévation simulée du gain normalisé et (b) du rapport axial à 1 GHz

Table 2: Polarisation en fonction des phases appliquées aux sources à $\theta = 0^\circ$, x correspond aux ports adaptés à 50Ω

	Port 1	Port 2	Port 3	Port 4	Polarisation
Configuration 1	0°	90°	180°	270°	Circulaire gauche
Configuration 2	0°	270°	180°	90°	Circulaire droite
Configuration 3	0°	x	180°	x	Linéaire horizontale
Configuration 4	x	0°	x	180°	Linéaire verticale

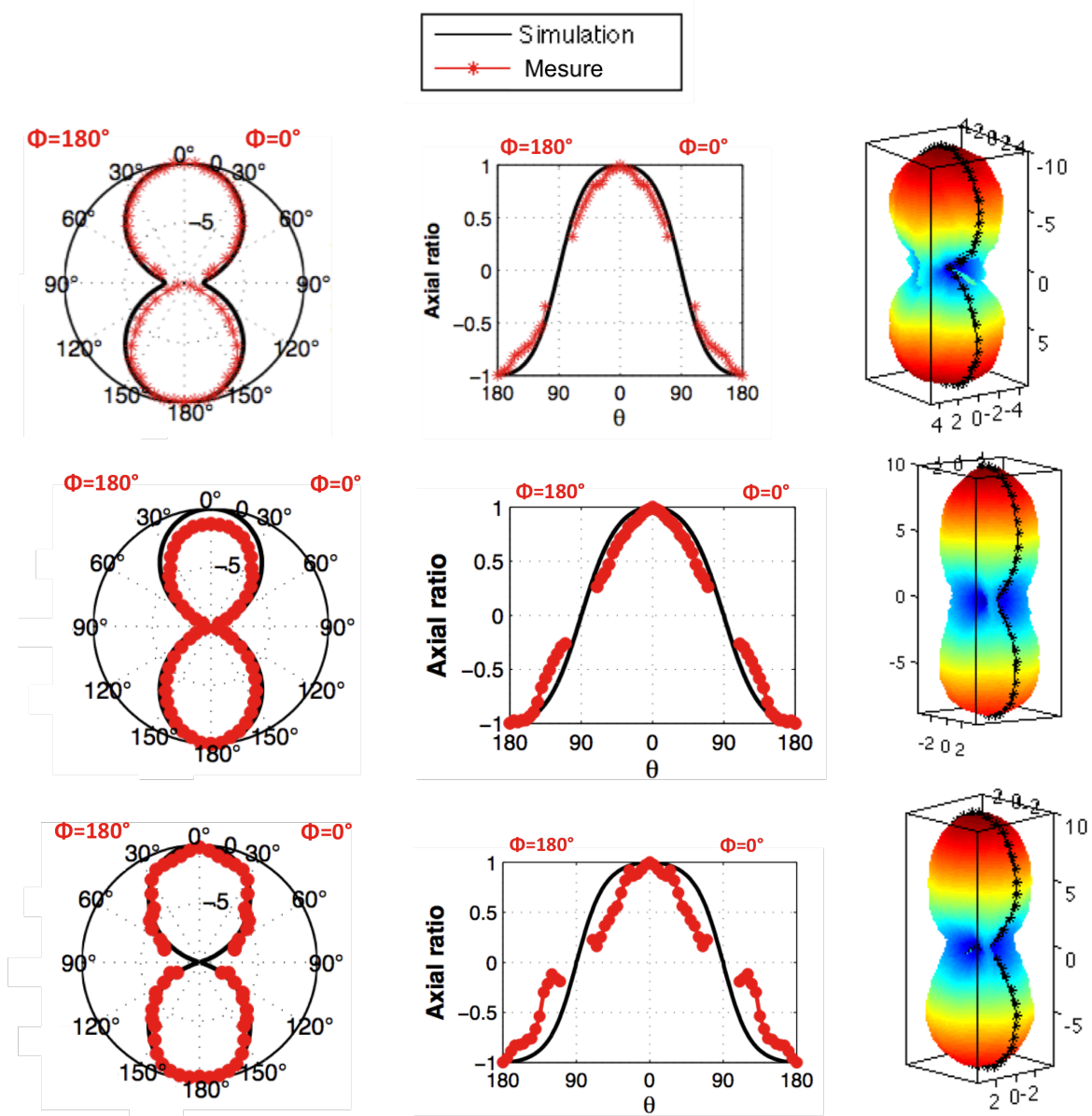


Figure 24: Antenne spirale à 4×2 bras : (gauche) comparaison de la coupe en élévation simulée et mesurée du gain normalisé, (milieu) du rapport axial et (droite) une vue 3D du diagramme mesuré à 800 MHz (haut), 1100 MHz (milieu) et 1500 MHz (bas)

Conclusion

Au cours de ce travail de thèse, différentes configurations d'antennes spirales alimentées par l'extérieur ont été développées pour palier le problème d'alimentation, lié à l'intégration du réseau sur l'enveloppe du dirigeable (voir tableau 3). La première solution combine la géométrie de la spirale d'Archimède avec deux sources contenues dans le même plan. Des charges résistives sont placées sur les bras périphériques et au centre de l'antenne, pour éviter des réflexions du courant, qui dégradent la pureté de la polarisation et la largeur de bande. Ainsi, la polarisation circulaire est rayonnée sur une plage de fréquence élargie de 120 MHz. Cependant, l'utilisation de ces charges résistives induit des pertes de puissance, ce qui affecte l'efficacité de l'antenne.

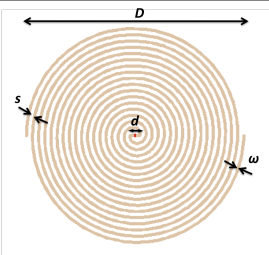
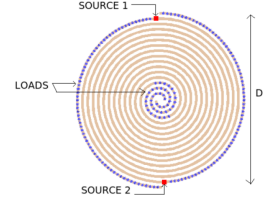
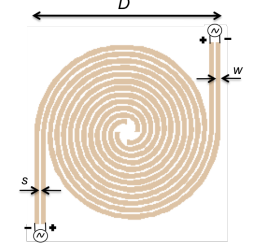
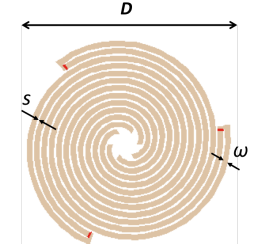
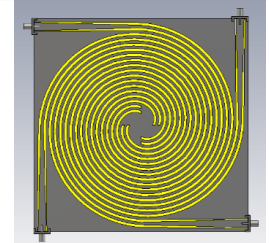
Afin d'éviter l'utilisation de charges sur la spirale, une autre antenne alimentée par deux sources a été conçue. Les performances obtenues sont intéressantes du point de vue de la largeur de bande qui est élargie de 150 MHz. Néanmoins, la polarisation rayonnée est circulaire uniquement sur une bande étroite de fréquence. Un prototype de cette antenne a été fabriqué et mesuré en chambre anéchoïque. Les mesures du champ électrique concordent avec les résultats de simulation. Toutefois, les baluns utilisés pour symétriser et réaliser une adaptation d'impédance de l'alimentation dégradent les performances large bande de l'antenne. L'étude des réseaux à géométrie circulaire, couplés aux techniques de rotations séquentielles, permet d'obtenir une polarisation circulaire quelle que soit la polarisation des éléments. Ainsi, à partir de trois éléments, une polarisation circulaire pure ($|AR|=1$) est rayonnée dans l'axe de l'antenne et une bonne polarisation ($|AR|\geq 0.7$) sur une large plage angulaire.

Ces techniques ont été appliquées à la spirale et deux nouvelles antennes alimentées par l'extérieur ont été développées. La première est l'antenne à 3×2 bras. Grâce à ses 3 sources, l'antenne rayonne une polarisation circulaire sur une plage angulaire égale à $\pm 20^\circ$. De plus, la polarisation est reconfigurable en circulaire droite ou gauche en fonction du jeu de phase appliqué aux sources. Le prototype de cette antenne inclut les baluns ce qui induit les mêmes inconvénients sur la largeur de bande observés que pour l'antenne à 2×2 bras. Toutefois, les résultats de mesure du champ électrique correspondent bien à la simulation.

La dernière antenne développée dans cette étude est l'antenne à fente à 4×2 bras. L'antenne est alimentée par quatre sources asymétriques. Chaque piste connectée aux sources subit une transition pour adapter l'impédance de l'antenne aux $50\ \Omega$ d'un câble coaxial. Ainsi, les baluns ne sont plus nécessaires et les résultats de mesures du coefficient de réflexion et du champ électrique concordent très bien avec la simulation. La bande passante est comprise

entre 1.25 GHz et 2 GHz. La polarisation rayonnée est circulaire sur une plage angulaire égale à $\pm 40^\circ$. De plus, grâce aux quatre sources, la polarisation est reconfigurable en linéaire horizontale/verticale ou circulaire droite/gauche. Cette solution présente des avantages pour l'obtention d'une bonne polarisation sur une large bande de fréquence tout en étant alimentée par l'extérieur directement par des câbles coaxiaux. Il est donc maintenant plus facile d'intégrer la spirale sur des plates-formes qui ne permettent pas l'accès à son centre.

Table 3: Résumé des performances des antennes

<i>Antenne</i>	<i>Nb de sources</i>	<i>F_{min} du RL</i>	<i>Diagramme de rayonnement</i>	<i>Polarisation</i>
	1	$f_{min}=800$ MHz	Symétrique	$f_{AR \geq 0.7} = 1$ GHz
	2	$f_{min}=830$ MHz	Symétrique	$f_{AR \geq 0.7} = 880$ MHz
	2	$f_{min}=650$ MHz	Symétrique	$f_{AR \geq 0.7} = 1-1.05$ GHz
	3	$f_{min}=1.05$ GHz	Symétrique	$f_{AR \geq 0.7} = 0.7-1.5$ GHz
	4	$f_{min}=1.25$ GHz	Symétrique	$f_{AR \geq 0.7} = 0.7-1.5$ GHz

**Ph.D THESIS
OF THE UNIVERSITY PIERRE ET MARIE CURIE
PARIS 6**

**Specialty
ELECTRICAL ENGINEERING**

**Thesis Submitted for the Degree of
DOCTOR OF PHILOSOPHY**

**By
Karim LOUERTANI**

**MULTI-ARMS MULTI-PORTS EXTERNALLY-FED
SPIRAL ANTENNA FOR RADAR APPLICATIONS
CARRIED BY AN AIRSHIP**

Jury:

Pr. Raphaël GILLARD, INSA Rennes	Reviewer
Dr. Xavier BEGAUD, TELECOM ParisTech	Reviewer
Pr. BENLARBI-DELAÏ, Université Pierre et Marie Curie	Examiner
Dr. Nicolas RIBIÈRE-THARAUD, DRE-L2S, SUPELEC	Supervisor
Dr. Régis GUINVARC'H, SONDRÀ, SUPELEC	Supervisor
Pr. Marc HÉLIER, Université Pierre et Marie Curie	Supervisor
Mr. Marc LESTURGIE, Directeur SONDRÀ, SUPELEC	Invited

Contents

Contents	0
List of figures	7
Glossary	9
Introduction	11
1 General Review	13
1.1 Airship	13
1.1.1 Antenna platform	13
1.1.2 Applications	14
1.2 Antenna Element	14
1.2.1 Spiral antenna	15
1.2.2 Feeding issue	21
1.3 State of the Art	21
1.4 Conclusion of Chapter 1	25
2 First Solutions of Externally-fed Spiral Antennas	27
2.1 Resistively Loaded Spiral Antenna	27
2.1.1 Antenna design	28
2.1.2 Antenna characteristics	29
2.2 2×2 Arms Spiral Antenna	33
2.2.1 Antenna design	33
2.2.2 Antenna performances	34
2.3 Measurement	37
2.3.1 Antenna prototype	37

2.3.2	Anechoic chamber	37
2.3.3	Measurement method and results	39
2.4	Conclusion of Chapter 2	40
3	From Circular Array with Sequential Rotation Technique to Multi-ports Antenna	43
3.1	Circular Array with Sequential Rotation Technique (CASRT)	44
3.1.1	Geometry and feeding configuration of the CASRT	44
3.1.2	Polarization of the CASRT	46
3.2	Examples of CASRT	47
3.2.1	Dipole antenna array	47
3.2.2	LPDA antenna array	53
3.3	Conclusion of Chapter 3	56
4	Multi-arms Multi-ports Externally-fed Spiral Antennas	61
4.1	3×2 Arms Spiral Antenna	61
4.1.1	Antenna design	61
4.1.2	Feeding configuration	62
4.1.3	Measurement and simulation results	63
4.2	4×2 Arms Spiral Antenna	69
4.2.1	Antenna design	69
4.2.2	Feeding configuration	70
4.2.3	Measurement and simulation results	70
4.3	Conclusion of Chapter 4	76
	Conclusion	79
	Publications	83
	Appendix	85
	A Substrate and balun datasheets	87
	B Typon of the prototypes	93

List of Figures

1	High Altitude Airship	i
2	Antenne spirale d'Archimède : (a) géométrie et (b) distribution du courant à 1.1 GHz	iii
3	Antenne spirale d'Archimède : (a) vue 3D du diagramme de rayonnement du champ électrique et (b) coupe en élévation à 860 MHz, 1000 MHz et 1100 MHz	iv
4	Antenne spirale d'Archimède : rapport axial en fonction de la fréquence à la position $\theta = 0^\circ$ et $\phi = 0^\circ$	iv
5	Antenne spirale d'Archimède : schéma d'alimentation	v
6	Solutions d'antennes spirale à alimentation coplanaire	vi
7	Antenne spirale à 2×2 bras : (a) géométrie et (b) distribution du courant à 1.1 GHz	vii
8	Antenne spirale à 2×2 bras : (a) rapport axial et (b) efficacité en fonction de la fréquence à $\theta=0^\circ$ et $\phi=0^\circ$	viii
9	Antenne spirale à 2×2 bras : (a) géométrie et (b) distribution du courant à 1.1 GHz	ix
10	Antenne spirale à 2×2 bras : (a) coefficient de réflexion et (b) rapport axial à $\theta=0^\circ$ et $\phi=0^\circ$ en fonction de la fréquence	ix
11	Antenne spirale à 2×2 bras : (a) prototype, (b) schéma et (c) photographie de la chambre anéchoïque à SUPELEC	x
12	Antenne spirale à 2×2 bras : (a) comparaison des coupes en élévation du diagramme de rayonnement du champ électrique simulé et mesuré à 700 MHz, 900 MHz et 1 GHz avec une vue 3D du diagramme mesuré à 900 MHz	xi
13	(a) vue 3D et (b) vue de dessus de la géométrie du réseau	xii
14	Réseau d'antennes LPDA : (a) vue de dessus et (b) vue 3D	xiii

15	Réseau d'antennes LPDA : (gauche) comparaison de la coupe en élévation simulée et mesurée du gain normalisé et (droite) du rapport axial à 1GHz (a), 1.1GHz (b), 1.2GHz (c) and 1.4GHz (d)	xiv
16	Antenne spirale à 3×2 bras : (a) prototype et (b) distribution du courant à 750 MHz	xv
17	Antenne spirale à 3×2 bras : rapport axial en fonction de la fréquence à $\theta = 0^\circ, 10^\circ$ et 20°	xvi
18	Antenne spirale à 3×2 bras : (a) simulation de la coupe en élévation du gain normalisé et (b) du rapport axial à 1 GHz	xvi
19	Antenne spirale à 3×2 bras : (gauche) comparaison de la coupe en élévation simulée et mesurée du gain normalisé, (milieu) du rapport axial et (droite) une vue 3D du diagramme mesuré à 1 GHz (haut) et 1.04 GHz (bas)	xvii
20	Antenne spirale à 4×2 bras : (a) modélisation et (b) prototype	xviii
21	Antenne spirale à 4×2 bras : comparaison des coefficients de réflexion simulé et mesuré en fonction de la fréquence pour $Z_c=50 \Omega$	xix
22	Antenne spirale à 4×2 bras : rapport axial en fonction de la fréquence pour $\theta= 0^\circ$ à 50°	xix
23	Antenne spirale à 4×2 bras : (a) coupe en élévation simulée du gain normalisé et (b) du rapport axial à 1 GHz	xx
24	Antenne spirale à 4×2 bras : (gauche) comparaison de la coupe en élévation simulée et mesurée du gain normalisé, (milieu) du rapport axial et (droite) une vue 3D du diagramme mesuré à 800 MHz (haut), 1100 MHz (milieu) et 1500 MHz (bas)	xxi
1.1	High Altitude Airship	14
1.2	Archimedean spiral antenna: (a) geometry and (b) current distribution at 1.1 GHz	15
1.3	Archimedean spiral antenna: (a) input impedance calculated for a reference impedance $Z_c = 200 \Omega$ and (b) reflection coefficient	17
1.4	Archimedean spiral antenna: (a) 3D view of the far field pattern and (b) cuts in elevation at three frequencies	18
1.5	Archimedean spiral antenna: (a) cut in elevation of the axial ratio at 1.5 GHz and (b) over the frequency range for $\theta = 0^\circ$ and $\phi= 0^\circ$	19
1.6	Archimedean spiral antenna: current distribution at (d) 700 MHz, (c) 900 MHz, (b) 1 GHz and (a) 1.5 GHz	20

1.7	Archimedean spiral antenna: feeding configuration	21
1.8	Three arms spiral antenna externally-fed	22
1.9	Two arms spiral antenna externally-fed	23
1.10	Single arm spiral antenna with inner and outer feeding	24
2.1	Resistively loaded spiral antenna: (a) geometry and (b) current distribution at 1.1 GHz	28
2.2	Resistively loaded spiral antenna: return loss calculated for a reference impedance $Z_c = 250 \Omega$	30
2.3	Resistively loaded spiral antenna: (a) 3D view of the far field pattern and (b) cuts in elevation at 860 MHz, 1 GHz and 1.1 GHz	31
2.4	Resistively loaded spiral antenna: (a) axial ratio over the frequency range at $\theta=0^\circ$ and $\phi=0^\circ$ and (b) efficiency	31
2.5	2×2 arms spiral antenna: (a) design and (b) current distribution at 1.1 GHz	33
2.6	2×2 arms spiral antenna: simulated return loss calculated for a reference impedance $Z_c = 200 \Omega$	34
2.7	2×2 arms spiral antenna: (a) 3D view of the far field pattern and (b) cuts in elevation at 900 MHz, 1.1 GHz and 1.5 GHz	35
2.8	2×2 arms spiral antenna: axial ratio against frequency at $\theta=0^\circ$ and $\phi=0^\circ$	36
2.9	2×2 arms spiral antenna: prototype	38
2.10	(a) scheme and (b) picture of the anechoic chamber at Supelec (<i>Sesame</i>)	38
2.11	2×2 arms spiral antenna: decomposition of the measurement, the total far field pattern (c) is equal to the sum of the two patterns (a) and (b)	39
2.12	2×2 arms spiral antenna: comparison of the measured and simulated patterns in elevation at 700 MHz, 900 MHz and 1 GHz with a 3D view of the measured pattern at 900 MHz	42
3.1	Antenna array geometry: (a) 3D view and (b) top view	45
3.2	Dipole antenna array: (a) top view and (b) 3D view	48
3.3	Dipole antenna array: (a) simulated axial ratio with and without phase and amplitude errors at $\theta=0^\circ$ and $\phi=0^\circ$ and (b) reflexion coefficient of the elements	49
3.4	Dipole antenna array: (a) axial ratio and (b) total gain at 50 MHz	50
3.5	Dipole antenna array: geometries of the arrays for N=3, 4 and 5	50
3.6	Dipole antenna array: (a) simulated axial ratio and (b) total gain at 45.625 MHz	51
3.7	Dipole antenna array: (a) simulated axial ratio and (b) total gain at 27.75 MHz	52

3.8	LPDA antenna array: (a) top view and (b) 3D view of the 4×LPDA antennas modeled with CST Microwave studio	53
3.9	LPDA antenna array: (a) top view and (b) 3D view of the measured 4×LPDA antennas	54
3.10	LPDA antenna array: measured S_{11} of an element.	55
3.11	LPDA antenna array: measured and simulated cuts in elevation of the normalized total gain (left) and AR (right) of an element at 1GHz (a), 1.1GHz (b), 1.2GHz (c) and 1.4GHz (d).	57
3.12	LPDA antenna array: measured and simulated cuts in elevation of the normalized total gain (left) and AR (right) of the array at 1GHz (a), 1.1GHz (b), 1.2GHz (c) and 1.4GHz (d).	58
3.13	LPDA antenna array: (a) top view and (b) 3D view of the 3×LPDA and (c) top view and (d) 3D view of the modified 3×LPDA.	59
3.14	LPDA antenna array: (a) axial ratio of the 3×LPDA and (b) modified 3×LPDA.	59
4.1	3×2 arms spiral antenna: (a) modeled and (b) built	62
4.2	3 × 2 arms spiral antenna: simulated current distribution at 750 MHz and sources phase shift	63
4.3	3 × 2 arms spiral antenna: simulated return loss for a reference impedance $Z_c = 200 \Omega$	64
4.4	3×2 arms spiral antenna: (a) simulated 3D view of the far field pattern at 1 GHz and (b) cuts in elevation of the total gain in dBi at 900 MHz, 1 GHz and 1.1 GHz	65
4.5	3×2 arms spiral antenna: axial ratio against frequency for $\theta = 0^\circ, 10^\circ$ and 20°	65
4.6	3×2 arms spiral antenna: (a) simulated cuts in elevation of the normalized gain and (b) the AR at 1 GHz	66
4.7	3×2 arms spiral antenna: comparison of the measured and simulated cuts in elevation of the normalized gain (left), AR (center) and a 3D view of the measured gain (right) at 1000 MHz (top) and 1040 MHz (bottom)	68
4.8	4×2 arms spiral antenna: (a) modeled and (b) built	69
4.9	4×2 arms spiral antenna: comparison of the measured and simulated return loss against frequency for a reference impedance $Z_c=50 \Omega$	71
4.10	4×2 arms spiral antenna: (a) 3D view of the simulated far field pattern at 1 GHz and (b) elevation cuts of the total gain in dBi at 0.8 GHz, 1 GHz, 1.2 GHz and 1.4 GHz	72

4.11	4×2 arms spiral antenna: simulated axial ratio against frequency for $\theta= 0^\circ$ to 50°	72
4.12	4×2 arms spiral antenna: (a) simulated cuts in elevation of the normalized gain and (b) AR at 1 GHz	73
4.13	4×2 arms spiral antenna: comparison of the measured and simulated cuts in elevation of the normalized gain (left), AR (center) and a 3D view of the measured gain (right) at 0.8 GHz (top), 1.1 GHz (middle) and 1.5 GHz (bottom)	75
B.1	Typon of the 2×2 arms spiral antenna	94
B.2	Typon of the 3×2 arms spiral antenna	95
B.3	Typon of the 4×2 arms spiral antenna	96

Glossary

AR: Axial Ratio

RHCP: Right Hand Circular Polarization

LHCP: Left Hand Circular Polarization

RL: Return Loss

HAA: High Altitude Airship

VSWR: Voltage Standing Wave Ratio

LPDA: Log-Periodic Dipole Antenna

CASRT: Circular Array with Sequential Rotation Technique

Introduction

Ordinarily used as an advertising platform in the sky, the airship is now considered as an antenna platform for radar applications. Particularly, new dirigibles called HAA for high altitude airship are under development in several countries. This kind of airship should be able to fly at 20 km above the ground and could be a cheap alternative to satellites for communications, detection or earth observation. During the previous Ph.D thesis, F. Chauvet [1] has studied the feasibility of a spiral antenna array on an airship. In this work, the conformal aspect of the array has been investigated and the feasibility of a spiral antenna array able to scan over a wide angular range has been demonstrated. The conclusion of this previous thesis has highlighted the interest of the spiral antenna for such applications on airship. However, the feeding of this antenna is located in its center which is not accessible when the spiral is mounted on the hull of the airship. This PhD thesis focuses on the feeding of the spiral antenna with the aim to design antennas that can be easily integrated on the airship. This work has been undertaken within the framework of SONDRA, a joint research laboratory between Singapore and France, gathering four partners, Supelec and ONERA from France and the National University of Singapore and the Defence Science and Technology Agency from Singapore.

Chapter 1 describes the context of this study. A general overview of the airships, especially the HAA is given. The behavior of the classical Archimedean spiral antenna is studied and the feeding issue of this solution is stressed. Several solutions of externally-fed spiral antenna found in the literature are investigated. For each case, their advantages and their drawbacks are highlighted. Despite the interesting characteristics of the designs, they are not suitable for our applications. Compared to the center-fed spiral antenna, the geometry and the current distribution on these antennas are not symmetric about the boresight axis and the frequency band is shifted about a factor 2 toward the higher frequencies.

Chapter 2 deals with two first solutions of spiral antennas with an external feeding. These antennas have been built following the principle of symmetry in the geometry and in the current distribution while being fed in the plane of the antenna. This is achieved by using two sources to feed the spiral. Due to the principle of symmetry, the behaviors of these designs are similar or even better regarding certain characteristics, compared to the Archimedean spiral. The first design increases the polarization characteristic. However, resistive loads are used which decrease the efficiency due to the dissipation of the power in the loads. The second design increases the functional frequency band, although the polarization does not behave as that of the center-fed spiral. Measurements of this antenna have been done in an anechoic chamber and are given in this chapter. These designs can be used when an external feeding is required without a strong need for high efficiency or pure circular polarization. This is not the case in this study and further investigations have been performed to increase the performances of the antennas.

Chapter 3 is about the circular antenna array with a sequential feeding. Since the antennas are fed with more than one source, they can be seen as a small array. In order to improve the performances of the antennas, studies of the circular antenna array are required. The theory of the circular array is explained and particularly the radiated polarization of this kind of array. According to the theory, a circular polarization is achieved whatever the polarization of the elements in the array. This has been verified with a simulated dipole antenna array. The theory has also been verified with an array of 4 Log-periodic Dipole Antenna (LPDA) with simulations and measurements done in anechoic chamber. Good results have been obtained in terms of radiated pattern and polarization.

Chapter 4 exhibits two last solutions of spiral antennas with an external feeding designed from the theory of the circular array with sequential feeding to generate a circular polarization. A microstrip antenna fed by 3 sources and a slot antenna fed by 4 sources have been developed. For each case, measurements have been done and compared to the simulations results. Good results have been obtained in terms of radiated pattern and polarization as expected. These designs overcome the feeding issue of the center-fed spiral and can be integrated on the airship or on various platforms that do not allow to feed the spiral in its center.

Chapter 1

General Review

1.1 Airship

The airship [5] [6] also called dirigible is an aircraft that belongs to the family of the lighter-than-air craft. It is filled by a lifting gas, usually helium or hot air, that is lighter than the surrounding air. Hence, due to the principle of Archimedes, a lifting force makes the airship flying. To generate a lifting force strong enough to lift an airship, a wide quantity of light gas is required that explains the usual volume of the dirigible. Unlike the balloons that simply follow the direction of the winds, the dirigible is able to control its direction. This is achieved by rudders placed on the hull. The kind of airship considered here is a High Altitude Airship (HAA). These dirigibles could operate at more than 20 kilometers of altitude. At this altitude, the airship is above the jet stream and the effect of the wind is minimized. It is then easier to maintain a geostationary position without spending a lot of energy to compensate for the effect of the wind. Moreover, photovoltaic cells could be carried on the hull to supply the airship and to increase its autonomy.

1.1.1 Antenna platform

In this study, HAA is considered to be used as an antenna platform for radar applications. An example of HAA is presented in Figure 1.1. This kind of airship has the advantage to provide a low operating cost and to be able to operate continuously. Furthermore, from the point of view of the antennas, the large surface on the hull of the airship to mount the array is an important advantage. However, the weight is a strong constraint on the antenna array. Therefore, the requirements on the antennas is the low profile and light weight for

aerodynamic reasons. All these aspects have been taken into account in order to choose the antenna element.



Figure 1.1: *High Altitude Airship*

1.1.2 Applications

The aim here is to achieve an antenna array carried by an airship for radar applications. These applications require specific characteristics on the antennas. The array should be able to scan in a wide angular range to be suitable for airborne reconnaissance or surveillance operations. The antenna array is also considered to be used for radar polarimetry. Therefore, a dual polarization is required. Among the radar applications, the detection under the canopy also called FOPEN for FOliage PENetration requires a wide frequency band in VHF/UHF band (400 MHz to 600 MHz).

1.2 Antenna Element

A previous PhD thesis led by F. Chauvet [1] has studied the feasibility of such an antenna array on airship. His investigations focused on the conformal aspect of the platform. The chosen antenna for this array is the Archimedean spiral antenna [7] [8]. This antenna has

been chosen for its ultra wideband feature, its dual polarization and its light weight. Hence, the spiral antenna is a good candidate that meets the requirements of the platform and the applications. The antenna characteristics are detailed in the next part.

1.2.1 Spiral antenna

The design of the Archimedean spiral antenna is given in Figure 1.2(a). The antenna has been modeled with the software *Feko* [9] based on the Method of Moments. Due to its geometry, this antenna belongs to the frequency independent antennas [10] [11].

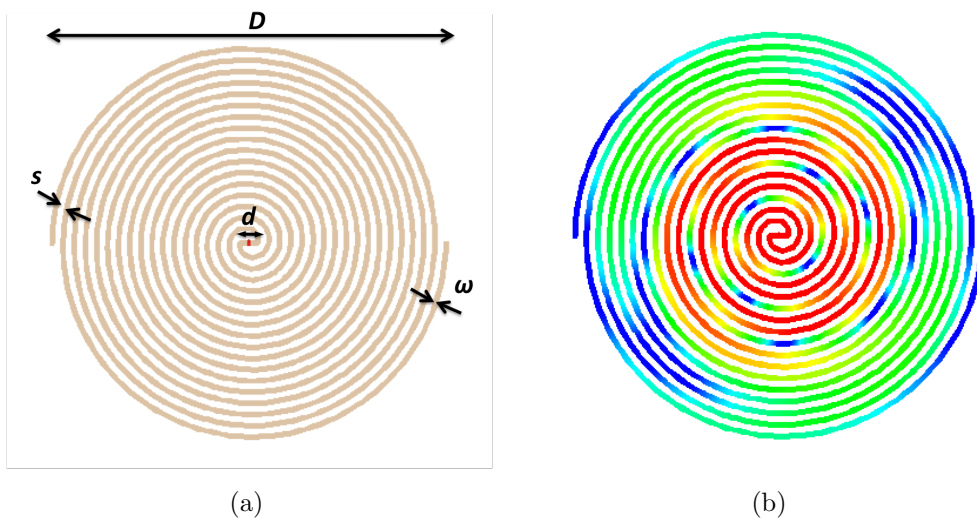


Figure 1.2: Archimedean spiral antenna: (a) geometry and (b) current distribution at 1.1 GHz

Two arms are wound around the center in a spiral shape. The geometry of an arm is described by equation 1.1 where r is the radius at the angle θ expressed in radian, a is the growth factor of the spiral and $d/2$ is the inner radius. The second arm is obtained by a rotation of 180° about the center of the first one. Therefore, the geometry is symmetric with respect to the center.

$$r = a\theta + d/2 \quad (1.1)$$

The parameters have been chosen to build an antenna with a diameter of 12.5 cm. Each arm makes 8.5 turns with a width of 2.4 mm. The growth factor is chosen to be 0.153 and the inner radius is equal to 4.9 mm. All the geometrical characteristics are summarized in Table 1.1.

Table 1.1: Geometrical characteristics

<i>Description</i>	<i>Symbol</i>	<i>Value</i>
<i>Outer diameter</i>	<i>D</i>	125 mm
<i>Inner diameter</i>	<i>d</i>	9.8 mm
<i>Arm width</i>	<i>w</i>	2.4 mm
<i>Space between arms</i>	<i>s</i>	2.4 mm
<i>Number of turns</i>	<i>N</i>	8.5

The feeding represented by a red square in the center of the antenna on Figure 1.2(a), supplies a balanced signal. Hence, a phase shift of 180° is achieved between the two arms. This leads to a symmetrical current distribution as shown in Figure 1.2(b). Indeed, the absolute value of the current at a given position is the same at the position symmetric about the center. Hence, the geometry and the current distribution exhibit a symmetry about the boresight axis of the antenna. Moreover, the geometry of the antenna is self-complementary i.e. the width of the arm is equal to the spacing between two arms. According to Babinet's principle [12], the input impedance of the antenna Z_{in} is expressed by equation 1.2 where $Z_{microstrip}$ and Z_{slot} correspond to the input impedances of the microstrip and slot parts and where η is the intrinsic impedance of the vacuum. The antenna is considered in free space therefore η is equal to 120π .

$$Z_{in} = \sqrt{Z_{microstrip} \times Z_{slot}} = \sqrt{\frac{\eta^2}{4}} = 188.5 \Omega \quad (1.2)$$

The spiral antenna is a frequency independent antenna. However, since the geometry is not infinite, the bandwidth is limited by two frequencies. These limits are linked to the geometry in equation 1.3 where c_0 is the celerity of light in free space. The lower frequency is set by the antenna diameter while the higher frequency is defined by the inner diameter. Hence, the frequency band is inversely proportional to the external diameter. Considering a $\frac{\lambda}{2}$ equally spaced antenna array, the frequency band is limited by grating lobes that appear at 600 MHz. It is interesting to note that this limit could be shifted toward higher frequency by using techniques such as interleaved array [13]. For measurements purpose, the antenna has been scaled to operate from 800 MHz to 1.2 GHz. Thus, the required frequency band is multiply by 2 and the diameter is divided by 2. In this case, the lower frequency limit of the spiral is around 800 MHz and the theoretical higher frequency is around 10 GHz.

$$f_{low} \approx \frac{c_0}{\pi D} \leq bandwidth \leq f_{high} \approx \frac{c_0}{\pi d} \quad (1.3)$$

The input impedance of the spiral antenna is plotted in Figure 1.3(a). As expected by the theory, the input impedance is close to 200Ω over a wide frequency range. The reflection coefficient expressed in equation 1.4 is then calculated with a reference impedance $Z_0 = 200 \Omega$ and plotted in dB in Figure 1.3(b). The incident wave is considered radiated for a reflection coefficient under -10 dB. Here again, according to the theory, $|S_{11}|$ is under -10 dB from around 800 MHz over the frequency range. Another representation of the radiation of the incident wave is the VSWR (Voltage Standing Wave Ratio). The expression is given in equation 1.5. For a $VSWR \leq 2$, the incident wave is considered radiated.

$$S_{11} = \frac{Z_{in} - Z_0}{Z_{in} + Z_0} \quad (1.4)$$

$$VSWR = \frac{1 + |S_{11}|}{1 - |S_{11}|} \quad (1.5)$$

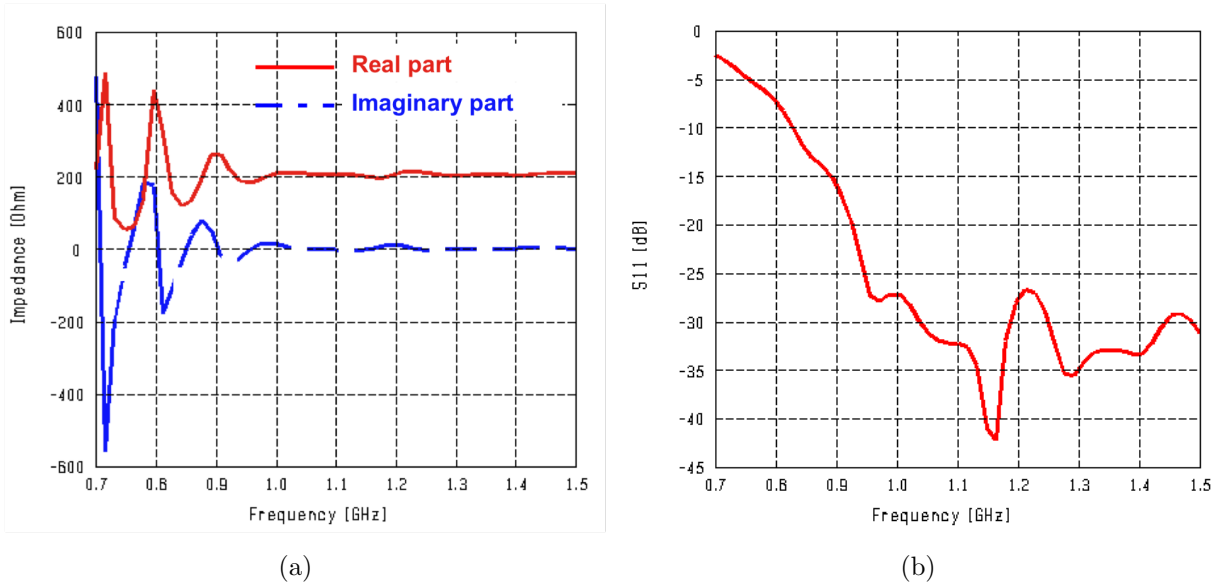


Figure 1.3: Archimedean spiral antenna: (a) input impedance calculated for a reference impedance $Z_c = 200 \Omega$ and (b) reflection coefficient

The radiation pattern is detailed in Figure 1.4 by a 3D view at 1.1 GHz and cuts in elevation at three different frequencies. According to the 3D view, the antenna radiates two main beams in two directions perpendicular to the plane of the spiral. This is expected since the geometry and the current are symmetric. Moreover, the shape of the far field pattern remains the same over the frequency range as shown by the cuts at 860 MHz, 1 GHz and 1.1 GHz.

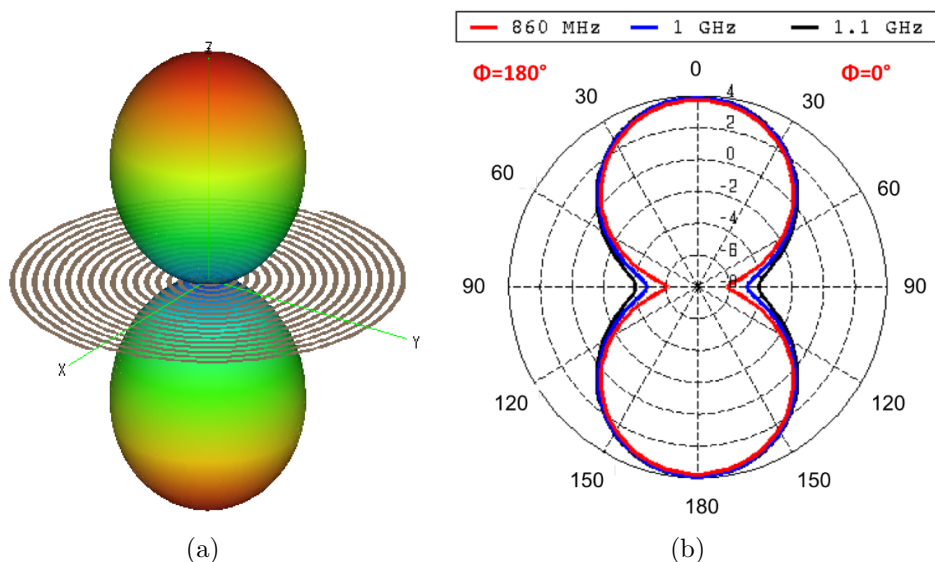


Figure 1.4: Archimedean spiral antenna: (a) 3D view of the far field pattern and (b) cuts in elevation at three frequencies

In order to study the polarization of the antenna, a cut in elevation of the axial ratio (AR) is plotted in Figure 1.5 at 1.5 GHz and over the frequency range for $\theta = 0^\circ$ and $\phi = 0^\circ$. The convention of the AR follows that given by the software feko [9] and corresponds to the ratio of the major and minor axis defined by the radiated electric field (which is the inverse of the standard definition). Hence, the AR is a representation of the polarization that varies from 0 for a linear polarization to ± 1 for a perfect circular polarization. The values comprised between 0 and 1 or -1 to 0 represent an elliptic polarization. However, the polarization is considered circular for an $|\text{AR}| \geq 0.7$. This value corresponds to a rejection of the cross-polarization of -15 dB. In order to distinguish the right hand circular polarization (RHCP) from the left hand circular polarization (LHCP), the positive values of the AR are affected to the RHCP and the negative values to the LHCP. From Figure 1.5(a), we can see that the polarization is RHC at the position $\theta = 0^\circ$ with an $\text{AR} \geq 0.7$. The value of the AR decreases when the angle θ moves away from the boresight until it reached 0 at $\theta = 90^\circ$. Therefore, a

linear polarization is radiated in the plane of the antenna. From this position, the AR becomes negative and the minimum is reached at $\theta = 180^\circ$ with an $AR \leq -0.7$, which represents the radiation of a LHCP. As a result, the spiral antenna radiates most of its power with two opposite circular polarizations in two opposite directions. According to Figure 1.5(b), the polarization becomes circular from 1 GHz to 1.5 GHz. Radiated polarization between 800 MHz and 1 GHz is elliptic. Although, a circular polarization is required. Hence, the spiral antenna is considered as suitable for the applications starting at 1 GHz.

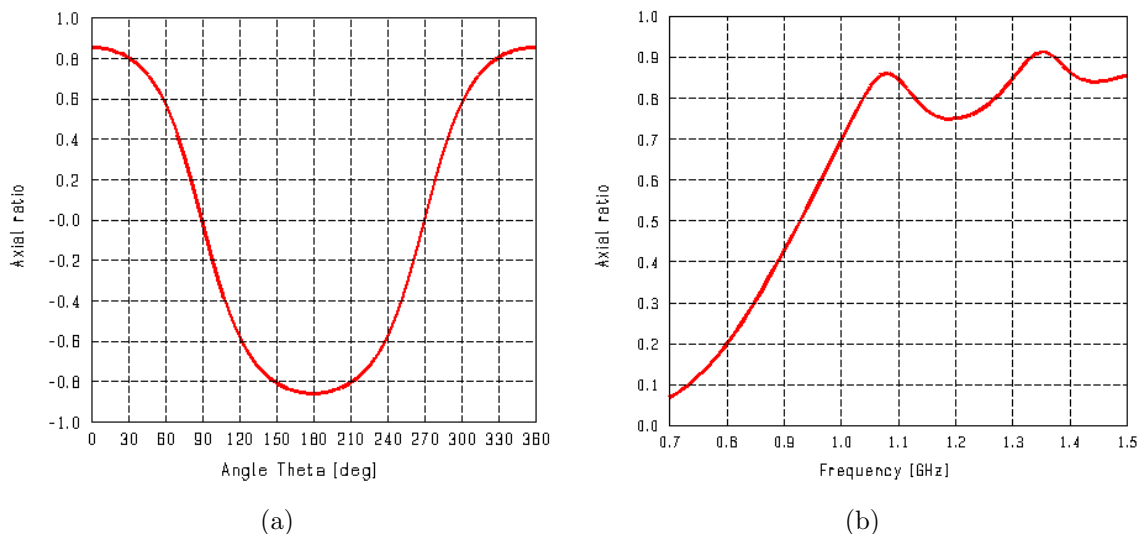


Figure 1.5: Archimedean spiral antenna: (a) cut in elevation of the axial ratio at 1.5 GHz and (b) over the frequency range for $\theta = 0^\circ$ and $\phi = 0^\circ$

Another way to understand the behavior of the spiral antenna is to look at the evolution of the current distribution with the frequency. Especially, four cases detailed in Figure 1.6 are interesting. The first one is the current distribution at 1.5 GHz. At this frequency, the current is concentrated in the center. As a result, the polarization is circular and $|S_{11}|$ is under -10 dB. For the second case at 1 GHz, the current occupies all the surface of the antenna but the wave is not reflected at the end of the arms. In this case, $|S_{11}|$ and the AR are still good. However, at 900 MHz, the waves are reflected at the end of the arms but do not reach the center of the antenna. A cross-polarization is then radiated, the AR decreases and the S_{11} is still good. This corresponds to the frequency band where the antenna radiates an elliptic polarization. For the last case at 700 MHz, the current waves are reflected at the end of the arms and have reached the center. Most part of the current is not radiated and the performances of the AR and $|S_{11}|$ decreases.

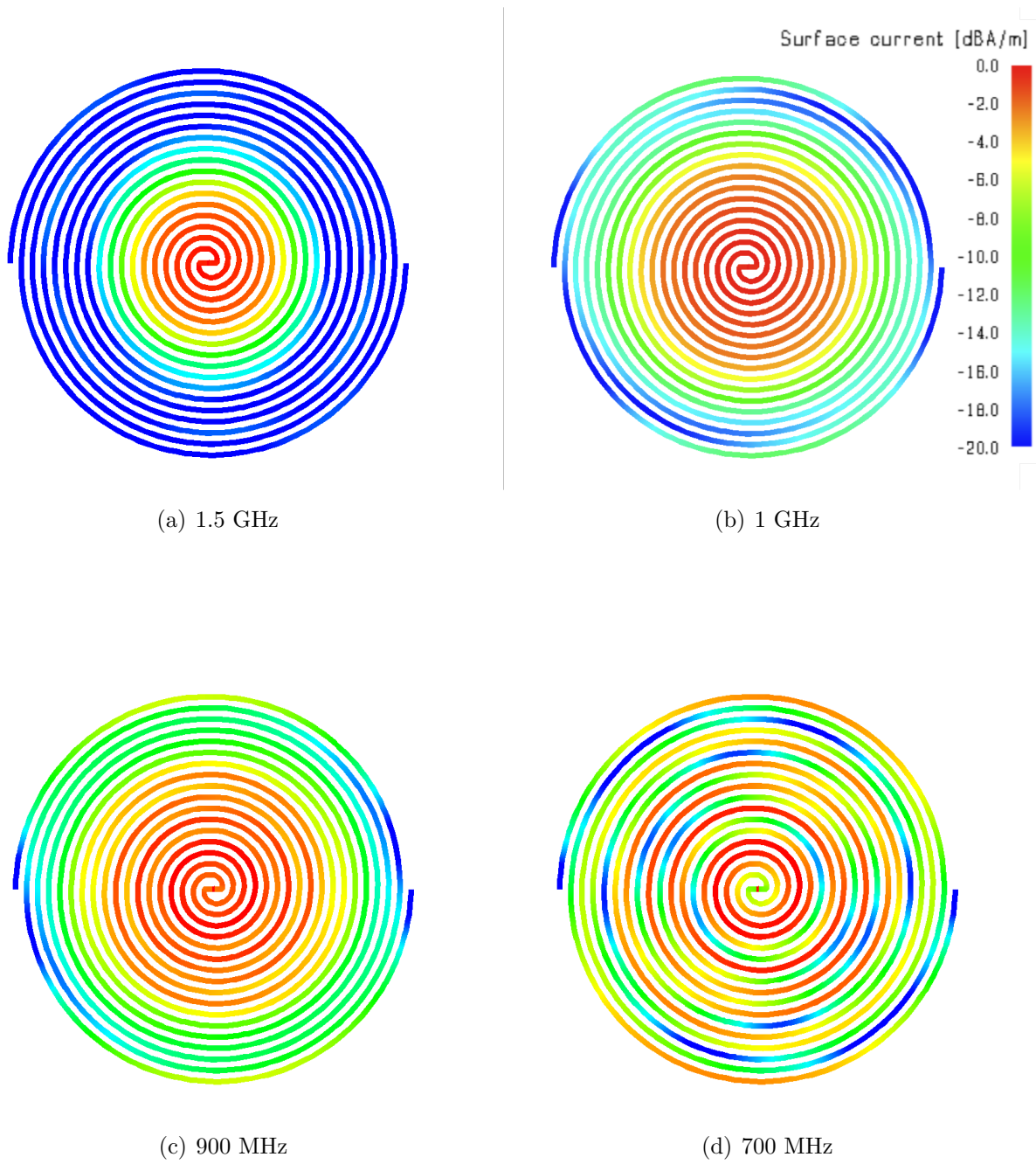


Figure 1.6: Archimedean spiral antenna: current distribution at (d) 700 MHz, (c) 900 MHz, (b) 1 GHz and (a) 1.5 GHz

1.2.2 Feeding issue

A coaxial cable supplies an unbalanced feeding with a reference impedance of 50Ω . However, the antenna needs a balanced feeding with a reference impedance of 200Ω . This can be achieved by a balun that achieves a matching impedance and a balanced feeding. The configuration of the feeding is summarized in Figure 1.7. The design is then fed in the center by a coaxial cable on the plane perpendicular to the antenna. This configuration is not suitable regarding the airship. Indeed, the array is supposed to be integrated on the hull of the dirigible and it is not conceivable to pierce the airship to feed the antennas. This feeding issue does not concern only the airship but all platforms that do not allow to feed the spiral in the center. A solution has to be found to feed the spiral antenna on its plane. This Ph.D work focuses on the feeding of the spiral antenna. The aim is to obtain an antenna externally-fed with a behavior similar or better to that of the center-fed spiral.

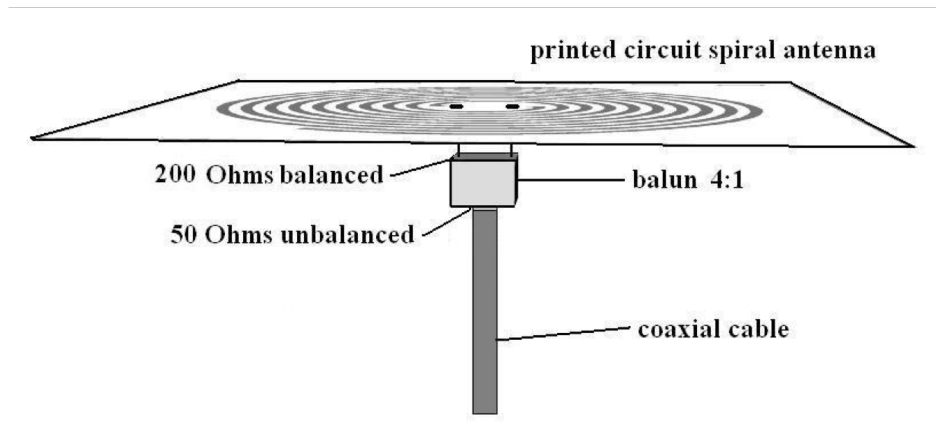


Figure 1.7: *Archimedean spiral antenna: feeding configuration*

1.3 State of the Art

Studies have been done on the antenna designs to shift the feeding from the center to the outermost arms. In this case, the feeding can be coplanar i.e. the feeding can be in the same plane as the antenna. Several proposed solutions have been found in the literature. Advantages and drawbacks of these designs regarding our applications are discussed in this part.

Externally-fed antenna

An interesting design has been proposed by D. J. Muller and K. Sarabandi in [2]. The antenna described in Figure 1.8 is composed by three arms that are wound together around the center. At the end of the spiral, all the arms are linked to the feeding by straight lines. As a result, the antenna is fed on its plane and it is no more required to reach the center of the spiral. The design is fed by an unbalanced feeding such as a coaxial cable. This is a very interesting feature that avoids the use of an external circuitry like baluns to balance the feeding. Moreover, the straight lines could be used as a matching transition to match the input impedance of the antenna to 50Ω . Resistive loads are placed in the center at the end of the arms to absorb the incident wave and to minimize the reflections that degrade the bandwidth and polarization characteristics.

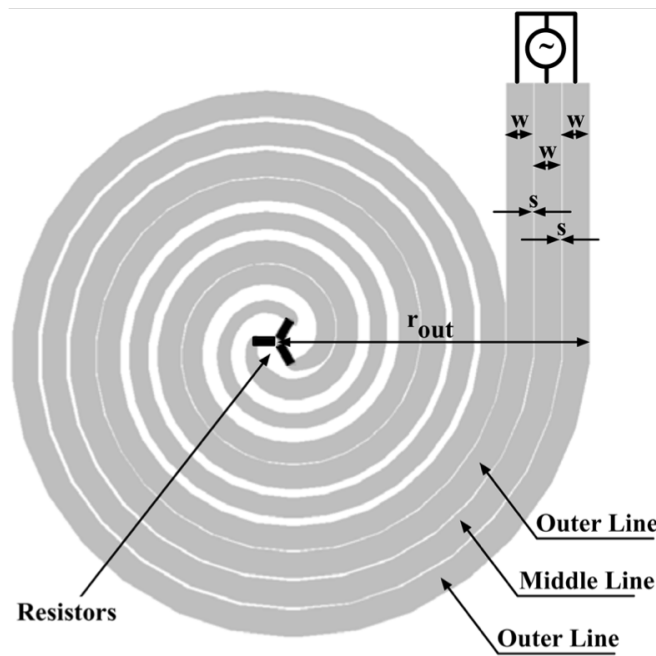


Figure 1.8: *Three arms spiral antenna externally-fed*

However, according to the author, the lower frequency of this design is around twice that of a center fed spiral. Hence, for the same diameter, the 3 arms spiral antenna starts to radiate much higher in frequency. This is not suitable in our case, especially for an antenna array objective. Moreover, the feeding and the geometry are not symmetric. As a result,

the current distribution is not symmetric on the antenna. Therefore, the radiated far field pattern is also not symmetric and the maximum of radiation is shifted from the boresight.

Another design of a spiral antenna with an external feeding is presented by E. Gschwendtner and W. Wiesbeck in [3]. The antenna geometry given in Figure 1.9 corresponds to a classical spiral for which an arm is extended half a turn. Like the previous antenna design, the two arms are linked to the feeding by straight lines. A balanced signal is delivered to the antenna which means that the arms are fed out-of-phase and a balun is needed. In this case, the feeding is symmetric, but not the geometry. This does not always achieve a symmetrical current distribution on the surface of the antenna. Therefore, the radiated characteristics varies over the frequency and the maximum of radiation moves away from the boresight at high frequency. Moreover, the lower frequency is here again multiplied by a factor about 2 compared to a conventional center fed spiral.

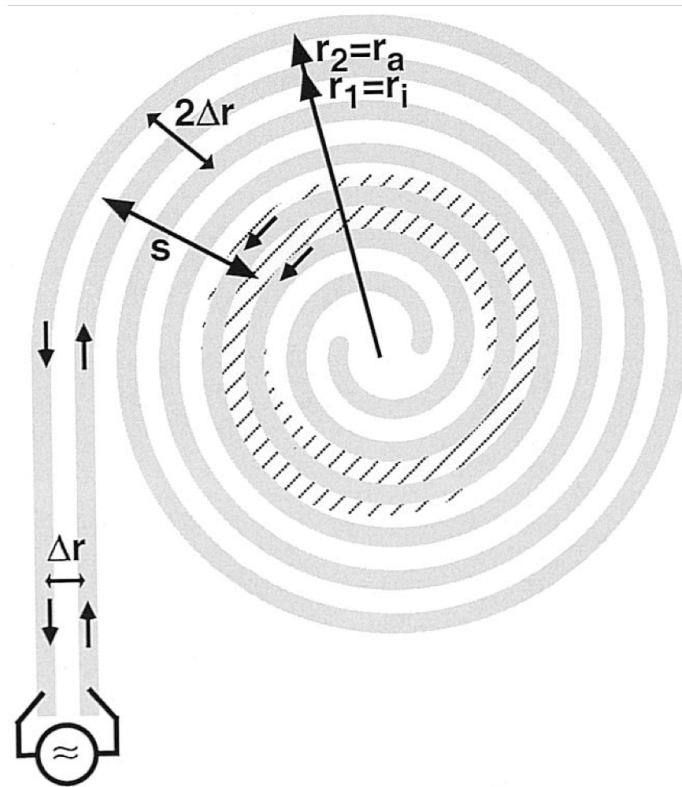


Figure 1.9: *Two arms spiral antenna externally-fed*

The antenna designed by C. W. Jung and investigated in [4] exhibits interesting characteristics in terms of polarization. The configuration is shown in Figure 1.10. A single arm is fed either in the center or on the outermost arm. Hence, the incident wave could be propagated from the center to outside or reversely. In this way, the radiated polarization is reconfigurable on either RHCP or LHCP. The aim of the design is also to generate a tilted beam by changing the length of the arm for the same frequency range. This is understandable regarding the current distribution. Indeed, the lack in the symmetry of current leads to a modification of the radiation pattern. Despite these interesting characteristics, this antenna is not suitable due to its non symmetric radiation pattern.

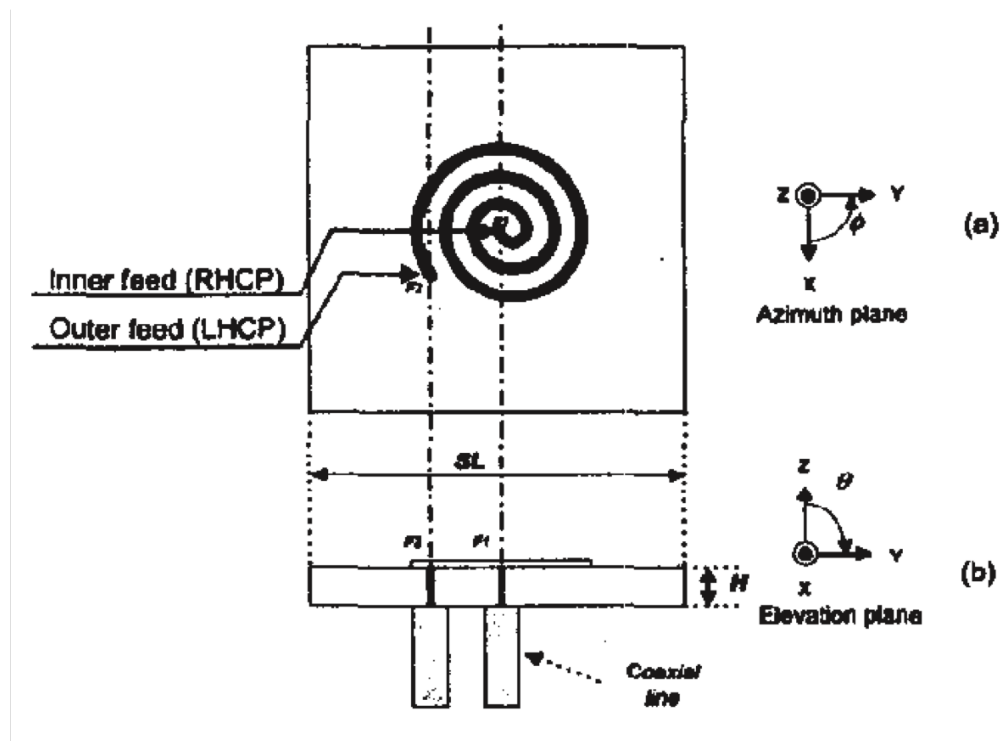
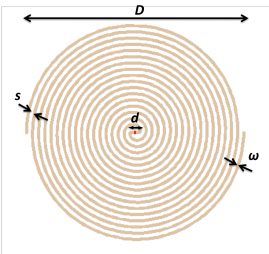
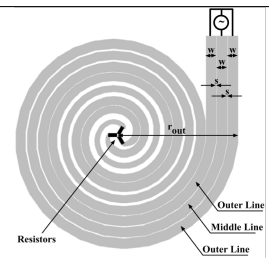
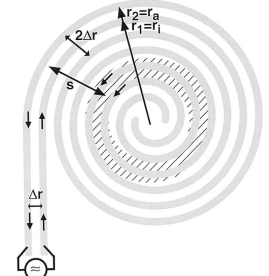
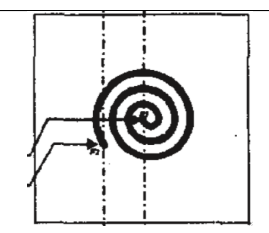


Figure 1.10: Single arm spiral antenna with inner and outer feeding

1.4 Conclusion of Chapter 1

Airship as a host of a spiral antenna array for radar applications exhibits several advantages. Therefore, there is a big interest to solve the feeding issue of the spiral antenna in order to be able to mount it on the airship. When fed in its center, the spiral antenna radiates in two opposite directions with two opposite polarizations, over a wide frequency band. The design of D. J. Muller and K. Sarabandi [2] exhibits an external and coplanar feeding but the frequency band is shifted about a factor of 2 toward the higher frequencies compared to the center-fed case. Moreover, the radiated beam is not symmetric around the boresight axis of the antenna. The frequency band is also shifted by a factor of 2 in the design presented by E. Gschwendtner and W. Wiesbeck [3] and the far field pattern is not symmetric. These two designs do not meet the requirements of our applications. In each configuration, unlike the Archimedean spiral, the geometry does not exhibit a symmetry about the boresight axis of the antenna. Therefore, the current distribution is not symmetric on the antenna, which affects its behavior. The spiral antenna of C. W. Jung [4] offers the possibility to reconfigure the radiated polarization by feeding the spiral in its center or in the outermost arm. It is an interesting design, however it does not meet the requirements due to its non symmetric radiation pattern. Advantages and drawbacks of each antenna are summarized in Table 1.2.

Table 1.2: Summary of the antennas characteristics

Design	Nb of feed	F_{min} for $RL_{\leq -10}$ dB	Radiation pattern	Polarization
	1	$f_{min} = 800$ MHz	Symmetric	$f_{AR \geq 0.7} = 1$ GHz
	1	$f_{min} \simeq 1.6$ GHz	Non symmetric	$f_{AR \geq 0.7} = N/A$
	1	$f_{min} \simeq 1.6$ GHz	Non symmetric	$f_{AR \geq 0.7} = N/A$
	2	$f_{min} = N/A$	Non symmetric	$f_{AR \geq 0.7} = N/A$

Chapter 2

First Solutions of Externally-fed Spiral Antennas

Spiral antennas with an external feeding investigated in the literature present interesting characteristics but they do not meet the requirements of our applications. In contrast with the well known Archimedean spiral antenna, all the designs mentioned previously do not achieve a symmetrical geometry with a symmetrical current distribution. Worst, most of them have a lower frequency limit much higher than the reference Archimedean spiral. In this section, two new designs of externally-fed spiral antennas are investigated. In both cases, the principle of symmetry in the geometry and in the feeding has been used to design the antennas.

2.1 Resistively Loaded Spiral Antenna

The principle of this antenna is to use the geometry of the traditional Archimedean spiral considering an external feeding. A symmetrical current distribution is achieved on the antenna thanks to the use of two sources. Moreover, resistive loads are used to damp the current [14] in the center and on the outermost arms in order to avoid strong reflections and to improve the antenna characteristics. The antenna behavior is studied with the software Feko. This antenna shows the same characteristics as a traditional spiral antenna while being fed outside with a coplanar feeding solution.

2.1.1 Antenna design

The antenna geometry is shown in Figure 2.1(a). Its shape is identical to that of the classical Archimedean spiral. The first arm is parametrized by equation $r=a \phi$ and the second one by $r=a(\phi+ 180^\circ)$. The arm width is $w=3.8$ mm and the growth factor is $a=0.24$. Each arm makes 7.5 turns, resulting in an antenna with a diameter D of 12.5 cm. Geometrical characteristics are summarized in Table 2.1. Two sources placed symmetrically on the outermost arms of the antenna are used to feed the spiral. Each source provides a balanced signal to the two connected arms. As a result, the currents on the antenna are symmetric with respect to its center as shown by the current distribution at 1.1 GHz in Figure 2.1(b). Resistive loads are added to the structure on the outermost turns and in the center. Sixty seven loads are located along a half turn of the outermost arms, and twenty one loads along 1.5 turns in the center. Outermost loads start from the sources with a value of 0Ω and increase linearly to 150Ω . Inner loads start from the center at 50Ω and decrease until 0Ω . As shown by the current distribution, the outer loads make the current decrease on the uttermost turns. Thus, the current flows only on the inner arms. The inner loads reduce the current on the center which improves the lower frequency of the return loss. The axial ratio is also improved by eliminating the return waves that would radiate an orthogonal crossed polarization. This design can be further improved by optimizing the values and the positions of the resistive loads. For instance, it could be possible to use a function (log, sinusoidal or exponential) to set the values of the loads in order to increase the efficiency of the antenna.

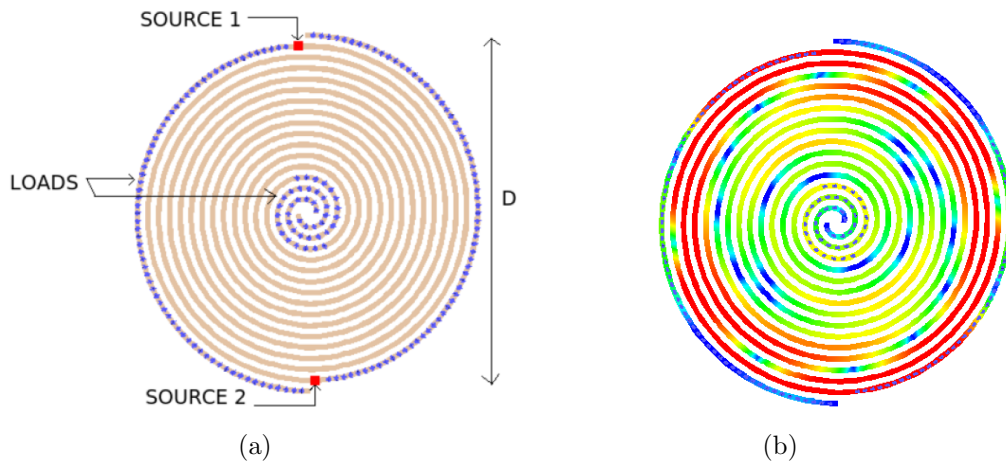


Figure 2.1: Resistively loaded spiral antenna: (a) geometry and (b) current distribution at 1.1 GHz

Table 2.1: Geometrical characteristics

<i>Description</i>	<i>Symbol</i>	<i>Value</i>
<i>Diameter</i>	<i>D</i>	125 mm
<i>Arm width</i>	<i>w</i>	3.8 mm
<i>Space between arms</i>	<i>s</i>	3.8 mm
<i>Number of turns</i>	<i>N</i>	7.5

2.1.2 Antenna characteristics

The antenna can be considered as a quadripole since two sources are used. In this case, the antenna is characterized by its scattering parameters given in equation 2.1. Moreover, due to the symmetry of the geometry, equation 2.1 can be simplified since $S_{11} = S_{22}$. As the antenna is a passive and reciprocal element, $S_{12} = S_{21}$.

$$\begin{pmatrix} b_1 \\ b_2 \end{pmatrix} \begin{bmatrix} S_{11} & S_{12} \\ S_{21} & S_{22} \end{bmatrix} \begin{pmatrix} a_1 \\ a_2 \end{pmatrix} \quad (2.1)$$

Moreover, the phase shift of each source implies that $a_2 = a_1 \exp(j\pi)$. Due to the high coupling between the arms, the return loss (RL) is not equal to the S_{11} parameter. Hence, we need to consider the contribution of the other sources. After simplification, the RL_i at each $\#i$ port is expressed as follows:

$$\begin{cases} RL_1 = \frac{b_1}{a_1} = S_{11} + S_{12} \exp(j\pi) \\ RL_2 = \frac{b_2}{a_2} = S_{12} \exp(-j\pi) + S_{11} \end{cases} \quad (2.2)$$

From this equation, we can see that $RL_1 = RL_2$. Hence, the return loss is the same at the two ports. Figure 2.2 shows the return loss from 700 MHz to 1.5 GHz calculated with FEKO for a reference impedance of 250 Ω . From this figure, it can be seen that the lowest operating frequency is around 830 MHz ($|RL| < -9$ dB) which is in agreement with the theory, i.e. around 800 MHz. The quasi-doubling of the lower frequency limit observed in the previous designs does not occur in this configuration.

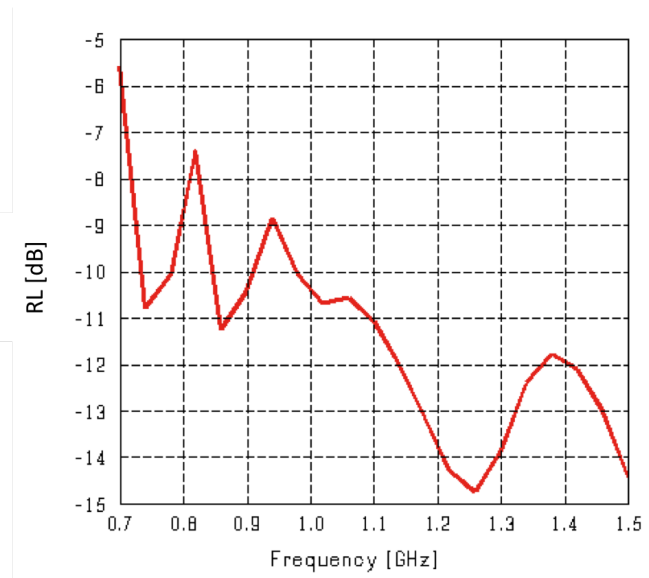


Figure 2.2: *Resistively loaded spiral antenna: return loss calculated for a reference impedance $Z_c = 250 \Omega$*

Figure 2.3 shows a 3D view of the radiated pattern at 1.1 GHz and three cuts of the gain in dBi of the antenna for $\theta = [0, 360^\circ[$ and $\phi = 0^\circ$. Due to the symmetry of the antenna geometry and sources, the shape of the far field pattern is similar to that of a traditional Archimedean spiral. Two main beams are radiated in two directions perpendicular to the plane of the antenna. Moreover, their shape remains similar over the frequency range according to Figure 2.3(b).

Axial ratio plotted for the same frequency range is given in Figure 2.4(a). From approximately 880 MHz, the antenna radiates a good circular polarization since the values are greater or equal to 0.7. Compared to the center-fed antenna, the frequency band that corresponds to an $|\text{AR}| \geq 0.7$ is improved about 120 MHz. This is due to the resistive load placed in the center that minimize the radiation of a cross-polarization. These loads decrease linearly and another tapering function or range of values could be tested to improve the AR. Though the antenna starts to radiate at 830 MHz, the antenna is considered suitable from 880 MHz due to the requirements of the applications.

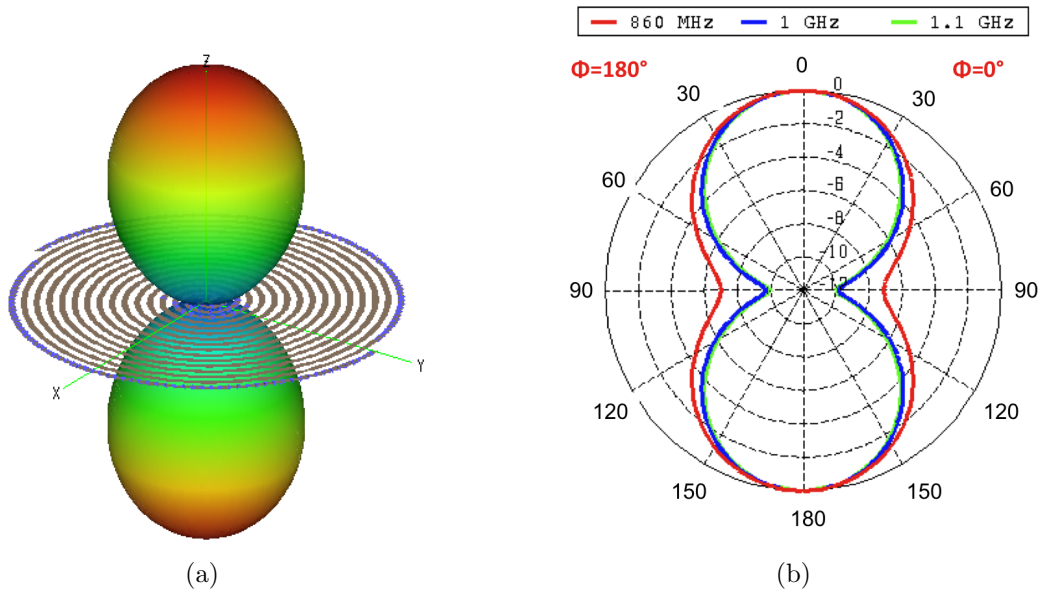


Figure 2.3: Resistively loaded spiral antenna: (a) 3D view of the far field pattern and (b) cuts in elevation at 860 MHz, 1 GHz and 1.1 GHz

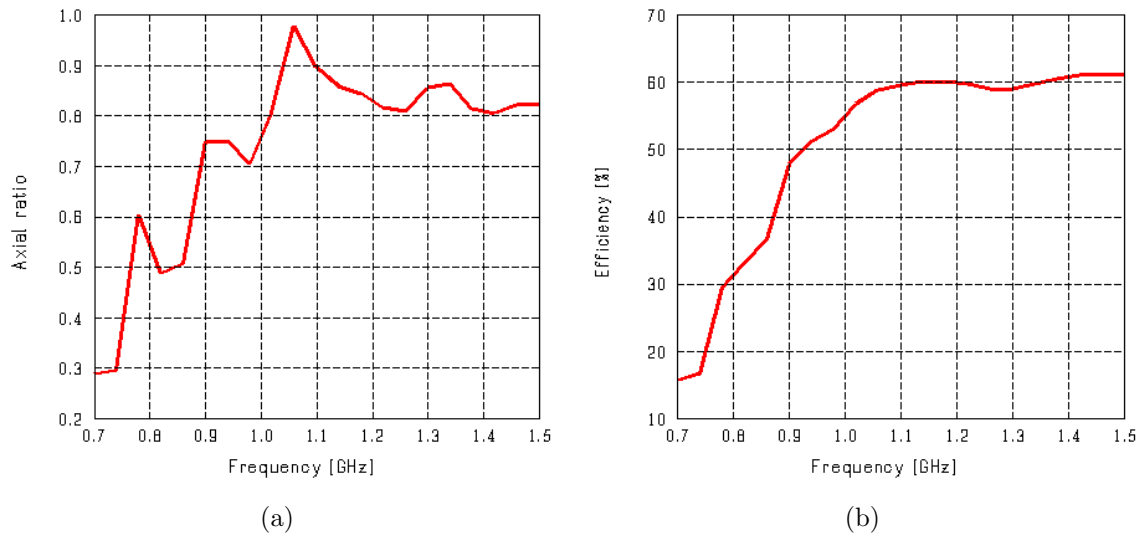


Figure 2.4: Resistively loaded spiral antenna: (a) axial ratio over the frequency range at $\theta=0^\circ$ and $\phi=0^\circ$ and (b) efficiency

Use of resistive loads implies that part of the power is not radiated but dissipated in the loads. A compromise has to be found between suppression of the reflections and losses of power due to the loads. In Figure 2.4(b), the efficiency reaches 60% around 1 GHz and remains constant over the frequency range. At lower frequencies, the current occupies the entire surface of the antenna, and is dissipated by all the loads, which explains the low efficiency. However, at higher frequencies, the current is located on the outermost arms and most part of the losses are due to the outermost loads.

This new design has the advantage to be externally fed by two sources located on the plane of the antenna. The center is then free from any feed and can be used to increase antenna performances. For instance, it could be interesting to design a transition in the center of the spiral to connect the arms in order to avoid strong reflections. This spiral antenna exhibits a lower frequency limit close to the theory and the shape of the far field pattern is similar to that of a classical center fed spiral. Moreover, the shape does not vary over the frequency range. Circular polarization is radiated within a frequency band increased of about 120 MHz compared to the center-fed spiral. Antenna characteristics described above show that this design is suitable for our applications and can be set on platforms that do not allow a central feeding. However, the use of resistive loads degrades the efficiency, since part of the power is not radiated but dissipated in the loads. Moreover, it is not easy to implement such resistive loads on the antenna.

2.2 2×2 Arms Spiral Antenna

In order to avoid losses due to the loads, a new design of externally-fed spiral antennas has been studied. This antenna consists of two double arms fed by two external sources out-of-phase. Instead of using resistive loads to suppress a part of the feeding, the principle is to wound the two arms connected to an outside feed point, around the center. This new design exhibits characteristics similar to that of the classical two arms center-fed spiral antenna.

2.2.1 Antenna design

The new design is presented in Figure 2.5(a). This spiral antenna is composed of four arms wound two by two around the center and ending by a short straight line to reach one of the feed points. Each arm makes a number of turns $N=3$ and has a width $w = 3.4$ mm. The spacing s between two arms is equal to $1/3$ of the width of an arm, hence $s = 1.13$ mm. This results in an antenna diameter D equal to 12.5 cm. All geometrical data are summarized in Table 2.2. This design is chosen to be geometrically symmetric about its center as for the classical spiral antenna.

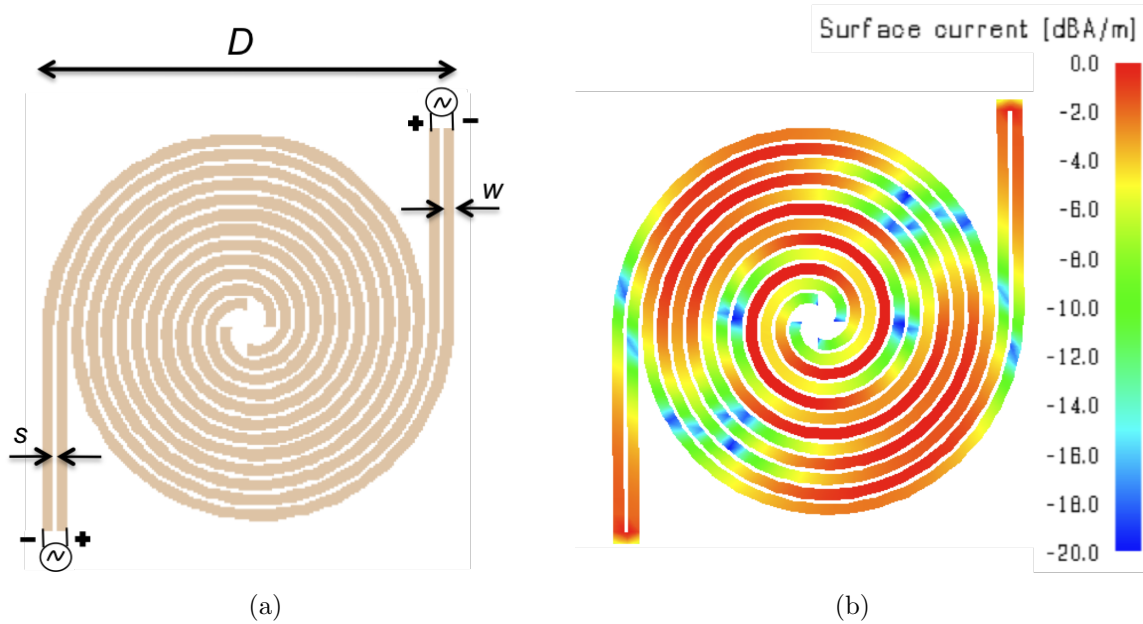


Figure 2.5: 2×2 arms spiral antenna: (a) design and (b) current distribution at 1.1 GHz

Table 2.2: Geometrical characteristics

<i>Description</i>	<i>Symbol</i>	<i>Value</i>
<i>Diameter</i>	<i>D</i>	125 mm
<i>Arm width</i>	<i>w</i>	3.4 mm
<i>Space between arms</i>	<i>s</i>	1.13 mm
<i>Number of turns</i>	<i>N</i>	3

Two sources are used to feed the spiral antenna. Each source is connected to two arms and provides a balanced signal (i.e. the two arms are fed out-of-phase). Moreover a phase shift of 180° is achieved between the two sources. As a result, the current distribution is symmetric on the entire surface of the antenna as shown by Figure 2.5(b).

2.2.2 Antenna performances

This antenna is modeled using the software Feko and considered without a ground plane. Return loss is plotted in Figure 2.6 from 500 MHz to 1.5 GHz. Reference impedance is chosen to be 200Ω .

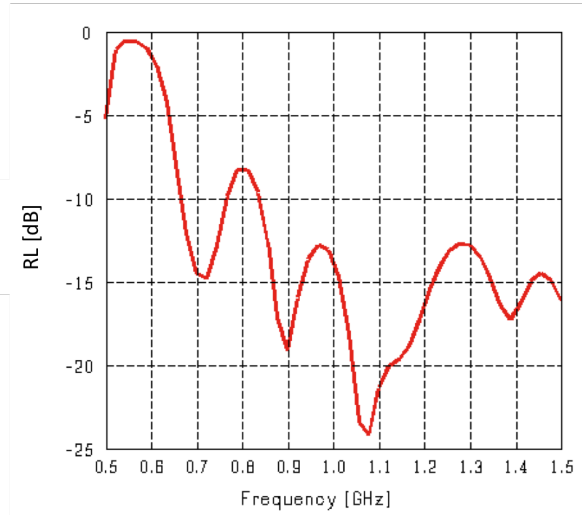


Figure 2.6: 2×2 arms spiral antenna: simulated return loss calculated for a reference impedance $Z_c = 200 \Omega$

As the previous antenna, the 2×2 arms spiral antenna can be seen as a passive and reciprocal quadripole since the sources are symmetric in position and in feeding. Consequently, the return loss expressed for the two ports in equation 2.3 are equal.

$$\begin{cases} \text{RL}_1 = S_{11} + S_{12} \exp(j\pi) \\ \text{RL}_2 = S_{12} \exp(-j\pi) + S_{11} \end{cases} \quad (2.3)$$

With an identical diameter, the 2×2 arms spiral antenna exhibits a return loss lower than -10 dB from 650 MHz (except from 770 MHz to 830 MHz where $|\text{RL}|$ is lower than -8 dB) while the Archimedean spiral antenna radiates above 800 MHz. Thus, we obtain an increase of around 150 MHz of the RL bandwidth. This extension is particularly interesting when the antenna is used in an array. For a $\lambda/2$ spaced array, this antenna improves the frequency band by around 37.5%. Figure 2.7 shows a 3D view of the far field pattern and cuts in elevation of the total gain in dBi of the 2×2 arms spiral antenna at 900 MHz, 900 MHz and 1 GHz. As for the classical center-fed antenna, the radiation pattern is symmetric about the plane of the antenna and its shape remains constant over the frequency range.

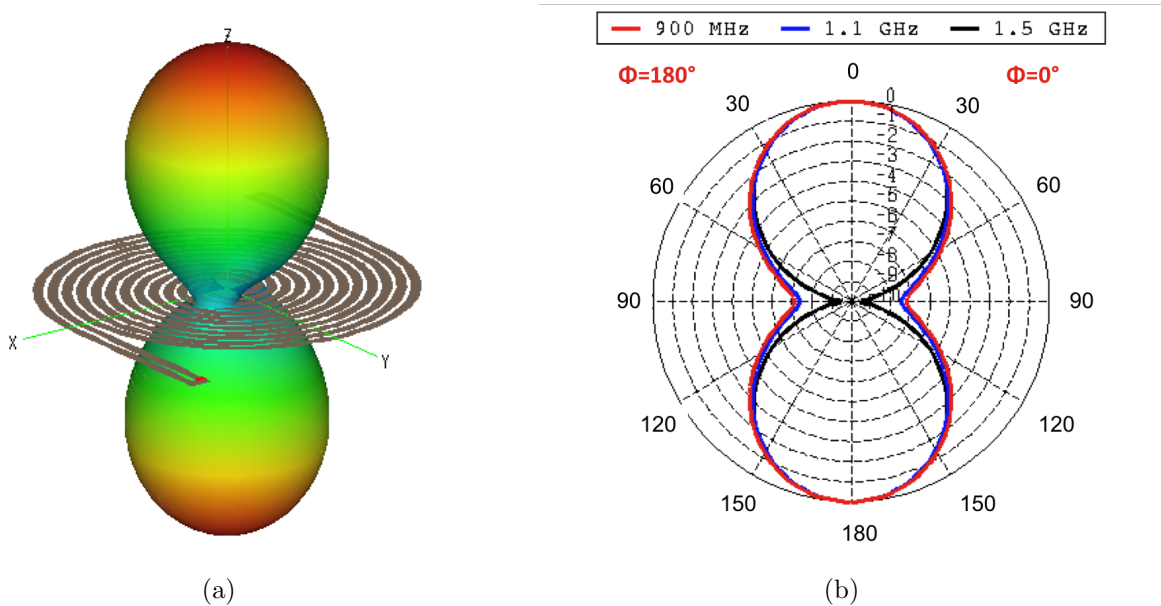


Figure 2.7: 2×2 arms spiral antenna: (a) 3D view of the far field pattern and (b) cuts in elevation at 900 MHz, 1.1 GHz and 1.5 GHz

However, the 2×2 arms spiral antenna radiates a circular polarization only for a narrow band as shown by the AR at position $\theta=0^\circ$ in Figure 2.8. Indeed, AR is above 0.7 only from 1 GHz to 1.05 GHz. For the remaining frequency range, the polarization is generally elliptic. This is partly due to the short lengths of the arms that create reflection in the center of the spiral. This in turn gives rise to a cross-polarization that diminishes the AR. Optimizing the center of the antenna could reduce these reflections.

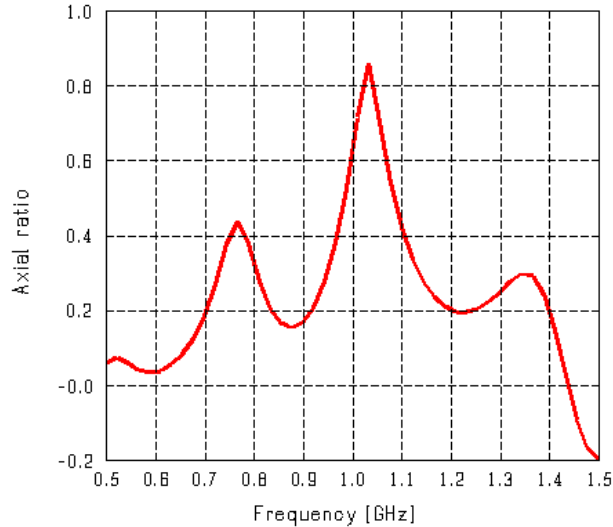


Figure 2.8: 2×2 arms spiral antenna: axial ratio against frequency at $\theta=0^\circ$ and $\phi=0^\circ$

This new design of spiral antenna is externally fed without using resistive loads. Hence, resistive losses are avoided and the theoretical value of the efficiency is equal to 100 % compared to Figure 2.4(b). The geometry is composed of two double arms and the feeding is achieved with two symmetrical sources in the same plane. Consequently, it is no more necessary for feeding the antenna, to have access to the center of the spiral. This antenna exhibits very good characteristics in terms of return loss. For the same diameter, the bandwidth is almost 150 MHz wider than that of the center-fed spiral antenna. Hence, the bandwidth is improved by around 37.5% when the antenna is used in an array. Thanks to the symmetry of the current distribution, the shape of the far field pattern does not change over the frequency range. Due to the reflections in the center, the AR of the 2×2 arms spiral antenna is worse than the center-fed case. However, the center of the antenna could be optimized to reduce reflection at the end of the arms to improve AR.

2.3 Measurement

An antenna prototype has been built and measurements in anechoic chamber have been done to be compared to the simulation results. This section details the prototype of the antenna as well as the anechoic chamber and its measurement configuration.

2.3.1 Antenna prototype

The prototype of the antenna is shown in Figure 2.9. According to the datasheet of the substrate given in Appendix A, the antenna has been printed on a square of 0.8 mm FR4 that has a permittivity equal to 4.2. Two SMA connectors are placed in the plane of the antenna. The unbalanced signal provided by the coaxial cable is balanced by two baluns located between the connectors and the beginning of the arms. Therefore, the two arms connected by the feed point are fed out-of-phase. Baluns characteristics are given in Appendix A. They are also used to achieve a matching impedance by multiplying the impedance characteristics of the feeding cable by a factor 4. Hence, since the reference impedance of a coaxial cable is 50Ω , the impedance from the point of view of the antenna should be equal to 200Ω . However, the insertion loss of the baluns degrades the efficiency of the antenna. Further investigations have to be done to obtain a better matching impedance. A solution could be to achieve a matching transition to 50Ω added to a circuitry that only balances the feeding. The phase shifter used to achieve a phase difference of 180° between the sources is not represented in this figure.

2.3.2 Anechoic chamber

All the measurements of the antennas have been done in the anechoic chamber at Supelec using a spherical near field test facility. A scheme and a picture of this chamber are given in Figure 2.10. The antenna under test is placed on a platform in the center of the chamber. A receiving antenna moves from 0° to 170° with a 5° step in the elevation plane. For each position of the receiving antenna, the antenna platform rotates from 0° to 360° with a 5° step in the azimuth plane. As a result, the radiated field is obtained over a spherical scan except for $\theta=[170^\circ,180^\circ]$ that corresponds to the antenna platform. The measurement of the polarization requires two orthogonal sets of data. This is achieved by rotating the probe about its axis of 90° at each position.

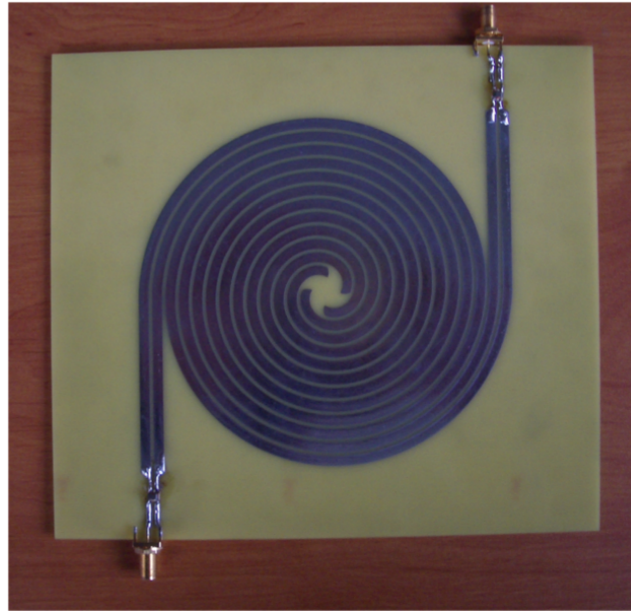
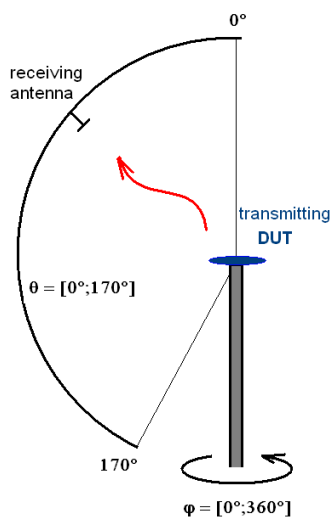


Figure 2.9: *2×2 arms spiral antenna: prototype*



(a)



(b)

Figure 2.10: (a) scheme and (b) picture of the anechoic chamber at Supelec (Sesame)

2.3.3 Measurement method and results

The antenna exhibits a symmetry about the boresight axis, both in the geometry and in the feeding. The spiral geometry is printed on the substrate and cannot be altered. However, the feeding can be decomposed by separating the effects of each source. Indeed, the antenna can be seen as a small array of two elements. In this case, the total far field radiated is given by equation 2.4.

$$\vec{E}_{Tot}(\theta, \phi) = \sum_{k=1}^N \vec{E}_k(\theta, \phi) \exp(j\Phi_k) \quad (2.4)$$

Where :

$\vec{E}_k(\theta, \phi)$ corresponds to the electrical far field of antenna k ;

N is the number of elements of the antenna array;

$\exp(j\Phi_k)$ is the phase of antenna k .

For the 2×2 arms spiral antenna, N is equal to 2 and the phase shift between elements is 180° . Hence, the total far field pattern is equal to the sum of the radiated patterns of the two sources. This corresponds to the superposition method illustrated in Figure 2.11. The first pattern (Figure 2.11(a)) is obtained by feeding one port and matching the second one with its reference impedance. Conversely, the second pattern (Figure 2.11(b)) corresponds to the first port matched and the second one fed. After adding the contributions of the two sources, the total far field pattern (Figure 2.11(c)) is obtained.

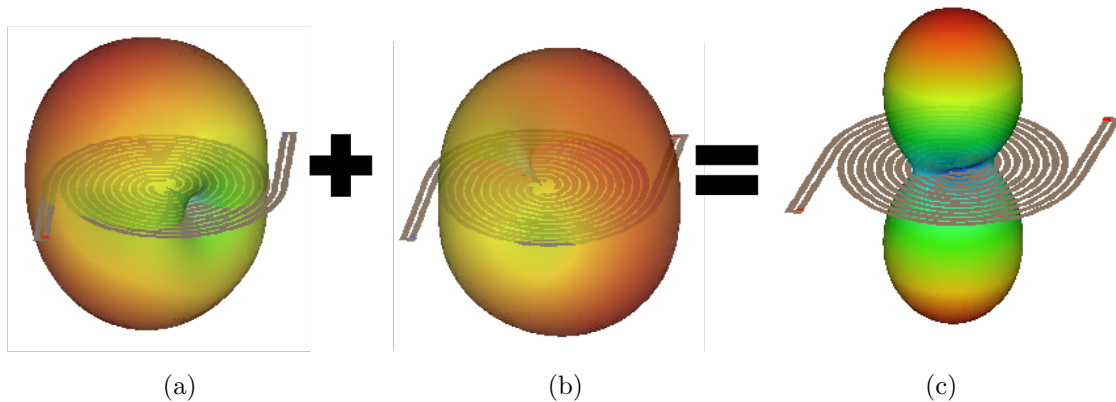


Figure 2.11: 2×2 arms spiral antenna: decomposition of the measurement, the total far field pattern (c) is equal to the sum of the two patterns (a) and (b)

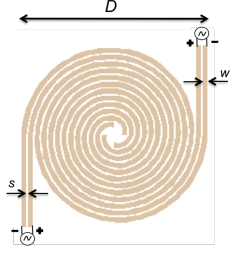
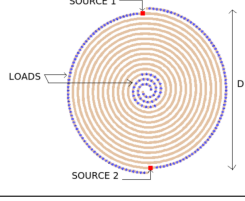
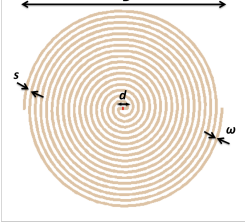
Due to the symmetry of the geometry, the second radiated pattern can be obtained by rotating the first one about the symmetrical axis. Therefore, the total pattern of the antenna can be calculated from only one pattern. The numerical technique used to rotate the far field pattern has been developed by F. Chauvet in [15]. Hence, for the measurements of the 2×2 arms spiral antenna, only one source has been fed and the second one matched. The obtained measured pattern has been rotated 180° about the boresight axis of the antenna and a phase shift of 180° has been added to the data before combining in order to determine the total pattern. In this case, the phase shift and the amplitude errors of a phase-shifter and power divider are avoided.

Measurement results compared with the simulated patterns are depicted in Figure 2.12. Three cuts in elevation of the far field pattern at 700 MHz, 900 MHz and 1 GHz are depicted with a 3D view at 900 MHz of the measured data. Black crosses on this figure represent the cut in elevation. Feeding is well balanced by the baluns and good agreement is shown between measurements and simulation. From the 3D view, it can be seen that the shape of the radiated pattern corresponds to that of a center-fed antenna.

2.4 Conclusion of Chapter 2

These two first solutions of externally-fed spiral antennas have been built following the principle of symmetry in the geometry and in the feeding. The first design using resistive loads in order to suppress reflections in the center and on the outermost arms, achieves good characteristics close to the center fed antenna. However, implementation of loads on the antenna is challenging. Moreover, losses of the radiated power due to the loads leads to a quite low efficiency. The second design takes into account these issues and no resistive loads are used. Antenna bandwidth is increased but the radiated polarization is circular only over a narrow frequency band. The 2×2 arms spiral antenna could be used for applications that require an external feeding without a need for good circular polarization. This is not the case in this study and another way to achieve an externally-fed spiral antenna with a circular polarization is investigated in the next chapter. All the characteristics of the designs are summarized in Table 2.3.

Table 2.3: Summary of the antennas characteristics

<i>Design</i>	<i>Nb of feed</i>	F_{min} for RL \leq -10 dB	<i>Radiation pattern</i>	<i>Polarization</i>
	2	$f_{min}=650$ MHz	Symmetric	$f_{AR \geq 0.7} = 1-1.05$ GHz
	2	$f_{min}=830$ MHz	Symmetric	$f_{AR \geq 0.7} = 880$ MHz
	1	$f_{min}=800$ MHz	Symmetric	$f_{AR \geq 0.7} = 1$ GHz

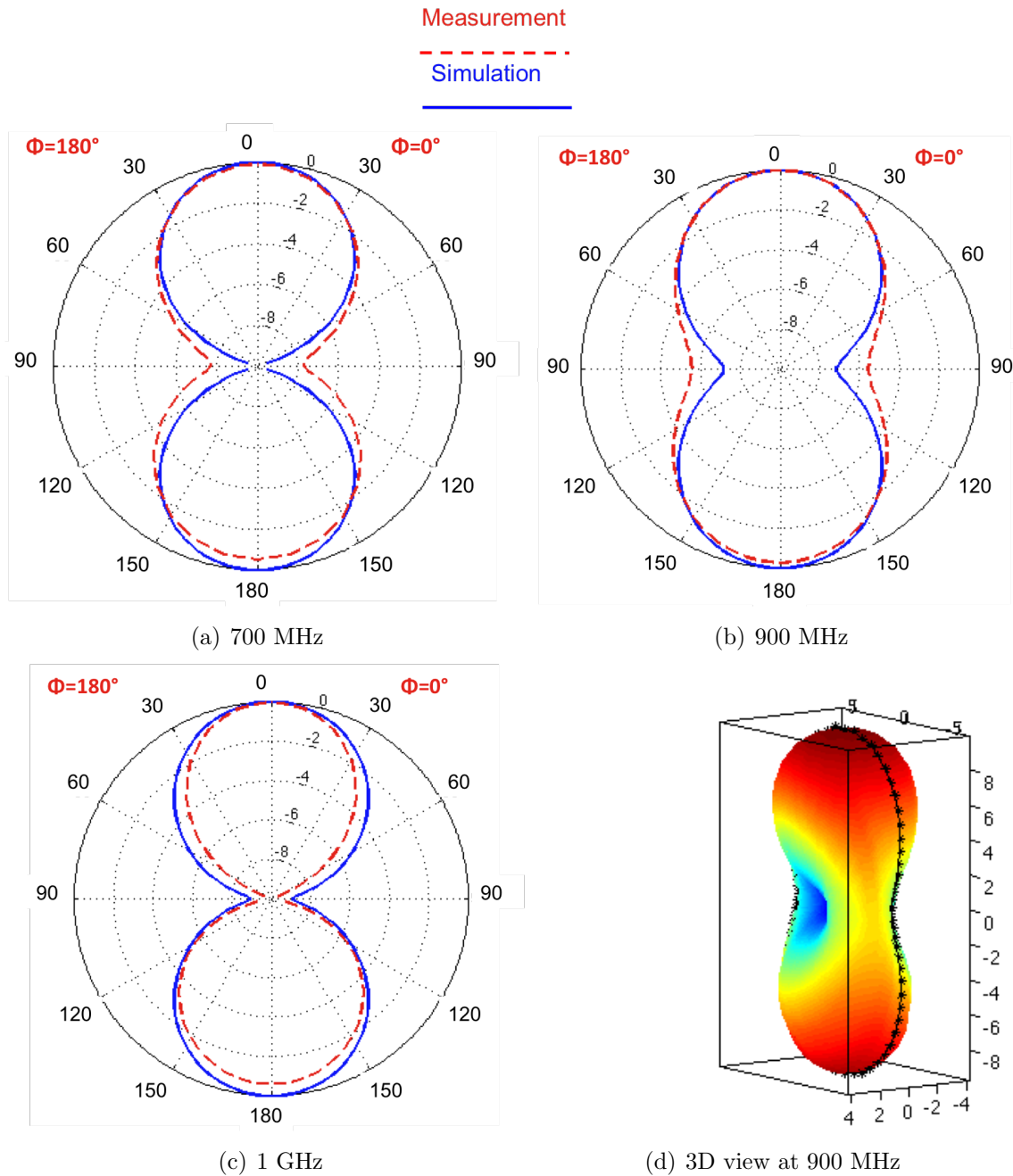


Figure 2.12: 2×2 arms spiral antenna: comparison of the measured and simulated patterns in elevation at 700 MHz, 900 MHz and 1 GHz with a 3D view of the measured pattern at 900 MHz

Chapter 3

From Circular Array with Sequential Rotation Technique to Multi-ports Antenna

The previous investigated designs are externally-fed by more than one source. Therefore, they can be seen as a small antenna array with highly coupled elements due to the short distance between them. Regarding the geometry, these elements are distributed along a circle. In order to improve the antenna array characteristics, especially in terms of polarization, investigation have been done in the area of the circular arrays with sequential rotation technique (CASRT). These arrays have been widely studied in the past to synthesize the radiation pattern [16] [17]. Studies have been done to optimize the antenna array characteristics [18] and to reduce coupling between elements [19]. In terms of polarization, the antenna array follows usually that of the elements. Hence, for an antenna array with Right Hand Circular Polarization and/or Left Hand Circular Polarization, the antenna element has to radiate the corresponding circular polarization. However, the geometry and the feeding of the array could also modify the polarization. Investigations in this area show that circular geometry of the array combined with sequential rotation techniques [20] may help to obtain a circular polarization. In some cases, the antennas are also optimized to achieve circular polarization [21]. In this chapter, different geometries of antenna array which achieve circular polarization independently of the polarization of the antenna element, are presented. The theory of the circular antenna array with sequential feeding is described and the influence of the number of elements on the polarization is illustrated with several examples. An antenna array has been built and measurements have been performed in order to verify the theoretical results.

3.1 Circular Array with Sequential Rotation Technique (CASRT)

The configuration of the array is described in this section. In a first part, the total electric far field calculated according to the position of all the elements is detailed. In a second part, the study focuses on the polarization that is radiated by this array.

3.1.1 Geometry and feeding configuration of the CASRT

The sequential rotation technique applied to the circular array improves the axial ratio. The principle of this technique is to rotate each element with respect to the center of the array and to add a phase shift that corresponds to the angle of rotation. In order to study the antenna array characteristics, the total far field pattern has to be calculated. For an antenna array, the far field pattern depends on the contributions of all the radiation patterns of the array elements. Hence, the radiation pattern for all antennas has to be known. The total electric far field of a CASRT is given by the following equation.

$$\vec{E}_{Tot}(\theta, \phi) = \sum_{k=1}^N \vec{E}_k(\theta, \phi) \exp(j\Phi_k) \quad (3.1)$$

Where $\vec{E}_k(\theta, \phi)$ is the active element pattern [22] of the element k . The active element pattern is the radiated field obtained by feeding one element of the array while the others are matched to their reference impedance. Hence, $\vec{E}_k(\theta, \phi)$ includes the rotation applied to element k and the coupling between the elements. N is the number of elements of the antenna array. The phase shift $\exp(j\Phi_k)$ of each antenna k corresponds to the phase configuration of the sequential rotation.

Thus, all the radiation patterns of the antennas are taken into account whatever their positions or directions. This study focuses on 2D antenna arrays with equally spaced elements in circular geometry. Hence, all antenna elements are placed along a circle where each element is equally spaced between the previous and the following one. In this configuration, the elements are arranged in such a way that each antenna is obtained from a rotation of the previous one about the center. An example is given in Figure 3.1, where a black cross denotes an antenna element.

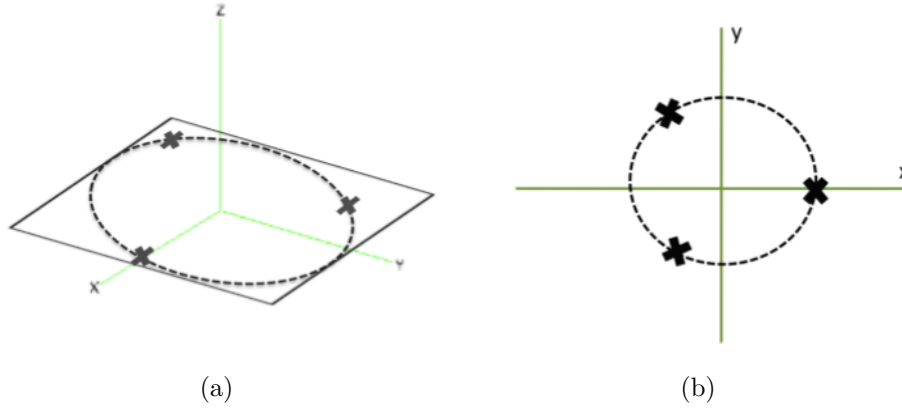


Figure 3.1: Antenna array geometry: (a) 3D view and (b) top view

In this example, 3 antennas are arranged along a circle in the plane xOy . Considering one of the antennas as a reference, it can be seen that the 2 others antennas are obtained from a rotation of this element about the center of 120° and 240° . Therefore, due to this rotational symmetry, the entire radiation pattern of the antenna array can be calculated from the radiation pattern of only one element. For simplicity, one of the elements is considered as an antenna reference in the array and its radiated pattern is $\vec{E}_{ref}(\theta, \phi)$. In this case, the total far field pattern is given by:

$$\vec{E}_{Tot}(\theta, \phi) = \sum_{k=1}^N \text{Rotation}_{\left(\frac{2\pi k}{N}\right)} \vec{E}_{ref}(\theta, \phi) \exp\left(j\frac{2\pi k}{N}\right) \quad (3.2)$$

Where :

$\vec{E}_{ref}(\theta, \phi)$ corresponds to the complex value of the electric far field of the antenna reference at position (θ, ϕ) ;

N is the number of elements in the antenna array;

$\exp\left(j\frac{2\pi k}{N}\right)$ is the phase of antenna k ;

The matrix *Rotation* applies a rotation of $\frac{2\pi k}{N}$ in radians about the z -axis.

The axis of rotation is always orthogonal to the plane of the antenna array. Since the antenna array is in the plane xOy , the rotations of the elements have to be done about z -axis. The rotation matrix is given in equation 3.3. The value of the far field of the antenna

reference at position (θ_i, ϕ_i) is converted from spherical to cartesian coordinates. Then a rotation about z -axis is applied to the cartesian coordinates and a last transformation is done from cartesian to spherical coordinates at position (θ_f, ϕ_f) .

$$Rotation = \begin{pmatrix} Cart \\ \downarrow \\ Sph \\ (\theta_f, \phi_f) \end{pmatrix} \begin{pmatrix} \cos(\frac{2\pi k}{N}) & \sin(\frac{2\pi k}{N}) & 0 \\ -\sin(\frac{2\pi k}{N}) & \cos(\frac{2\pi k}{N}) & 0 \\ 0 & 0 & 1 \end{pmatrix} \begin{pmatrix} Sph \\ \downarrow \\ Cart \\ (\theta_i, \phi_i) \end{pmatrix} \quad (3.3)$$

Moreover, a phase shift is applied to each element by multiplying the results by $\exp(j\frac{2\pi k}{N})$. This operation is done $N-1$ times before summation of each contribution. Thanks to the rotational symmetry, coupling between elements can be taken into account by assuming that $\vec{E}_{ref}(\theta, \phi)$ is calculated or measured with all the elements. In practice, this means that $\vec{E}_{ref}(\theta, \phi)$ is obtained by feeding only the antenna reference and matching all other antennas of the array with their reference impedance. Thus, coupling is included in the radiation pattern of the antenna reference.

3.1.2 Polarization of the CASRT

For a classical linear antenna array, the polarization depends on that of the antenna element. Hence, if the antenna array is composed with linear polarized elements, the polarization of the array will be linear. In this part, the influence of the CASRT is studied. For simplicity, the study focuses on the position in the boresight axis of the array at $\theta=0^\circ$ and $\phi=0^\circ$. At this position, the total far field pattern becomes:

$$\vec{E}_{Tot}(0, 0) = \sum_{k=1}^N \begin{pmatrix} 1 & 0 & 0 \\ 0 & \cos(\frac{2\pi k}{N}) & \sin(\frac{2\pi k}{N}) \\ 0 & -\sin(\frac{2\pi k}{N}) & \cos(\frac{2\pi k}{N}) \end{pmatrix} \vec{E}_{ref}(0, 0) \exp(j\frac{2\pi k}{N}) \quad (3.4)$$

Assume that $\vec{E}_{Tot}(\theta, \phi) = E_{\theta_{Tot}}(\theta, \phi)\vec{e}_\theta + E_{\phi_{Tot}}(\theta, \phi)\vec{e}_\phi$. To achieve a circular polarization, $E_{\theta_{Tot}}(\theta, \phi)$ and $E_{\phi_{Tot}}(\theta, \phi)$ have to satisfy the following conditions :

$$\begin{cases} |E_{\theta_{Tot}}| = |E_{\phi_{Tot}}| \\ Arg(E_{\theta_{Tot}}) - Arg(E_{\phi_{Tot}}) = \pm\pi/2 \end{cases} \quad (3.5)$$

The following table gives the phase difference with the formulas of $E_{\theta_{Tot}}$ and $E_{\phi_{Tot}}$ according to the number of elements N in the array. For the first two cases which correspond to only

one or two elements, the values of $E_{\theta_{Tot}}$ and $E_{\phi_{Tot}}$ depends on the element ones as well as the radiation pattern and polarization.

N	1	2	3	4
$E_{\theta_{Tot}}(\theta = 0, \phi = 0)$	E_{θ}	$2 \times E_{\theta}$	$\frac{3}{2} \times (E_{\theta} - iE_{\phi})$	$2 \times (E_{\theta} - iE_{\phi})$
$E_{\phi_{Tot}}(\theta = 0, \phi = 0)$	E_{ϕ}	$2 \times E_{\phi}$	$\frac{3}{2} \times (iE_{\theta} + E_{\phi})$	$2 \times (iE_{\theta} + E_{\phi})$
$\text{Arg}(E_{\theta_{Tot}}) - \text{Arg}(E_{\phi_{Tot}})$	x	x	$\pm\pi/2$	$\pm\pi/2$

However, from $N = 3$, the components of the far field can be written as in (3.6). $E_{\theta_{Tot}}$ and $E_{\phi_{Tot}}$ completely satisfy the conditions given in (3.5). Hence, for a minimum of 3 elements, the CASRT radiated field is perfectly circularly polarized whatever the polarization of the elements.

$$\begin{cases} E_{\theta_{Tot}} = \frac{N}{2} \times (E_{\theta} - iE_{\phi}) \\ E_{\phi_{Tot}} = \frac{N}{2} \times (iE_{\theta} + E_{\phi}) \end{cases} \quad (3.6)$$

Thanks to the circular geometry of the antenna array and to the sequential feeding, a perfectly circular polarization is achieved at position $\theta=0^\circ$ independently of the element polarization. To obtain this circular polarization over a wide angle, $E_{\theta_{Tot}}$ and $E_{\phi_{Tot}}$ have to satisfy the condition given in (3.5) as well as possible. This depends on the radiation pattern of the element.

3.2 Examples of CASRT

To illustrate the theory, a simulated dipole antenna arrays is studied in a first part. In a second part, the theory of the CASRT is also applied to a simulated and measured array of 4 LPDA.

3.2.1 Dipole antenna array

A dipole antenna is chosen as the element of the array. In the first part, a dipole antenna array of 3 elements is studied to illustrate the theory. The characteristics of both the antenna element and antenna array are presented. In the second part, several arrays are simulated to investigate the influence of the number of elements on the radiation pattern and the polarization. All the antennas are modeled using the software FEKO based on the Method of Moments.

The geometry of the antenna array is given in Figure 3.2. Antenna elements are placed along a circle and each element results from a rotation of 120° about the circle center of the previous one. Moreover, a phase shift is applied to the elements. Thus, all antennas are fed with the same voltage and a phase shift of 0° , 120° and 240° respectively. The antenna

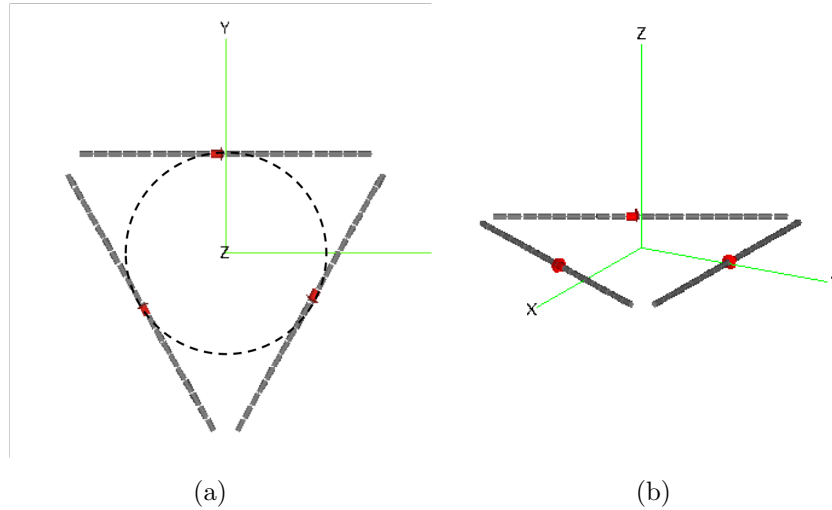


Figure 3.2: Dipole antenna array: (a) top view and (b) 3D view

length is chosen to be equal to half wavelength at the frequency of 50 MHz. The return loss of the elements are calculated with a reference impedance of 75Ω and displayed in dB in Figure 3.3(b). Here again, due to the geometry of the array, RL is identical for all the antennas and its absolute value is under -10 dB around 50 MHz.

The AR of the antenna array is depicted in Figure 3.3(a) against frequency at position $\theta=0^\circ$. As previously explained, the antenna array polarization is perfectly circular whatever the polarization of the elements. Simulations results show very good agreement with the theory since the AR is equal to 1 over the frequency range at position $\theta=0^\circ$. To emphasize the robustness of the circular array theory, the AR has been calculated with a phase shift error of $\pm 8^\circ$ and an amplitude error of 1 dB randomly affected to the sources. These values far exceed typical errors given by phase-shifter and power divider. At each frequency, 100 simulations have been done to calculate the means and means \pm standard derivation, depicted in Figure 3.3(a). Even though a phase shift and an erroneous amplitude are applied to the sources, all the curves of the AR are still above 0.8 and a good circular polarization is radiated.

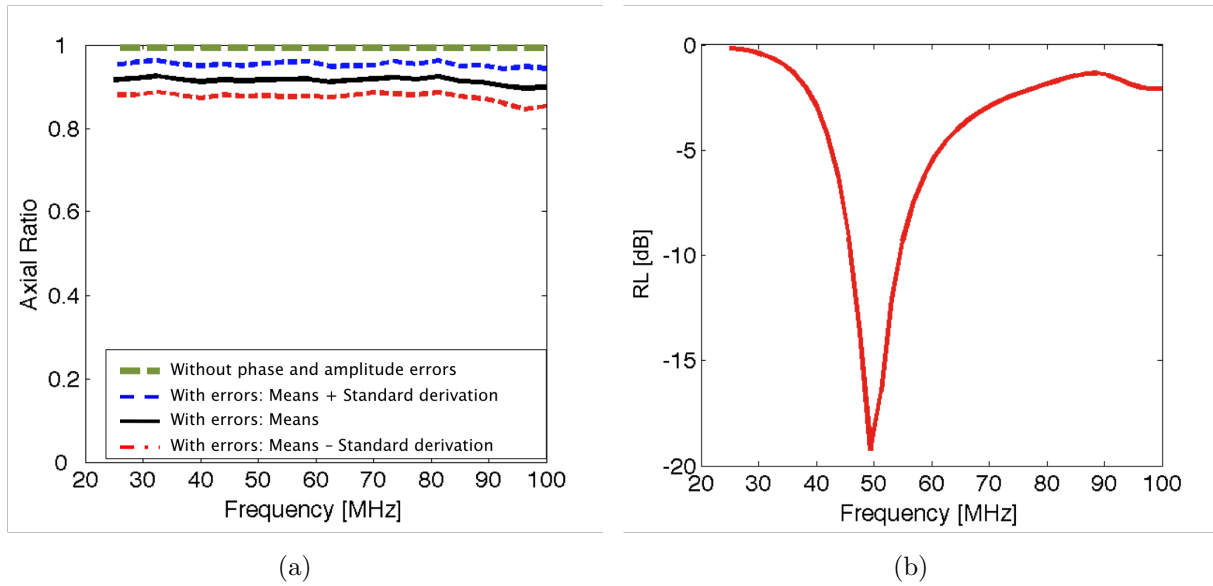


Figure 3.3: Dipole antenna array: (a) simulated axial ratio with and without phase and amplitude errors at $\theta=0^\circ$ and $\phi=0^\circ$ and (b) reflection coefficient of the elements

The AR of the array is depicted in Figure 3.4(a) for $\theta=[0^\circ, 360^\circ[$ and $\phi=0^\circ$ at the frequency 50 MHz, which is the maximum of radiation. Negative values corresponds to the radiation of a LHCP while positive values represent the radiation of a RHCP. Thus, the array radiates a right hand circular polarization for $\theta = 0^\circ$ and left hand circular polarization for $\theta = 180^\circ$. Circular polarization is radiated within an angular range of $\pm 25^\circ$ from the boresight. It is important to consider the gain compared to the AR to ensure that the antenna array radiates most of the power with a circular polarization.

The total gain in dBi is given in Figure 3.4(b) for $\theta=[0^\circ, 360^\circ[$ and $\phi=0^\circ$ at the same frequency. The antenna array radiates in both directions perpendicular to the plane of the antennas with an aperture of $\pm 50^\circ$ from the boresight. In this case, only a part of the power is radiated with a circular polarization. In order to study the influence of number of elements of the antenna array on the beamwidth of the gain and the polarization, three arrays containing 3, 4 and 5 dipoles are studied and their performances are compared. The geometries are given in Figure 3.5.

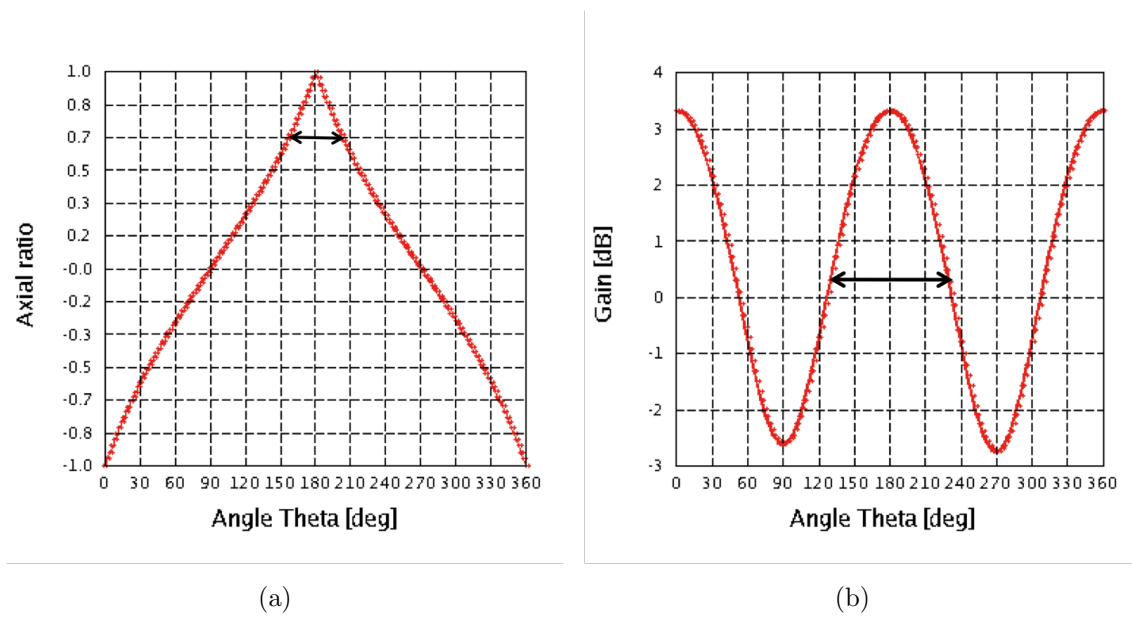


Figure 3.4: Dipole antenna array: (a) axial ratio and (b) total gain at 50 MHz

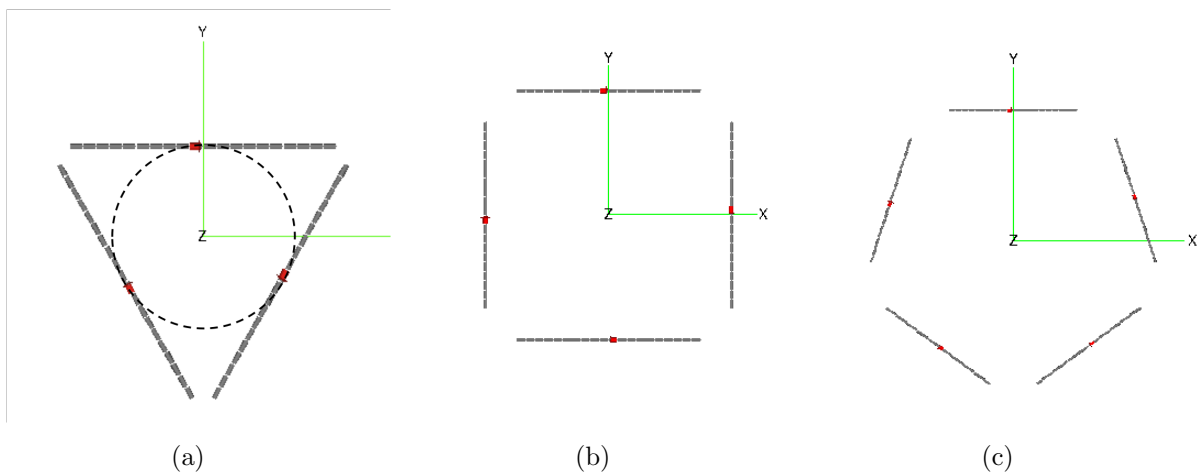


Figure 3.5: Dipole antenna array: geometries of the arrays for $N=3$, 4 and 5

The axial ratio and the gain are plotted in Figure 3.6 for $\theta=[0^\circ, 360^\circ]$ and $\phi=0^\circ$ at 45.625 MHz for the 3 cases. At this frequency, all the antenna array exhibit an absolute value of the return loss less than -10 dB. As the number of elements increases in the array, the beamwidth of the gain and the angular range corresponding to the radiation of a circular polarization, are enhanced except when the number of elements is equal to 5. In this case, the antennas are more directive and grating lobes appear in the total radiation pattern.

It is interesting to notice that a gap of around 3 dB is observed between the cases 3 and 4 dipoles in Figure 3.6(b). This is due to the coupling between elements that is different in both cases. Hence, the electric far field generated by these two arrays is different which explains this gap of the total gain.

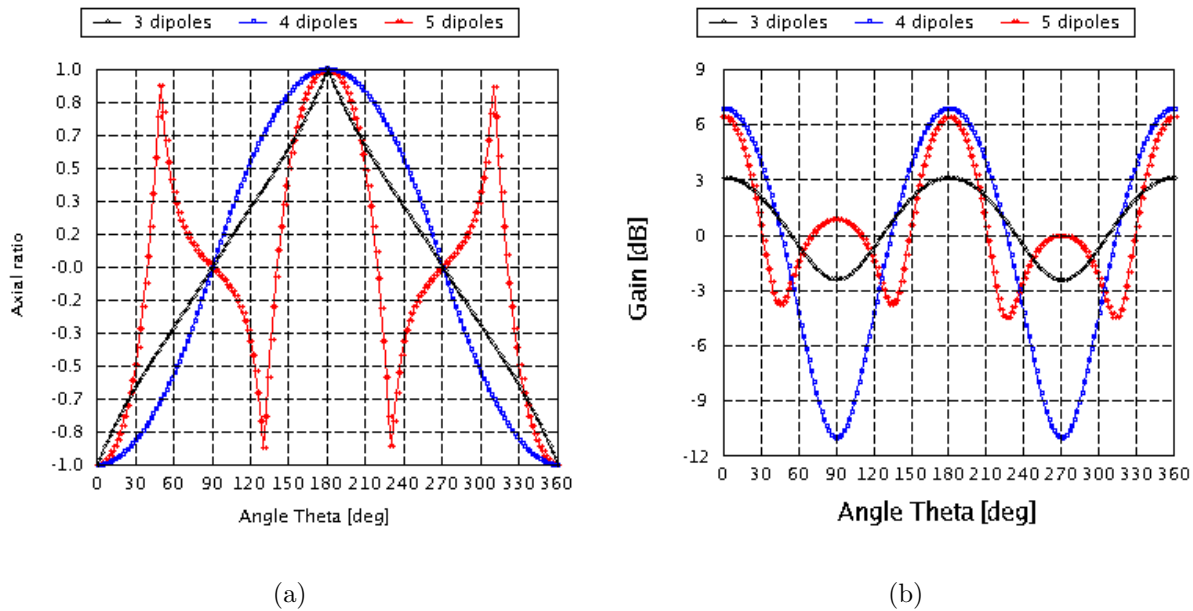


Figure 3.6: Dipole antenna array: (a) simulated axial ratio and (b) total gain at 45.625 MHz

The same cut of the total gain and the axial ratio is shown in Figure 3.7 at the frequency of 27.75 MHz. At this frequency, the antenna arrays exhibit a $|RL| \geq -10$ dB but the grating lobes are avoided. Thus, the study focuses only on the influence of the number of antennas on the axial ratio. The angular range for an $AR \geq 0.7$ increases clearly with the number of elements while the beamwidth of the total gain decreases. Hence, a trade-off has to be found between the gain and the polarization in order to radiate as much power as possible with a circular polarization. All the performances are summarized in the next table.

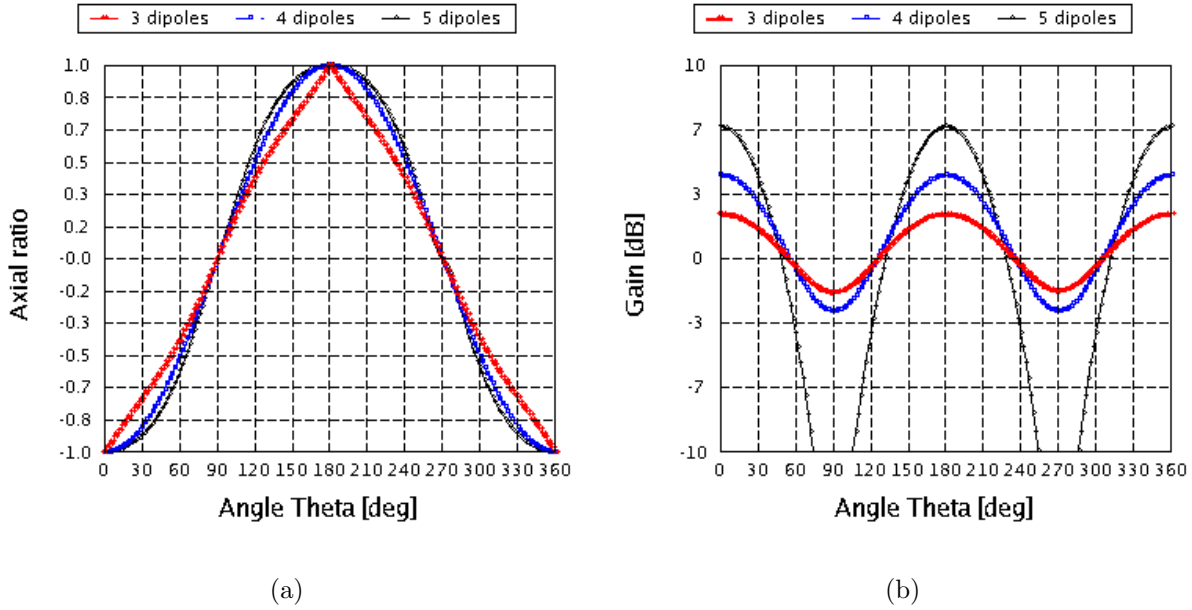


Figure 3.7: Dipole antenna array: (a) simulated axial ratio and (b) total gain at 27.75 MHz

N	3	4	5
AR at 45.625 MHz	$\pm 25^\circ$	$\pm 50^\circ$	$\pm 25^\circ$
Total gain at 45.625 MHz	$\pm 50^\circ$	$\pm 30^\circ$	$\pm 25^\circ$
AR at 27.75 MHz	$\pm 35^\circ$	$\pm 45^\circ$	$\pm 55^\circ$
Total gain at 27.75 MHz	$\pm 45^\circ$	$\pm 35^\circ$	$\pm 30^\circ$

All the previous examples show the influence of the circular geometry of the antenna array on the polarization. According to the theory given in the first section, a perfect circular polarization is obtained at position $\theta = 0^\circ$ and a good circular polarization over a large angular range. Moreover, this angular range grows with the number of elements. However, grating lobes could appear when they are too numerous. Thus, a compromise has to be found between the AR and the total gain. At last, all these performances should be obtained for a frequency range as wide as possible.

3.2.2 LPDA antenna array

In this part, the theory is applied to a $4 \times$ Log Periodic Dipole Antenna (LPDA) array. The antenna array has been modeled with CST Microwave Studio [23] and a prototype has been built. Firstly, simulation and measurement results of the array with only one antenna fed are compared. Secondly, the far field pattern of the antenna array calculated with the measurement results according to the theory is compared with the simulated array. Lastly, a modification of the LPDA is presented in order to improve the polarization of the array.

In this configuration, 4 elements are placed along a circle and a phase shift of 90° is applied between each element. The LPDA [24] antenna is built using 21 dipoles for a frequency range comprised between 1 GHz and 2 GHz. Modeled antenna array is presented in Figure 3.8 and the prototype in Figure 3.9. The array is placed in the center of a $40 \text{ cm} \times 40 \text{ cm}$ ground plane.

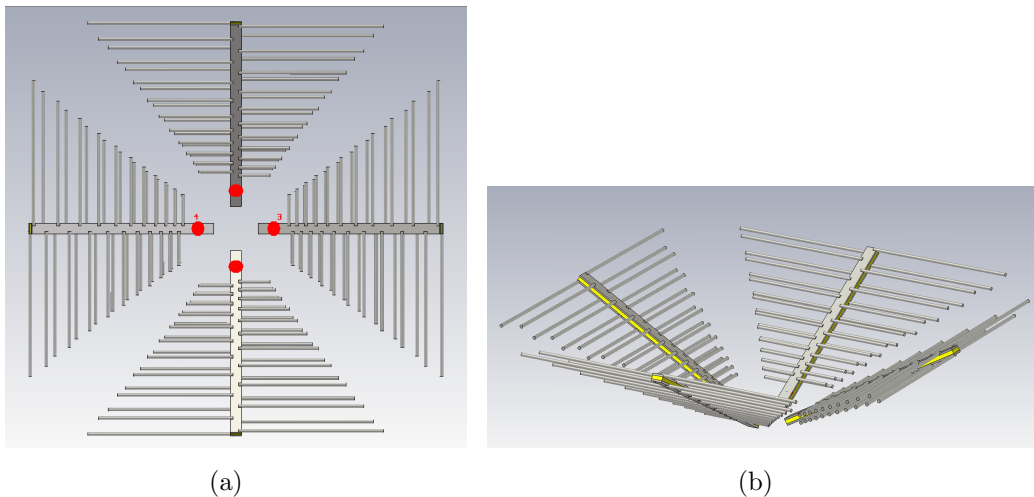


Figure 3.8: LPDA antenna array: (a) top view and (b) 3D view of the $4 \times$ LPDA antennas modeled with CST Microwave studio

The RL of an antenna element is plotted in Figure 3.10 for the frequency range starting from 1 GHz to 1.5 GHz. The antenna exhibits an absolute value of the reflexion coefficient under -10 dB over several frequency band marked by greened surfaces. $|\text{RL}|$ is almost always less than -7 dB over the remaining bandwidth.

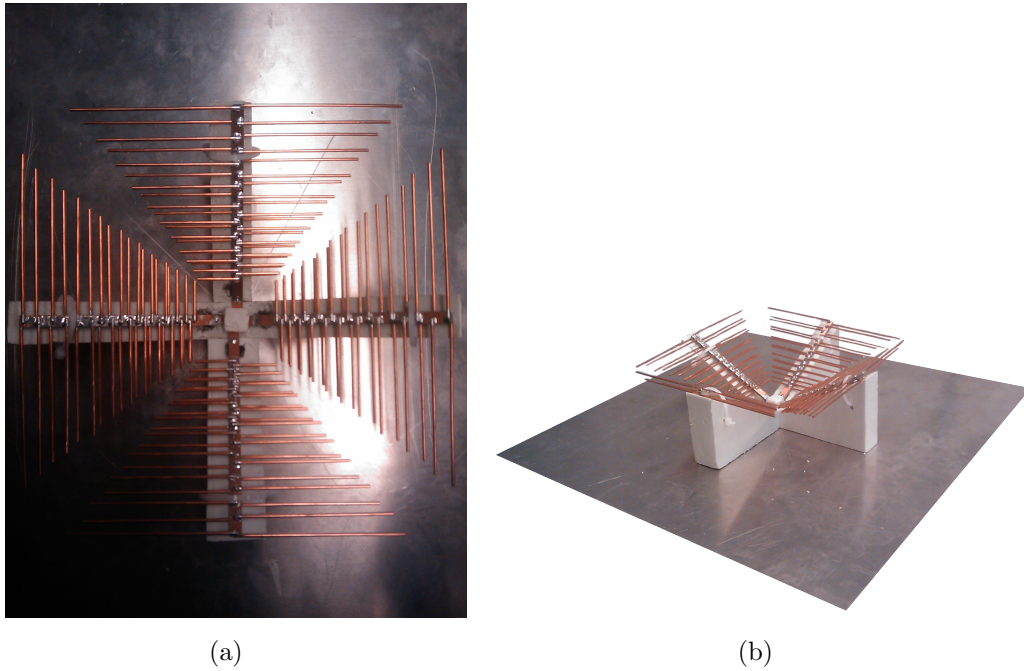


Figure 3.9: *LPDA antenna array: (a) top view and (b) 3D view of the measured $4 \times$ LPDA antennas*

Measurements of only one element is compared with simulation results at the frequencies of 1 GHz, 1.1 GHz, 1.2 GHz and 1.4 GHz in Figure 3.11. In this figure, cuts in elevation of the normalized total gain and the AR are compared. Red crosses represent the measurement results while the black lines show simulation results. Measurement results show good agreement with simulation results. The antenna element radiates a main beam in the perpendicular direction of the ground plane and, as expected, the polarization is not circular with only one element.

In order to obtain the radiation characteristics of the antenna array, measurements results of the antenna element are combined according to the theory and compared to the simulation results of the array in Figure 3.12. Here again, the red cross represent the measurement results and the black lines show simulation results. The total gain exhibits a main symmetrical beam on the perpendicular axis of the ground plane. As expected, the polarization is perfectly circular in the boresight for $\theta = 0^\circ$ and the AR is greater than 0.7 over a wide angular range. Measurements exhibit better results than the simulation for the polarization, especially at

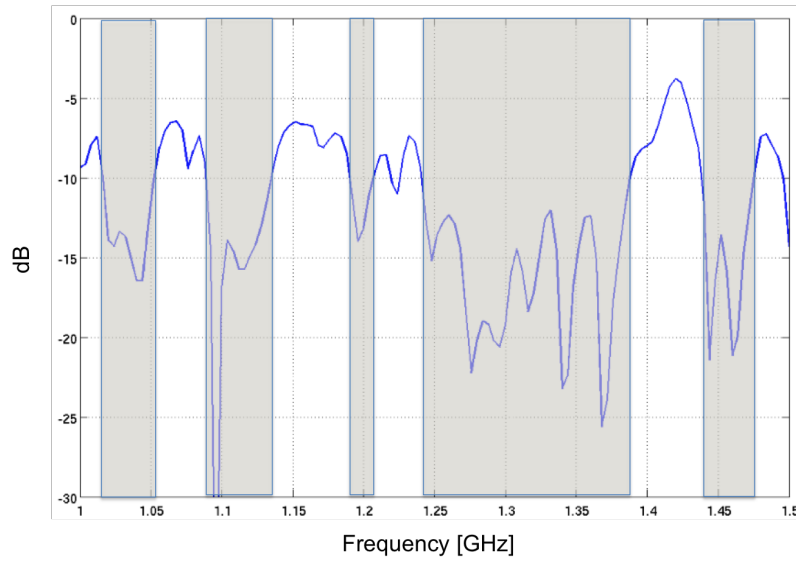


Figure 3.10: *LPDA antenna array: measured S_{11} of an element.*

1.1 GHz and 1.2 GHz where the polarization is circular over almost all the values of θ . The behavior of the antenna array depends on the antenna element. With the LPDA, good performances in terms of polarization are obtained over a wide frequency range.

To enhance the performances of the polarization of the array over a part of the frequency band, a modified array of $3 \times$ LPDA is modeled and compared to a non modified array of $3 \times$ LPDA. The geometries of the antennas are given in Figure 3.13. In both cases, the arrays are placed above a perfect ground plane. In this part, the study focuses only on the polarization characteristics. In order to increase the angular range that corresponds to an $AR \geq 0.7$, the dipoles of the LPDA have been bended. This affects the radiation pattern of the new antenna that becomes less directive. As a result, the total gain exhibits a wider beamwidth than for the classical case and a circular polarization is radiated over a wider angular range.

The axial ratio of both antenna arrays are plotted against frequency in Figure 3.14. For each case, several values of θ for $\phi = 0^\circ$ are plotted against frequency. For the $3 \times$ LPDA antenna array, the AR is greater than 0.7 over the frequency range for $\theta = 15^\circ$. From $\theta = 20^\circ$, the polarization is not circular at all the frequencies. However, for the modified $3 \times$ LPDA, the AR is better between 200 MHz and 350 MHz. Over this frequency band, the polarization remains circular for $\theta = 20^\circ$ and the AR decreases proportionally when θ grows.

Thus, the AR is enhanced over a wide part of the frequency range.

3.3 Conclusion of Chapter 3

In this chapter, the theory of the CASRT to obtain circular polarization whatever the elements of the array has been explained. With only the measurement of an antenna element, the entire far field pattern, including coupling between elements, is calculated. A perfect circular polarization is achieved at position $\theta = 0^\circ$ and the $|\text{AR}| \geq 0.7$ over an angular range depending on the antenna directivity. Good polarization performances are obtained with dipoles array and LPDA array. The performances of the polarization increase with the number of elements while the antennas become more directive. Hence, a trade-off has to be found to meet the requirements in terms of polarization and gain beamwidth. An antenna array of $4 \times \text{LPDA}$ has been built and the measurement results show good agreement with simulation results. A proposed modification of the LPDA increases the AR by decreasing the directivity of the antennas. This study could be applied to different types of antennas. In the next chapter, the theory of circular array to generate a circular polarization is applied to the externally-fed spiral antenna.

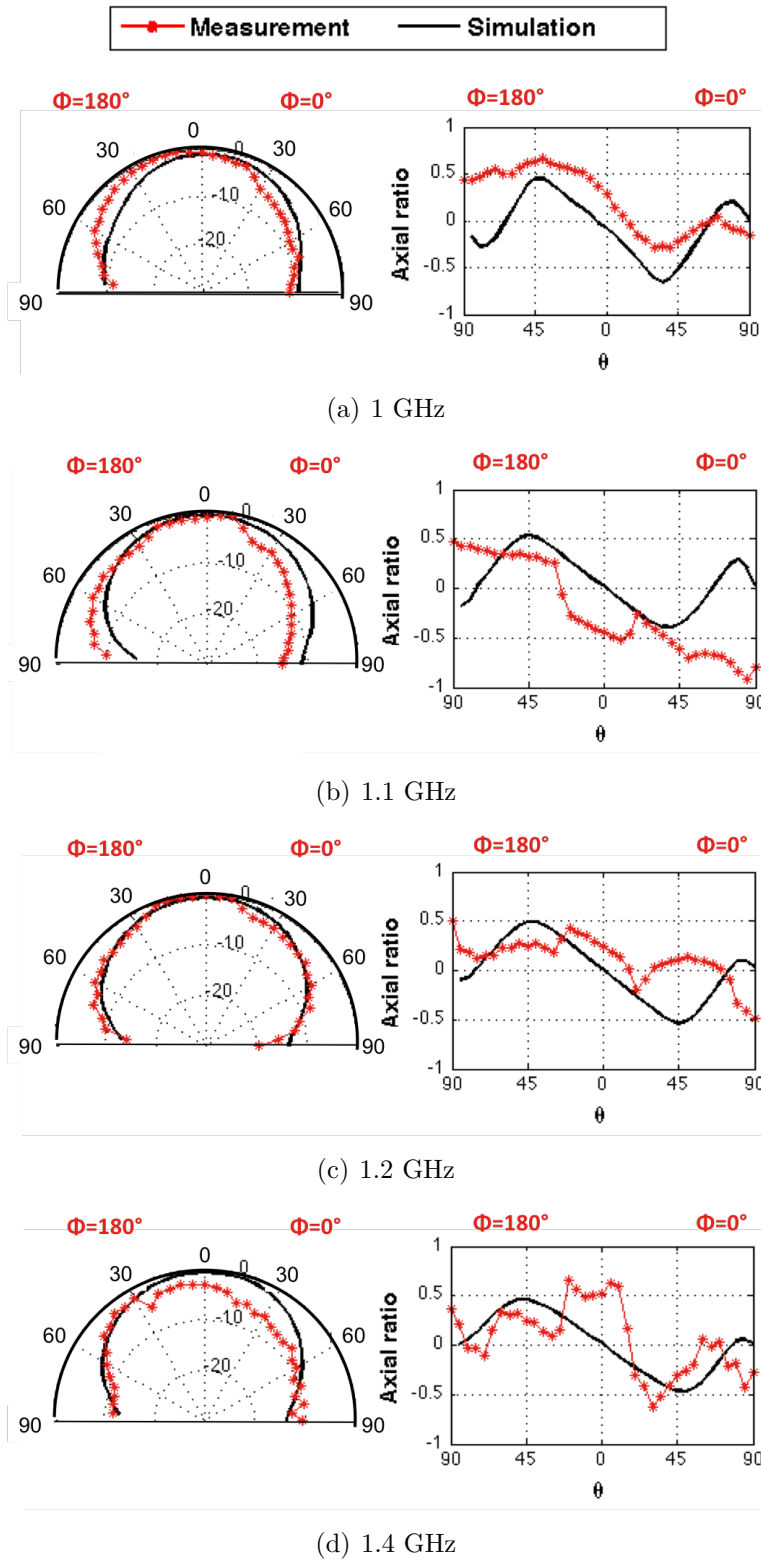


Figure 3.11: LPDA antenna array: measured and simulated cuts in elevation of the normalized total gain (left) and AR (right) of an element at 1GHz (a), 1.1GHz (b), 1.2GHz (c) and 1.4GHz (d).

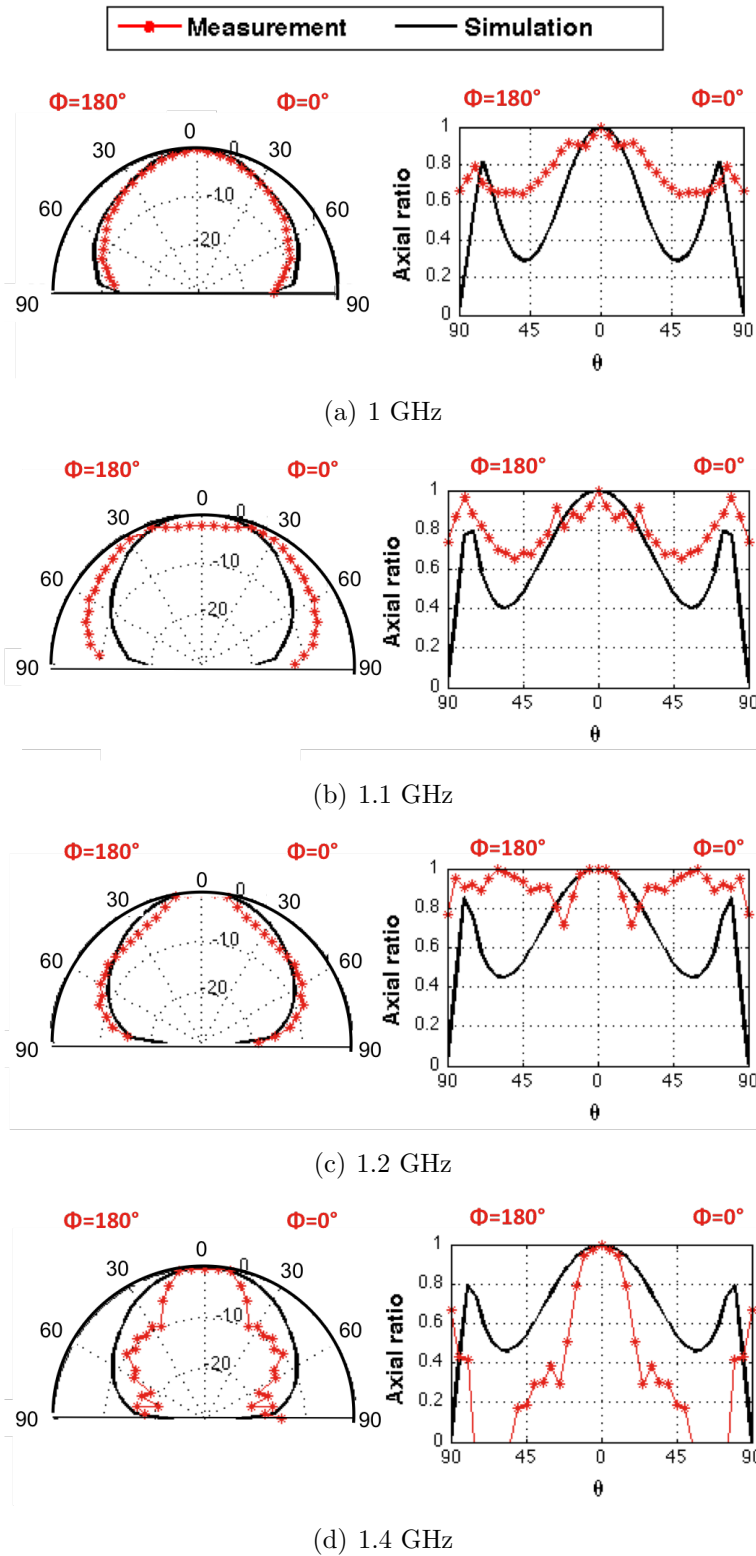


Figure 3.12: LPDA antenna array: measured and simulated cuts in elevation of the normalized total gain (left) and AR (right) of the array at 1GHz (a), 1.1GHz (b), 1.2GHz (c) and 1.4GHz (d).

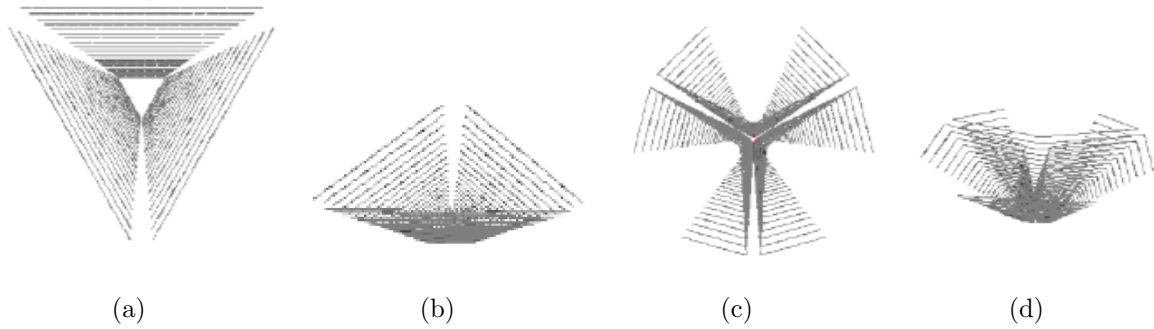


Figure 3.13: LPDA antenna array: (a) top view and (b) 3D view of the 3×LPDA and (c) top view and (d) 3D view of the modified 3×LPDA.

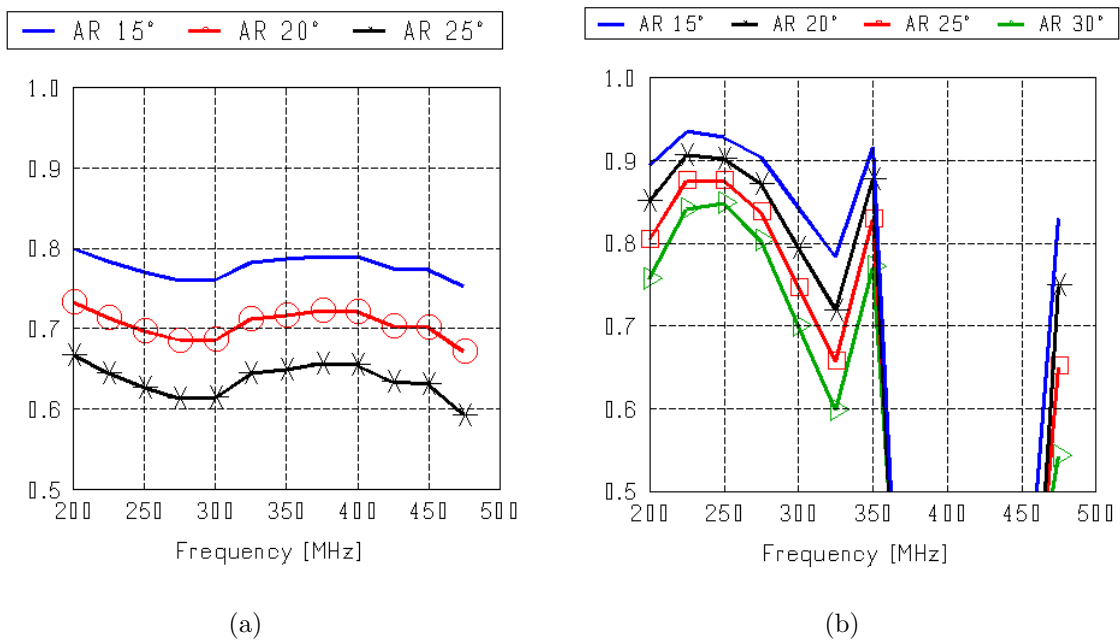


Figure 3.14: LPDA antenna array: (a) axial ratio of the 3×LPDA and (b) modified 3×LPDA.

Chapter 4

Multi-arms Multi-ports Externally-fed Spiral Antennas

The 2×2 arms spiral antenna described in chapter 2 exhibits good characteristics in terms of bandwidth while being externally-fed. The disadvantage of this solution is the radiation of a circular polarization only over a narrow frequency band. To overcome this issue, an investigation on circular arrays have been performed in the previous chapter and an appropriate configuration for externally-fed spiral has been found. In this chapter, two externally-fed spiral antennas designed according to the theory, are studied. In both cases, the antennas have been built and measured to supplement simulation results.

4.1 3×2 Arms Spiral Antenna

In this section, an antenna that meets the requirements is presented. The antenna has been modeled with the software Feko based on the Method of Moments and built. Results coming from simulation and measurements have been compared.

4.1.1 Antenna design

The design is depicted in Figure 4.1. The antenna is made of three couples of microstrip lines wound around the center, making 2 turns. Each couple of microstrip lines is connected to a feed point. The geometry is obtained by two rotations about the center of 120° and 240° of the first couple of lines. Hence, the design is symmetric with respect to the center. All the

geometrical characteristics are given in Table 4.1. The built antenna is printed on a square FR4 substrate with a thickness equal to 0.8 mm.

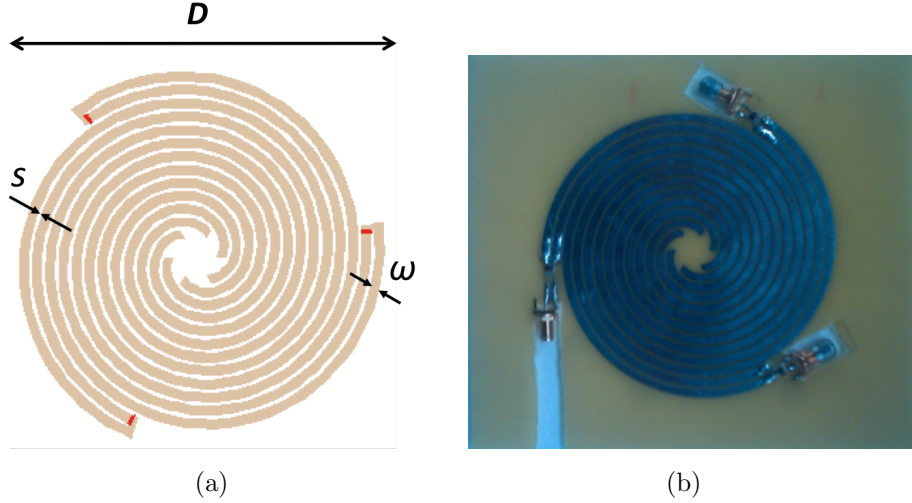


Figure 4.1: 3×2 arms spiral antenna: (a) modeled and (b) built

Table 4.1: Geometrical characteristics

Description	Symbol	Value
Diameter	D	125 mm
Arm width	w	3.3 mm
Space between arms	s	1 mm
Number of turns	N	2

4.1.2 Feeding configuration

The antenna is fed by three different sources. Each source provides a symmetrical feeding which means that each couple of microstrip lines is fed out-of-phase. Basically, this is done by three baluns that achieve the symmetry and an impedance matching. Moreover, a phase difference of 120° is applied between each source. Hence, the design is fed by three balanced

sources with equal amplitude and a phase shift of 0° , 120° and 240° respectively. This implies that the current is symmetric as shown by the current distribution at 750 MHz given in Figure 4.2. For a given position on the antenna, the value of the current is the same at positions corresponding to a rotation about the center of 120° and 240° of the initial one.

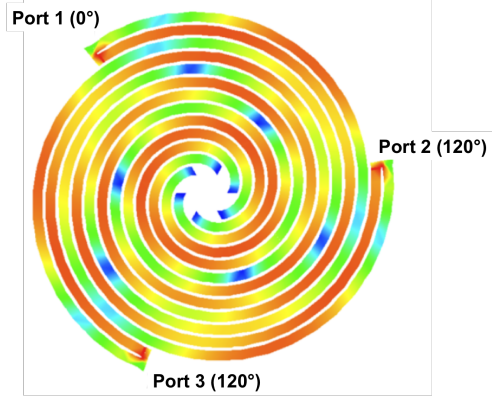


Figure 4.2: 3×2 arms spiral antenna: simulated current distribution at 750 MHz and sources phase shift

4.1.3 Measurement and simulation results

The antenna can be considered as a hexapole defined by its scattering parameters. Hence, the 3×2 arms spiral antenna is characterized by 9 parameters given in the following equation that includes all the coupling between the sources.

$$\begin{pmatrix} b_1 \\ b_2 \\ b_3 \end{pmatrix} = \begin{bmatrix} S_{11} & S_{12} & S_{13} \\ S_{21} & S_{22} & S_{23} \\ S_{31} & S_{32} & S_{33} \end{bmatrix} \begin{pmatrix} a_1 \\ a_2 \\ a_3 \end{pmatrix} \quad (4.1)$$

Here again, due to the symmetrical geometry and the fact that the antenna is a passive and reciprocal element, $S_{11} = S_{22} = S_{33}$ and $S_{12} = S_{21} = S_{13} = S_{31} = S_{32} = S_{23}$. Phase shift of each source implies that $a_2 = a_1 \exp(j\frac{2\pi}{3})$ and $a_3 = a_1 \exp(j\frac{4\pi}{3})$. The RL is then expressed as follows and it can be seen that $RL_1 = RL_2 = RL_3$.

$$\begin{cases} RL_1 = S_{11} + S_{12} \exp(j\frac{2\pi}{3}) + S_{12} \exp(j\frac{4\pi}{3}) \\ RL_2 = S_{12} \exp(-j\frac{2\pi}{3}) + S_{11} + S_{12} \exp(j\frac{2\pi}{3}) \\ RL_3 = S_{12} \exp(-j\frac{4\pi}{3}) + S_{12} \exp(-j\frac{2\pi}{3}) + S_{11} \end{cases} \quad (4.2)$$

Simulated RL calculated with a reference impedance $Z_c = 200 \Omega$ is plotted in Figure 4.3. The baluns do not achieve a good impedance matching and only the simulated RL is shown. Further investigations have to be done to overcome this issue. The antenna starts to radiate from 1.05 GHz where $|\text{RL}| \leq -10$ dB to the end of the frequency range except between 1.2 GHz and 1.29 GHz. For the same diameter, the center-fed spiral antenna achieves a return loss under -10 dB starting from 800 MHz. This difference in the lower frequency band is probably due to the short length of the arms that causes strong reflections in the center of the antenna. Indeed, for the same diameter of antenna, the more arms we add, the shorter the length of the arms becomes. The return loss could be improved by optimizing the center in order to avoid or minimize reflections. A possible solution could be the use of resistive loads in the center to dissipate the power at the cost of the efficiency. In this case, a trade-off has to be found between the RL and the efficiency [13].

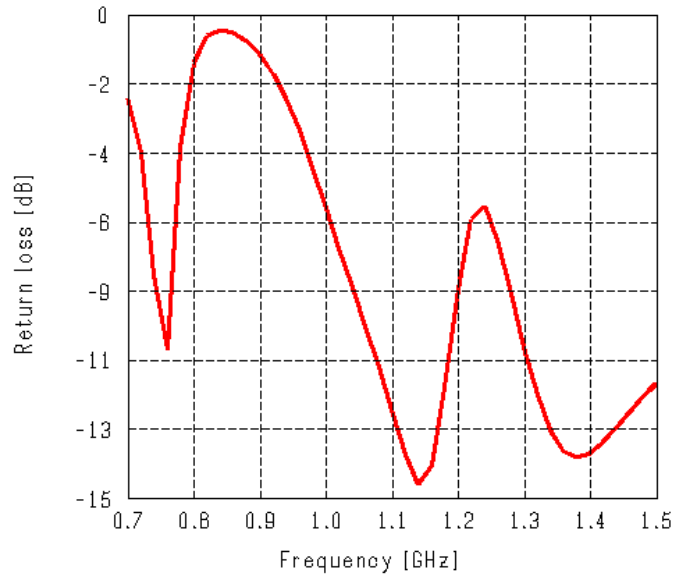


Figure 4.3: 3×2 arms spiral antenna: simulated return loss for a reference impedance $Z_c = 200 \Omega$

A 3D view of the far field pattern at 1 GHz and cuts in elevation of the total gain at three different frequencies are depicted in Figure 4.4. The new design radiates in two directions perpendicular to the antenna plane like the center-fed spiral antenna as shown by the 3D view in Figure 4.4(a). Moreover, the different cuts of the gain in Figure 4.4(b) show that the shape of the radiation pattern remains constant over the frequency range.

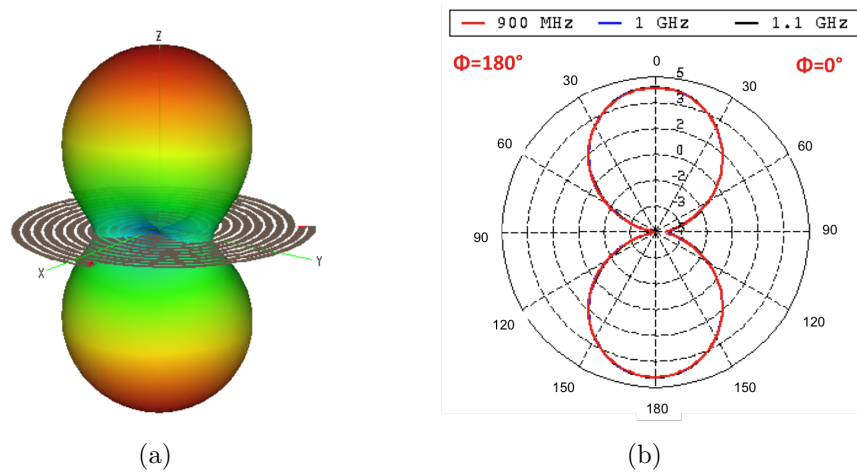


Figure 4.4: 3×2 arms spiral antenna: (a) simulated 3D view of the far field pattern at 1 GHz and (b) cuts in elevation of the total gain in dBi at 900 MHz, 1 GHz and 1.1 GHz

Two different polarizations are radiated, right-hand circular polarization in one direction and left-hand circular polarization in the opposite direction. The AR is plotted against frequency in Figure 4.5 for different values of theta. As expected, a quasi perfect circular

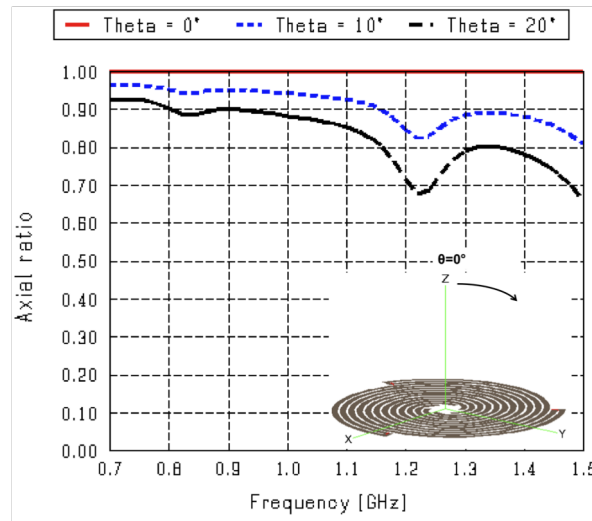


Figure 4.5: 3×2 arms spiral antenna: axial ratio against frequency for $\theta = 0^\circ$, 10° and 20°

polarization is achieved at position $\theta=0^\circ$ and a good circular polarization ($AR > 0.7$) over $\pm 20^\circ$ angle from the boresight. Hence, most part of the power is radiated with a circular polarization.

Due to the number of sources, the antenna is reconfigurable in terms of polarization. Depending on the phase shift between the sources, the antenna radiates a different polarization. The two configurations are given in Figure 4.6. For each case, a cut in elevation of the total gain and the AR is plotted at 1 GHz. In the first configuration plotted in blue, the three sources are fed with a phase shift of 0° , 120° and 240° respectively. For the second configuration, plotted in red line, the order of the phase shift of two sources is reversed, e.g. 0° , 240° and 120° . The two configurations are summarized in Table 4.2.

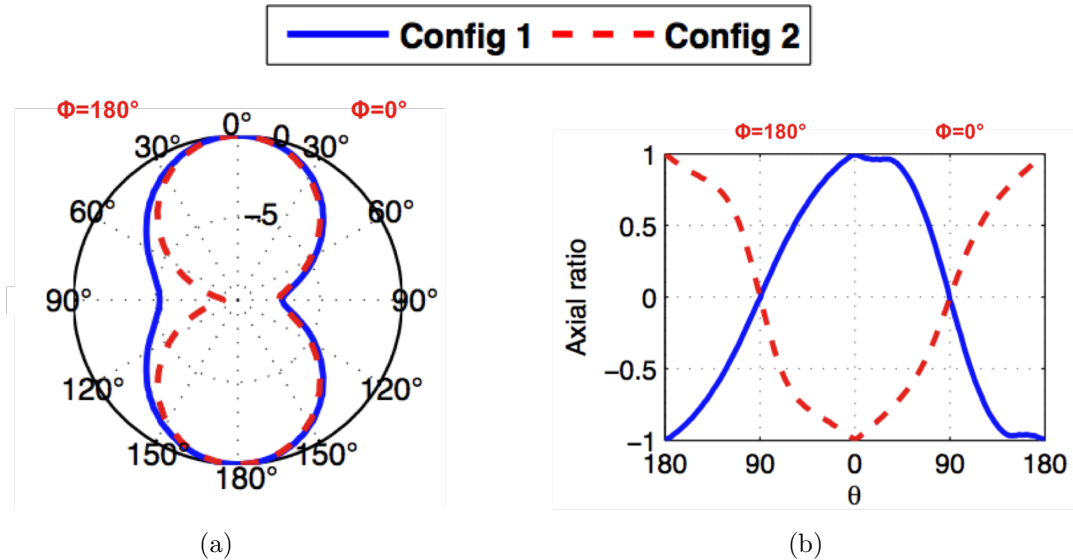


Figure 4.6: 3×2 arms spiral antenna: (a) simulated cuts in elevation of the normalized gain and (b) the AR at 1 GHz

In both cases, the electric far field patterns are symmetric about the plane of the antenna as shown in Figure 4.6(a). However, the patterns are not symmetric about the boresight axis due to the positions of the sources and a skewness is observed in the two opposite AR plotted in Figure 4.6(b). The radiated polarization at position $\theta = 0^\circ$, is perfectly right hand circular for configuration 1 and perfectly left hand circular for configuration 2. Hence, the radiated polarization is reconfigurable by only modifying the order of the phase shifts of the sources.

Table 4.2: *Phase shift configurations at $\theta=0^\circ$*

	Port 1	Port 2	Port 3	Polarization
Configuration 1	0°	120°	240°	RHCP
Configuration 2	0°	240°	120°	LHCP

The antenna has been measured in the anechoic chamber at SUPELEC. Here again, the measurement method presented in chapter 2 has been used. Therefore, the 3×2 arms spiral antenna has been measured feeding only one source, while the two others are matched to their reference impedance ($Z_c = 200 \Omega$). Far field pattern of the others sources are deduced by rotation of 120° and 240° of the first one around the axis perpendicular to the antenna plane and a phase shift of 120° and 240° is added to the rotated pattern. The total far field pattern is equal to the superposition of the three patterns.

The results are given in Figure 4.7 at two frequencies. For each frequency, cuts in elevation of the normalized gain and the AR is plotted with a 3D view of the measured total gain. Measurement results appear in red line with crosses and the simulation results are plotted in black. The symmetrical feeding is well achieved by the baluns and good agreement is shown between the simulation and measurement results. The cut of the total gain corresponds to the black cross in the 3D view. The antenna exhibits a far field pattern, with two main directions of propagation, which is similar to the simulation results. Moreover, the AR shows that two crossed polarizations are radiated. At position $\theta=0^\circ$ which belongs to the first main beam, the radiated polarization is perfectly right hand circular (AR is equal to 1). Symmetrically on the second main beam at $\theta=180^\circ$, the polarization is perfectly left hand circular (AR is equal to -1).

An externally-fed spiral antenna has been presented in this section. This design is fed by three sources located on its plane. Return loss under -10 dB is achieved in theory from 1.05 GHz to 1.5 GHz except from 1.2 GHz to 1.29 GHz and could be improved by reducing the reflections in the center. The measured antenna exhibits a perfect circular polarization in direction $\theta=0^\circ$ and a good circular polarization within a $\pm 20^\circ$ aperture from the boresight. Moreover, the polarization is reconfigurable in a right or left hand circular polarization. Simulation results have been compared to measurements achieved in an anechoic chamber and a good agreement is obtained. The balun performs a well balanced feeding but not a good matching. In order to improve the antenna characteristics, a new antenna has been studied to avoid the use of baluns. This antenna is presented in the next part.

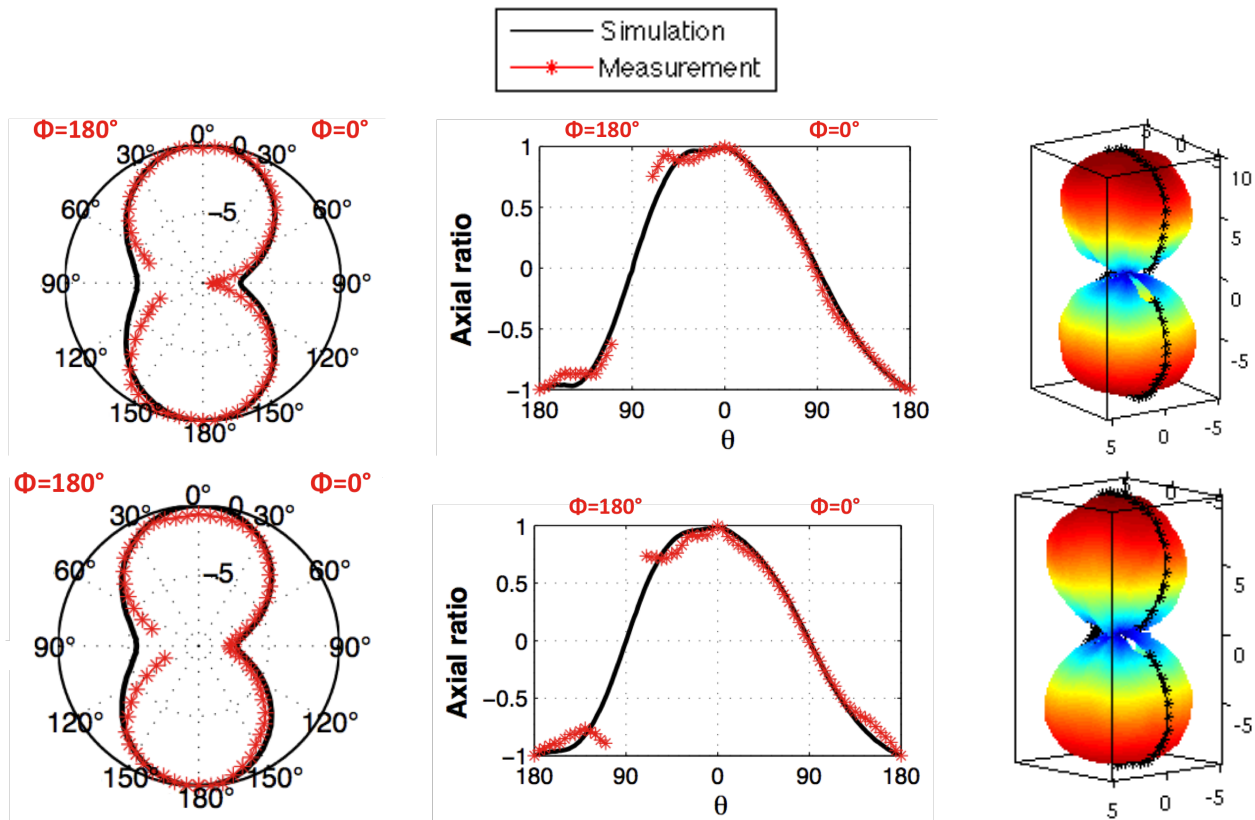


Figure 4.7: 3×2 arms spiral antenna: comparison of the measured and simulated cuts in elevation of the normalized gain (left), AR (center) and a 3D view of the measured gain (right) at 1000 MHz (top) and 1040 MHz (bottom)

4.2 4×2 Arms Spiral Antenna

In this section, an another externally-fed spiral antenna is studied. The antenna has been modeled with CST Microwaves Studio® software [23]. Measurements have been done and the results are compared with simulated ones.

4.2.1 Antenna design

Unlike the 3×2 arms spiral antenna, this new design is a slot antenna. In this case, the 4×2 arms spiral antenna consists of a slot cut in a plate of metal. The designed and built antennas are shown in Figure 4.8. Four couples of slot lines are wound around the center on a copper plate of 13 cm ×13 cm on a substrate of FR4 with a thickness of 0.8 mm. Taking a couple of slot lines as reference, the geometry of the antenna corresponds to three rotations of these lines of 90°, 180° and 270° around the center. This results in a symmetrical design with respect to the center. Each couple of line starts with a short straight tapered line before being wound in a spiral shape. The geometrical characteristics are provided in Table 4.3.

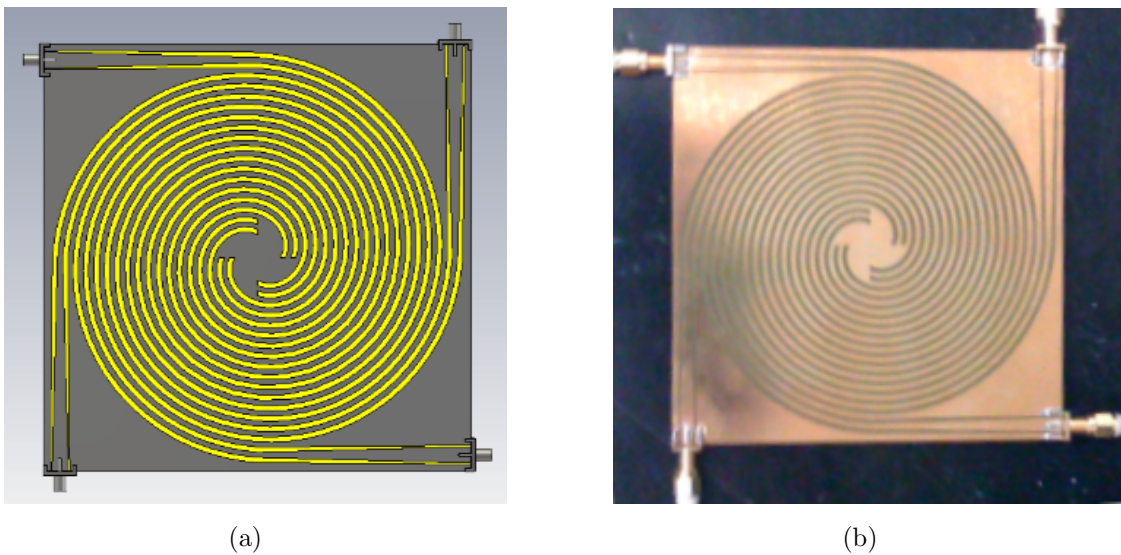


Figure 4.8: 4×2 arms spiral antenna: (a) modeled and (b) built

Table 4.3: *Geometrical characteristics*

<i>Description</i>	<i>Values</i>
<i>Diameter</i>	125 mm
<i>Slot width</i>	1.59 mm
<i>Space between slots</i>	1.59 mm
<i>Number of turns</i>	2

4.2.2 Feeding configuration

At each feed point, the slot lines provide three areas of copper connected to a SMA connector. The inner pin is connected between the slots and the outer conductor is connected on each side of the slots. Four sources provide thus an unbalanced signal to the antenna and a phase shift of 90° is applied between two consecutive sources. Hence, the antenna is fed by four unbalanced signal with a phase shift of 0° , 90° , 180° and 270° respectively. Due to the symmetry of the geometry and the feeding, the current is symmetric on the antenna. This property leads to a symmetrical far field pattern that is shown further in this section. The tapered coplanar slot lines are used as a matching transition from the input impedance of the antenna to 50Ω . In this case, baluns are not longer needed and the 4×2 arms slot antenna could be simply fed by coaxial cables. All the issues due to the baluns are then avoided.

4.2.3 Measurement and simulation results

Simulated and measured RL calculated with a reference impedance of 50Ω are depicted in Figure 4.9. Measurement result is plotted in red dashed line and the simulation is in black line. Like the 3×2 arms spiral antenna, the antenna is defined by its scattering parameters. Since there are four feed points, the design is an octopole. With the effect of all the sources, the RL is expressed as follow:

$$RL = S_{11} + S_{12} \exp(j\frac{\pi}{2}) + S_{13} \exp(j\pi) + S_{14} \exp(j\frac{3\pi}{2}) \quad (4.3)$$

Hence, the 16 scattering parameters have been measured to determine the return loss. The curve is the same at each feed point due to the symmetry in the design and feeding. Simulated curve fits very well with measurement of Figure 4.9. According to the measurement results, the antenna starts to radiate at 1.25 GHz up to 2 GHz with a $|RL| \leq -10$ dB. Here again, the

bandwidth could be improved by reducing the reflections in the center. Moreover, the transition slot lines could be further optimized to enhance the matching impedance at the lower frequencies. A possible solution could be the use of miniaturization techniques [25] [14] [26].

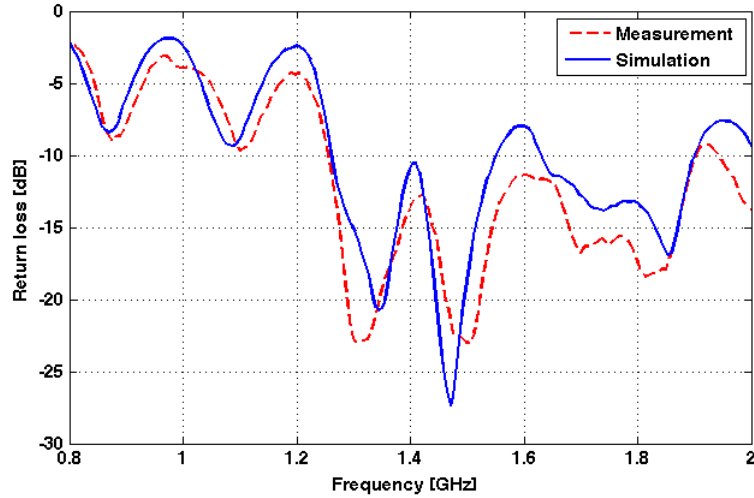


Figure 4.9: 4×2 arms spiral antenna: comparison of the measured and simulated return loss against frequency for a reference impedance $Z_c = 50 \Omega$

The 3D view of the far field pattern at 1 GHz and an elevation cut of the total gain in dBi at four different frequencies are given in Figure 4.10. From the 3D view, it could be seen that the plane of the antenna corresponds to a plane of symmetry of the radiation pattern. Moreover, the shape of the far field pattern is the same over the frequency band as shown in Figure 4.10(b). For all the frequencies, two main beams are radiated.

The performances in terms of polarization are described in Figure 4.11. The simulated AR is plotted against frequency for $\theta = 0^\circ$ to 50° by step of 10° . All the curves are above 0.7 except for $\theta = 50^\circ$. The 4×2 arms spiral antenna exhibits a perfect circular polarization on the boresight. The purity of the polarization decreases when θ moves away from the boresight until a value lying between 40° and 50° . Hence, the angular range corresponding to a good circular polarization is found at least between $\pm 40^\circ$ from the boresight, i.e. in an angle of 80° . As a result, most part of the power is radiated with a circular polarization.

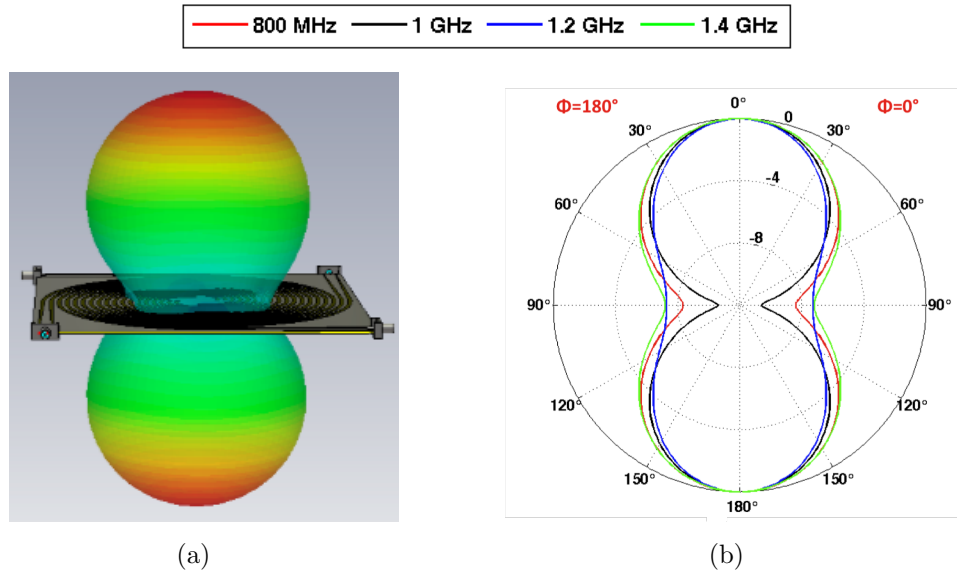


Figure 4.10: 4×2 arms spiral antenna: (a) 3D view of the simulated far field pattern at 1 GHz and (b) elevation cuts of the total gain in dBi at 0.8 GHz, 1 GHz, 1.2 GHz and 1.4 GHz

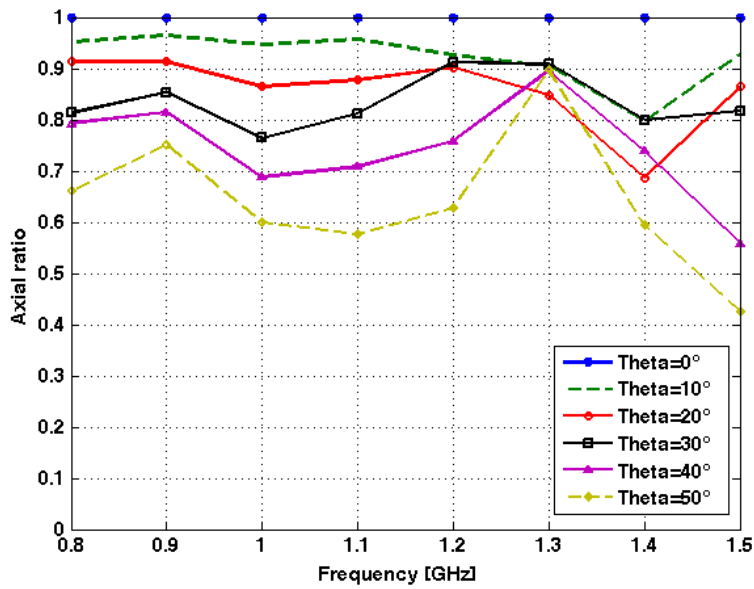


Figure 4.11: 4×2 arms spiral antenna: simulated axial ratio against frequency for $\theta = 0^\circ$ to 50°

Due to the number of sources, the antenna provides all polarizations. Depending on the phase shift and the voltage applied to the sources, different polarizations are radiated. For each case, a cut in elevation is plotted in Figure 4.12 with the associated axial ratio. All the configurations are summarized in Table 4.4. Whatever the case, the radiated pattern is the same as shown in Figure 4.12(a). This is not the case for the polarization. In the two first configurations, all the sources are fed with the same voltage and a phase shift of 0° , 90° , 180° and 270° or reversed. This leads to the radiation of a left or right hand circular polarization as described by the two curves symmetrical about the axis $AR=0$. For the two last configurations, only two of the four sources are fed with a phase shift of 180° . The two non-fed sources are matched to 50Ω and are designated by a cross in Table 4.4. When the sources 1 and 3 are fed, a linear horizontal polarization is radiated around $\theta=0^\circ$. However, when the sources 2 and 4 are fed, the radiated polarization is linear and vertical. In these cases, the AR is close to 0 around $\theta=0^\circ$. This antenna could be used as a multifunction antenna with a tunable polarization.

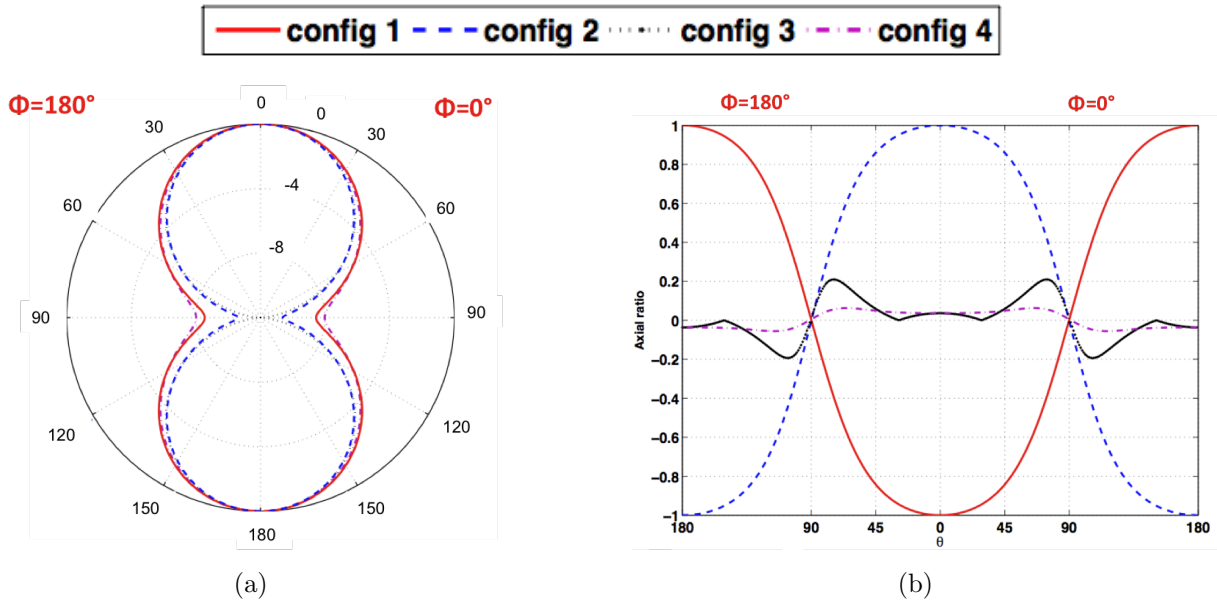


Figure 4.12: 4×2 arms spiral antenna: (a) simulated cuts in elevation of the normalized gain and (b) AR at 1 GHz

Table 4.4: *Phase shift configurations at $\theta=0^\circ$*

	Port 1	Port 2	Port 3	Port 4	Polarization
Configuration 1	0°	90°	180°	270°	LHCP
Configuration 2	0°	270°	180°	90°	RHCP
Configuration 3	0°	x	180°	x	H
Configuration 4	x	0°	x	180°	V

Measurement results and simulation ones are compared in Figure 4.13. The superposition method has been used as for the 3×2 arms spiral antenna. Hence, a measured far field pattern is obtained by feeding only one source and by matching the others. The total far field pattern is then constructed by adding the contribution of all the sources. The results are given at the frequencies 0.8 GHz, 1.1 GHz and 1.5 GHz in Figure 4.13. For all cases, a 3D view of the measured pattern is provided and a cut in elevation of the normalized gain and AR is plotted. The antenna has been measured in the same anechoic chamber as the previous antenna. Therefore, there is an angular range without data. Moreover, due to the rotations applied to obtain the total far field data, this angular range is also rotated. This leads to another area of θ without data. This is why the curves of the measurement results are not continuous. From the gain and the AR, it can be seen that the measurement results fit well with the simulation. For all cases, a perfect circular polarization is achieved in direction $\theta=0^\circ$ and the polarization remains good over a wide angular range. The 3D view of the radiated pattern exhibits two main beams as expected.

The 4×2 arms spiral antenna has the particularity to be an externally-fed slot antenna. The design is fed by four unbalanced sources on the same plane as the antenna. A matching transition is achieved to match the antenna to 50Ω . Therefore, a simple coaxial cable could be used and the issues with the baluns are avoided. The antenna exhibits a bandwidth starting from 1.25 GHz to 2 GHz and could be improved by optimizing the center and the matching transition. For this frequency band, a circular polarization is radiated over an angular range equal at least to $\pm 40^\circ$ from the boresight. Moreover, the antenna is reconfigurable in four different polarizations.

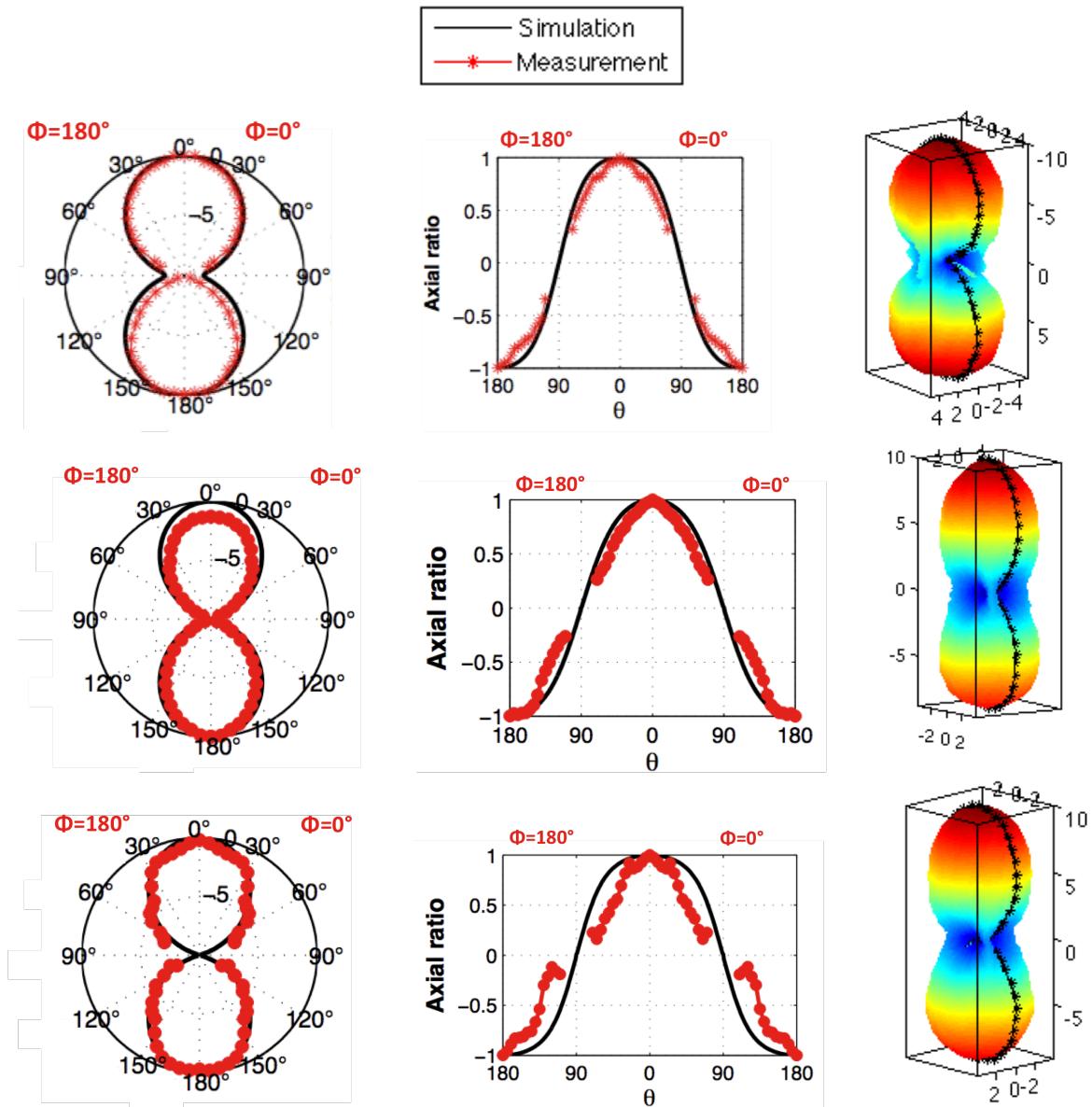
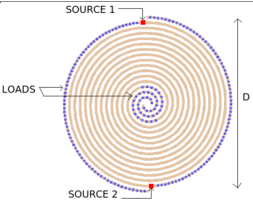
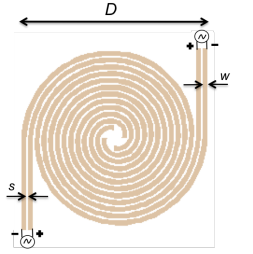
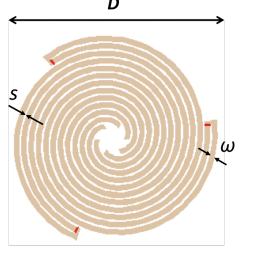
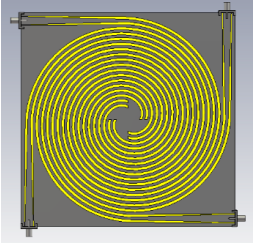


Figure 4.13: 4×2 arms spiral antenna: comparison of the measured and simulated cuts in elevation of the normalized gain (left), AR (center) and a 3D view of the measured gain (right) at 0.8 GHz (top), 1.1 GHz (middle) and 1.5 GHz (bottom)

4.3 Conclusion of Chapter 4

In this chapter, two externally-fed spiral antennas have been studied. The first one is a coplanar microstrip antenna fed by three sources. Three baluns are used to achieve a matching impedance and a balanced feeding. However, the matching impedance is not good and further investigations have to be done to overcome this issue. The signal is well balanced and a good agreement has been obtained between the measured and simulated far field. The antenna radiates a circular polarization over an angular aperture of $\pm 20^\circ$ from the boresight and is reconfigurable with two crossed polarizations. The second antenna is a slot antenna fed by four sources. The design exhibits an input impedance close to 50Ω , therefore the baluns are no more necessary. In this case, the feeding is simpler and a good agreement is observed between the measured and simulated return loss and far field data. The 4×2 arms spiral antenna radiates a good circular polarization within an angular range of 80° and is reconfigurable in four different polarizations (linear vertical/horizontal and circular right/left). In both cases, the antennas could be used when the center is not accessible for feeding. However, the 4×2 arms slot spiral antenna is a better candidate since it is easier to feed. Moreover, the radiated characteristics are better than those of the 3×2 arms spiral antenna. Finally, in order to feed all the sources of the antennas, a 90° and 120° wideband phase-shifter are needed. Here again, it is easier to find a 90° wideband phase-shifter than a 120° one.

Table 4.5: Summary of the antennas characteristics

<i>Design</i>	<i>Nb of feed</i>	F_{min} for RL ≤ -10 dB	<i>Radiation pattern</i>	<i>Polarization</i>
	2	$f_{min} = 830$ MHz	Symmetric	$f_{AR \geq 0.7} = 880$ MHz
	2	$f_{min} = 650$ MHz	Symmetric	$f_{AR \geq 0.7} = 1-1.05$ GHz
	3	$f_{min} = 1.05$ GHz	Symmetric	$f_{AR \geq 0.7} = 0.7-1.5$ GHz
	4	$f_{min} = 1.25$ GHz	Symmetric	$f_{AR \geq 0.7} = 0.7-1.5$ GHz

Conclusion

This PhD thesis work focuses on the feeding of the spiral antenna. In order to make the spiral suitable for radar application on airship, the feeding has been moved from the center to the outermost arms. Several solutions of externally-fed spiral antennas has been developed. For each case, the feeding is contained in the plane of the antenna, which makes easier to integrate the spiral on platforms that do not allow to reach its center. The investigated solutions can be decomposed in 5 items.

- The first solution combines the spiral geometry with two sources. Like the Archimedean center-fed spiral antenna, this design is based on the principle of a symmetrical geometry and current distribution. Resistive loads are added to the structure in the center and the outermost arms to avoid the reflections of the current wave that decrease both the purity of the polarization and the RL bandwidth. The behavior of this antenna is close to that of the center-fed one. Furthermore, a circular polarization is radiated over a frequency band improved of about 120 MHz, which increases the functional bandwidth. However, the low efficiency and the difficulty to mount the resistive loads on the spiral make this antenna not suitable.
- The 2×2 arms spiral antenna has been created following the same principles used for the previous spiral. Resistive loads have been avoided in this design by winding the two arms connected to the feed points. This antenna exhibits a frequency band extended about 150 MHz compared to the center-fed spiral. The far field pattern is symmetric about the plane of the antenna. However, unlike the Archimedean spiral antenna, the radiated polarization is circular only over a narrow frequency band. In order to supplement the simulation results, a prototype has been built. The two baluns used to balance the feeding introduce an insertion loss that degrades the measured return loss. However, the feeding is well balanced and good agreement is shown between simulation and measurement results. This antenna is a good solution for applications that require

a spiral antenna externally-fed without a circular polarization. Although, in our case, a circular polarization is required, therefore this design has not been chosen.

- The developed antennas are fed by more than one source on their plane. They can be seen as a small array highly coupled where the elements are placed around a circle. In order to improve the polarization of the antennas, investigations have been done on the antenna array with a circular geometry and on the sequential rotations techniques. These investigations have led to the conclusion that a circular polarization is obtained, whatever the polarization of the antennas inside the array, when the array is composed of at least three elements placed around a circle. The theory of this kind of array has been studied and simulated with an array of dipoles. Moreover, the theory has been applied to a simulated and measured array of 4 LPDA.
- The theory has been applied to the spiral which gave rise to the 3×2 arms externally-fed spiral antenna. This design is fed by 3 sources connected to three pair of microstrip lines. As expected, a circular polarization is achieved over an angular range of $\pm 20^\circ$ from the boresight. The functional frequency band starts from 1.05 GHz to 1.5 GHz. Due to the number of sources, the antenna is reconfigurable in a right or left hand circular polarization. A prototype has been built and measured. As for the 2×2 arms spiral antenna, baluns are used to balance the feeding which degrades the return loss. However, the feeds are well balanced and good agreement is obtained between simulation and measurement results. This design is very interesting but the use of baluns makes the antenna not usable. Moreover, 120° wideband phase-shifter are not easy to find.
- The 4×2 arms externally-fed spiral antenna has also been developed according to the theory of the array with a circular geometry combined with sequential rotation technique. This antenna has the particularity to be a slot antenna fed by 4 unbalanced sources on its plane. Moreover, a matching slot lines transition to 50Ω is achieved to match the impedance of the antenna to a coaxial cable. The baluns are then avoided in this design and good agreement is shown between the measured and simulated return loss. The antenna has been measured in anechoic chamber and good agreement is observed between the simulated and measured far field. The 4×2 arms spiral antenna exhibits a far field pattern similar to the center-fed spiral over a frequency range comprise between 1.25 GHz and 2 GHz. The radiated polarization is circular over an

angular range up to $\pm 40^\circ$. With 4 ports, the antenna is reconfigurable in 4 polarizations, linear horizontal/vertical and circular right/left.

Several perspectives could be mentioned to conclude this thesis work:

- The baluns used with the antennas achieve a well balanced feeding but not a good matching impedance. In order to overcome this issue and to improve the RL bandwidth, it could be interesting to design a transition lines to match the input impedance of the antenna to 50Ω and to use baluns only to balance the feeding.
- The 4×2 arms spiral antenna is fed without baluns and good agreement is shown between the measured and simulated RL. However, the RL bandwidth has to be improved, especially at the lower frequencies. This could be done by optimizing the design of the transition slot lines for a better matching impedance. Moreover, the center of the spiral could be modified to avoid or reduce reflections at these frequencies.
- The total far field pattern of the 4×2 arms spiral antenna has been obtained from the measured pattern of a single source fed while the others are matched to 50Ω . In order to fully characterize the antenna, the 4 sources should be fed simultaneously with the appropriate phase shifts.

Publications

Journals

- K. Louertani, R. Guinvarc'h, N. Ribiere-Tharaud and M. Hélier, "Multi-arms Multi-ports Externally Fed Spiral Antenna", submitted to IEEE transaction on ANTENNAS AND PROPAGATION

Conferences

- K. Louertani, N. Ribière-Tharaud, R. Guinvarc'h and M. Hélier, "External and Coplanar Feeding for Spiral Antenna," in *Proc. IEEE International Symposium on Antennas and Propagation*, Toronto, Canada, July 2010
- K. Louertani, R. Guinvarc'h , N. Ribière-Tharaud and M. Hélier, "Alimentation d'une antenne spirale par l'extérieur", in *GDR Ondes*, Paris, France, October 2009
- K. Louertani, N. Ribière-Tharaud, R. Guinvarc'h and M. Hélier, "Coplanar Feeding Solution For Spiral Antenna," in *Proc. IEEE International Symposium on Antennas and Propagation*, Charleston. SC, USA, June. 2009.
- K. Louertani, N. Ribière-Tharaud, R. Guinvarc'h and M. Hélier, "Solution d'alimentation planaire pour antenne spirale", in *Proc. Journée Nationales Microondes*, Grenoble, France, Juin. 2009.
- K. Louertani, R. Guinvarc'h, N. Ribière-Tharaud and M. Darces, "Design of a Spiral Antenna with Coplanar Feeding Solution," in *Proc. IEEE International Symposium on Antennas and Propagation*, San Diego. CA, USA, July. 2008.

Appendix

List of the components used for the antenna building

- **Substrate:** 25N (Cirly)
- **Transformer:** TC4-14+ (Minicircuits)
- **Antenna prototype:** 2x2 arms typon
- **Antenna prototype:** 3x2 arms typon
- **Antenna prototype:** 4x2 arms typon

Appendix A

Substrate and balun datasheets



MULTI-FUNCTIONAL FR-4 LAMINATE Tg-130 °C

Approvals	UL	: File No. E124601	Designation: EEL-145
Description	Multi-functional FR-4 Laminates Tg-130 °C with single- or double-sided copper-clad manufactured by using precise blend of tetrafunctional and difunctional epoxy resin with flame retardant property , reinforced with Electrical grade (E-glass) glass fabric to provide the exceptional printed wiring board (PWB) performance.. Superior low coefficient of Thermal Expansion (CTE Z-axis) to be advantage to lead free PCBA assembly process.		
Type	Epoxy/Woven E- Glass Fabric – flame resistant UL V-0, NEMA FR4,		
Copper Foil	Electrodeposited, standard ductility , HTE type. Thickness: 18, 35, 70 , 105, 140 and 175 μ m Other thickness and foil types upon request		
Surface Quality	Class A of IPC-4101		
Thickness	Range	: 0.1 mm ~ 1.6 mm (4 mil ~ 63 mil)	
	Tolerance	: In accordance with IPC-4101 Class B/L Special tolerance upon request.	
Size	Full sheet	: 914 mm x 1219 mm (36" x 48") 939 mm x 1244 mm (37" x 49") 990 mm x 1244 mm (39" x 49") 1041 mm x 1244 mm (41" x 49") 1092 mm X 1244 mm. (43" X 49") Tolerance: -0 mm, \leq +2 mm Cut-to-size panels also available upon request. Panel Tolerance: -0 mm, \leq +2 mm	
Special Feature	UV Block effects to prevent shoot through (Mirror effect). Laser Fluorescence effect for better AOI performance.		
Applications	Communications, Measuring Instruments, Digital home appliances, Computers and peripherals, Industrial controls, and automotive.		

**LAMINATE SPECIFICATION**

Description	IPC-TM-650 Method	Unit	Requirement	Typical value (as 59 mils)
Peel Strength After thermal stress (< 20 mil/≥ 20 mil)				
A. Low profile Copper foil	2.4.8	lb/inch	3.9/3.9	6.5/6.8
B. STD Foil	2.4.8	lb/inch	4.5/5.9	11.0/13.0
Water Absorption	2.6.2.1	%	≤ 0.35	0.10
Glass Transition Temperature (8 x 7628) by DSC	2.4.25	°C	≥ 130	135-140
Dimensional Stability (≤ 20 mil)	2.4.39	mil/inch	≤ 0.5	0.1
Thermal stress 10 sec @ 288°C	2.4.13.1	sec	Pass Visual	Pass (Max. 200 sec)
Volume Resistivity After moisture resistance	2.5.17.1	MΩ . cm.	≥ 10 ⁶	1.84 x 10¹⁰
Surface Resistivity After moisture resistance	2.5.17.1	MΩ	≥ 10 ⁴	1.9 x 10⁷
Permittivity at 1 MHz	2.5.5.4	-	≤ 5.4	4.45
Dissipation Factor at 1MHz	2.5.5.4	-	≤ 0.035	0.015
Permittivity at 1 GHz	2.5.5.4	-	N/A	4.20
Dissipation at 1 GHz	2.5.5.4	-		0.019
Electric Strength (< 20 mil)	2.5.6.2	kV/mm	≥ 30	N/A
Dielectric Breakdown (≥ 20 mil)	2.5.6	kV	≥ 40	50
Flexural Strength (≥ 20 mil)				
A. Length Direction	2.4.4	Kg/M ²	4.23 x 10 ⁷	6.23 x 10⁷
B. Cross Direction			3.52 x 10 ⁷	6.77 x 10⁷
Flammability	UL 94	-	V-0 (UL Approved)	V-0
Comparative Tracking Index	IEC 112	-	UL Approved	Class 3
Coefficient Thermal Expansion (Z-axis)				
- Pre Tg	2.4.24	ppm/°C	N/A	40
- Post Tg		ppm/°C		250
- 50 C to 260 C.		%		3.5
Thermal degradation temperature , Td	2.4.24.6	Deg.C	N/A	300
Time to Delamination , T260	2.4.24.1	Minutes	N/A	20
Time to Delamination , T288	2.4.24.1	Minutes	N/A	1



Remarks:

1. Test results are determined in the company laboratory and government approved outside laboratories.
2. All data given in this specification sheet are based on IPC-4101/21 and IPC-TM-650 test methods except those marked with UL approval. The above data is guaranteed when using the test methods referenced. We cannot assure these results when different methods and applications are used.
3. Refer to IPC-4101, IPC-TM-650 for other laminate properties or specifications not described herein.
4. Any other laminate properties and specifications require shall be clearly stated on the customer's material specification or purchase order.
5. RoHS Compliance.

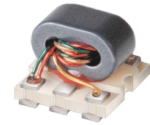
PACIFIC INSULATING MATERIAL (THAILAND) LIMITED

1/68 Moo 5 Rojana Industrial Park,
Rojana Rd, Tambon Khanham, Amphur Uthai,
Pranakornsriyayuthaya, Thailand 13210
Tel: 66-35- 330774, 330776 Fax: 66-35-330775
E-mail: suwanna@elecektek.com

Surface Mount RF Transformer

TC4-14+

50Ω 200 to 1400 MHz



CASE STYLE: AT224-1
PRICE: \$1.29 ea. QTY (100)

+ RoHS compliant in accordance
with EU Directive (2002/95/EC)

The +Suffix has been added in order to identify RoHS
Compliance. See our web site for RoHS Compliance
methodologies and qualifications.

Maximum Ratings

Operating Temperature	-20°C to 85°C
Storage Temperature	-55°C to 100°C
RF Power	0.25W
DC Current	30mA

Pin Connections

PRIMARY DOT	6
PRIMARY	4
SECONDARY DOT	3
SECONDARY	1
SECONDARY CT	2

Features

- good return loss
- wideband, 200 to 1400 MHz
- plastic base with leads
- aqueous washable

Applications

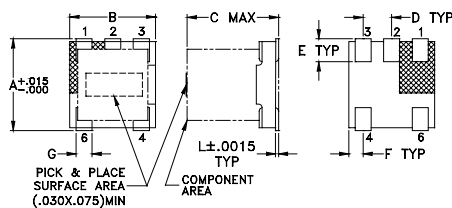
- push-pull amplifiers
- impedance matching

Transformer Electrical Specifications

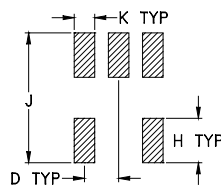
Ω RATIO (Secondary/Primary)	FREQUENCY (MHz)	INSERTION LOSS*		
		3 dB MHz	2 dB MHz	1 dB MHz
4	200-1400	200-1400	300-1300	800-1100

* Insertion Loss is referenced to mid-band loss, 0.7 dB typ.

Outline Drawing AT224-1



PCB Land Pattern



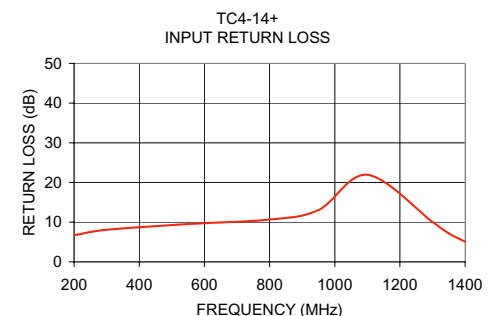
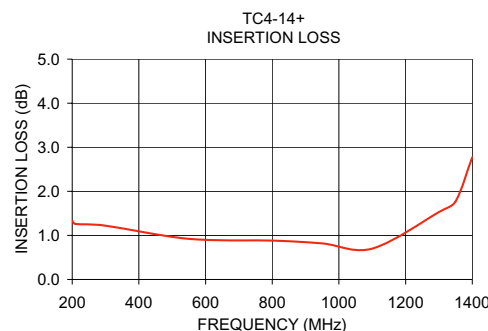
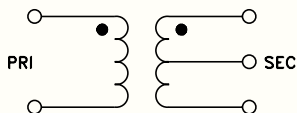
Outline Dimensions (inch/mm)

A	B	C	D	E	F
.150	.150	.160	.050	.040	.025
3.81	3.81	4.06	1.27	1.02	0.64
G	H	J	K	L	wt
.028	.065	.190	.030	.007	grams
0.71	1.65	4.83	0.76	0.18	0.15

Typical Performance Data

FREQUENCY (MHz)	INSERTION LOSS (dB)	INPUT R. LOSS (dB)
200.00	1.33	6.74
210.00	1.26	6.88
300.00	1.22	8.07
550.00	0.92	9.54
800.00	0.88	10.68
950.00	0.82	13.05
1100.00	0.70	21.93
1300.00	1.53	10.04
1350.00	1.77	7.15
1400.00	2.77	5.05

Config. A



Mini-Circuits®
ISO 9001 ISO 14001 CERTIFIED

ALL NEW
minicircuits.com

P.O. Box 350166, Brooklyn, New York 11235-0003 (718) 934-4500 Fax (718) 332-4661 For detailed performance specs & shopping online see Mini-Circuits web site



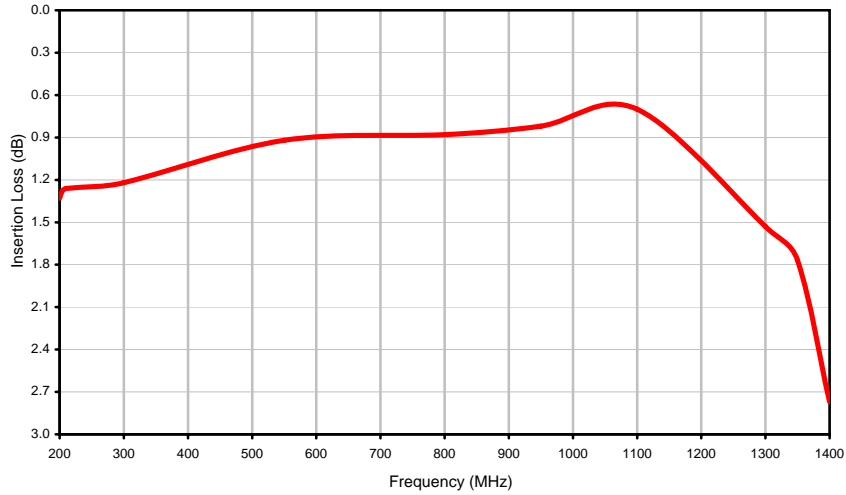
The Design Engineers Search Engine Provides ACTUAL Data Instantly From MINI-CIRCUITS At: www.minicircuits.com

RF/IF MICROWAVE COMPONENTS

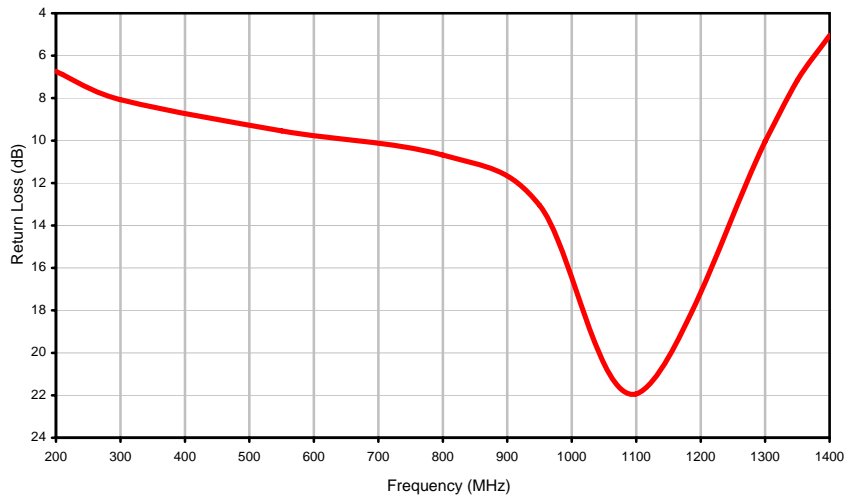
REV. B
M111888
TC4-14+
IG/TD/CP/AM
070625

Typical Performance Curves

Insertion Loss



Return Loss



Appendix B

Typon of the prototypes

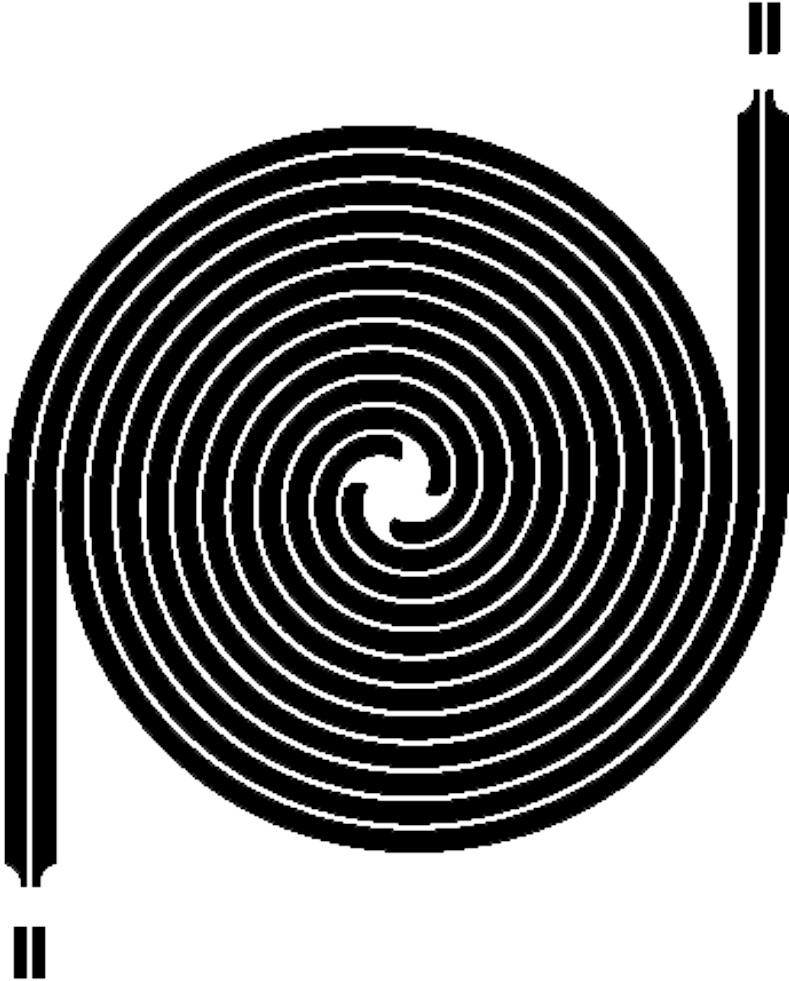


Figure B.1: *Typon of the 2x2 arms spiral antenna*

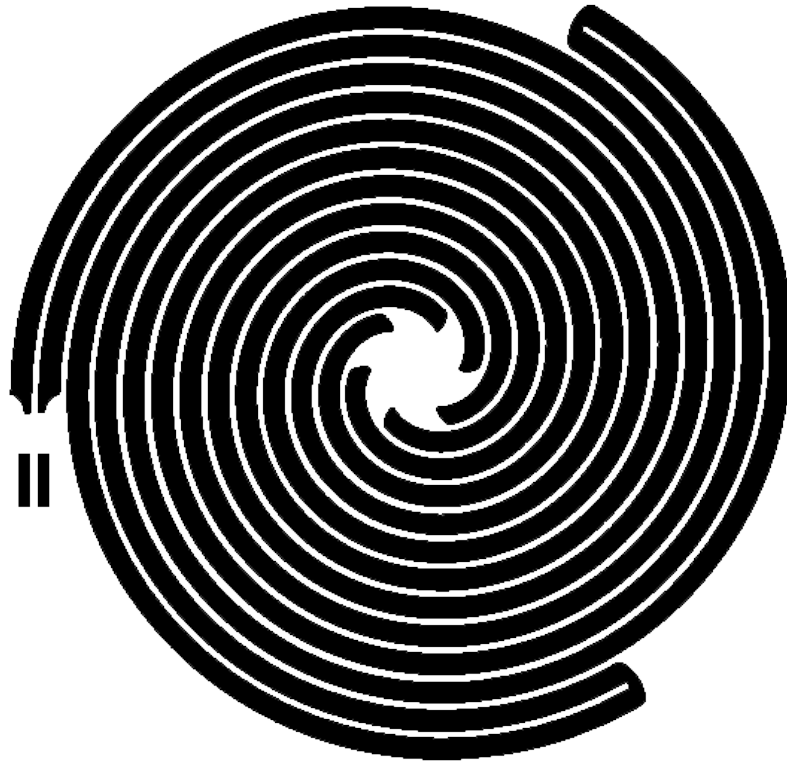


Figure B.2: *Typon of the 3×2 arms spiral antenna*

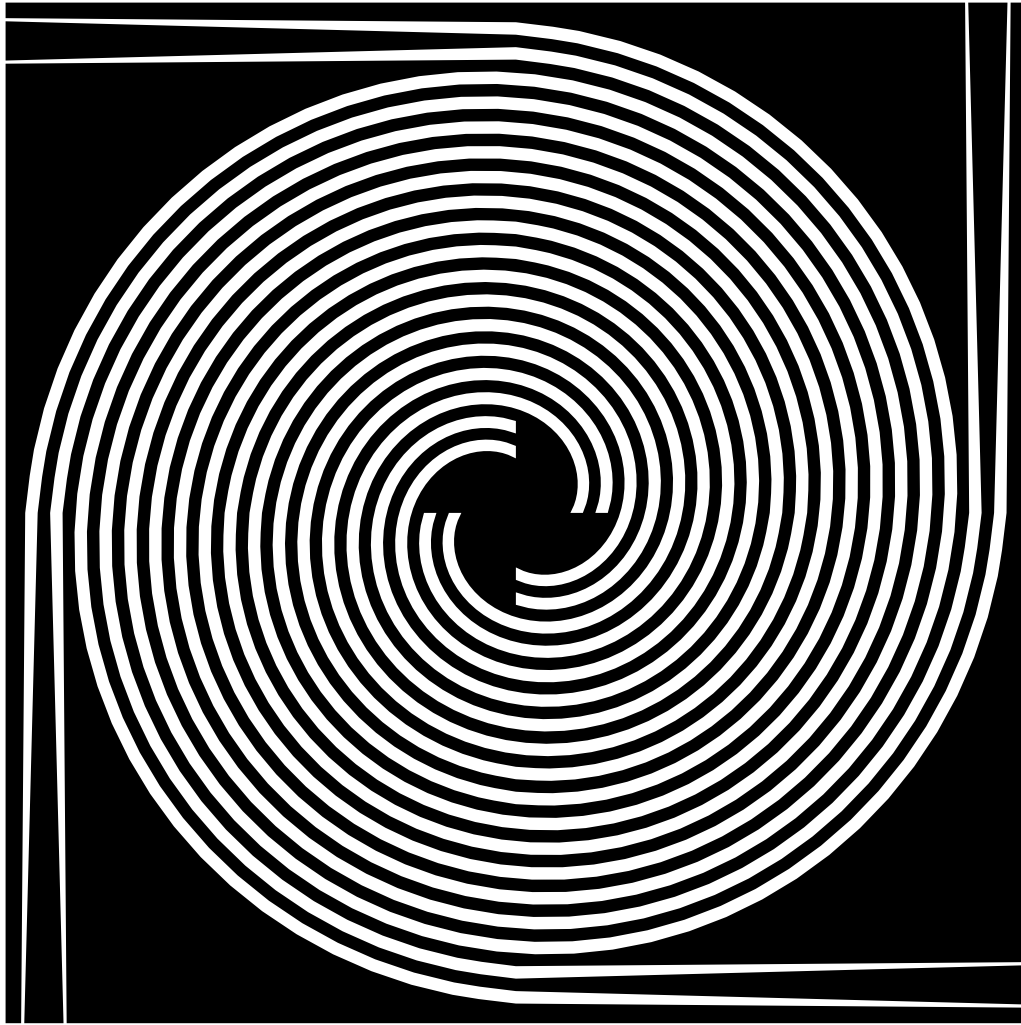


Figure B.3: *Typon of the 4×2 arms spiral antenna*

Bibliography

- [1] F. Chauvet, *Conformal, wideband, dual polarization phased antenna array for UHF radar carried by airship*, Ph.d, UPMC/Sondra, Paris 6, Jan. 2007.
- [2] D. J. Muller and K Sarabandi, "Design and analysis of a 3-arm spiral antenna," *IEEE Transactions on Antennas and Propagation*, vol. 55, no. 2, pp. 258–266, Feb. 2007.
- [3] E. Gschwendtner and W. Wiesbeck, "Ultra-broadband car antennas for communications and navigation applications," *IEEE Transactions on Antennas and Propagation*, vol. 51, no. 8, pp. 2020 – 2027, aug. 2003.
- [4] C. W. Jung, B. A. Cetiner, and F. De Flavis, "A single-arm circular spiral antenna with inner/outer feed circuitry for changing polarization and beam characteristics," *IEEE Antenna and Propagation Society International Symposium*, vol. 4, pp. 474–477, June 2003.
- [5] Airshipvision, "<http://www.airshipvision.org>," 2007.
- [6] MyAirship, "<http://www.myairship.com>," 2007.
- [7] J. D. Kraus and R. J. Marhefka, *Antennas for all applications*, McGraw Hill, third edition, 2002.
- [8] R. G. Corzine and J. A. Mosko, *Four-Arm Spiral Antennas*, Artech House, first edition, 1990.
- [9] FEKO, *EM Software & Systems-S.A.*, 32 Techno lane, Technopark, Stellenbosch, 7600 South Africa, 2004.
- [10] V. H. Rumsey, *Frequency Independent Antennas*, Academic Press, 1966.

- [11] H. G. Shantz, "Introduction to ultra-wideband antennas," in *IEEE UWBST Conference*, 2003.
- [12] C. B. Balanis, *Antenna Theory, Analysis and Design*, John Wiley and Sons, Inc, second edition edition, 1997.
- [13] R. Guinvarc'h and R.L. Haupt, "Dual polarization interleaved spiral antenna phased array with an octave bandwidth," *IEEE Transactions on Antennas and Propagation*, vol. 58, no. 2, pp. 397–403, feb. 2010.
- [14] Ming Lee, B.A. Kramer, Chi-Chih Chen, and J.L. Volakis, "Distributed lumped loads and lossy transmission line model for wideband spiral antenna miniaturization and characterization," *IEEE Transactions on Antennas and Propagation*, vol. 55, no. 10, pp. 2671–2678, oct. 2007.
- [15] F. Chauvet R. Guinvarc'h and M. Hélier, "Approximated method neglecting coupling for conformal array," *Applied Computational Electromagnetics Society Journal, Special Issue on ACES 2006 Conference*, vol. 22, no. 1, pp. 105–111, Mar. 2007.
- [16] H. Neff and J. Tillman, "An electronically scanned circular antenna array," *IRE International Convention Record*, vol. 8, pp. 41–47, Mar. 1960.
- [17] T. Simpson and J. Tillman, "Parasitic excitation of circular antenna arrays," *IRE Transactions on Antennas and Propagation*, vol. 9, no. 3, pp. 263–267, May 1961.
- [18] M. Shihab, Y. Najjar, N. Dib, and M Khodier, "Design of non-uniform circular antenna arrays using particle swarm optimization," *Electrical Engineering*, vol. 59, pp. 216–220, 2008.
- [19] D. E. N. Davies, "Correspondence: Mutual coupling compensation for small, circularly symmetric planar antenna arrays," *IEE Proceedings H Microwaves, Optics and Antennas*, vol. 129, no. 5, pp. 281–283, Oct. 1982.
- [20] J. Huang, "A technique for an array to generate circular polarization with linearly polarized elements," *IEEE Trans. Antennas Propagat*, vol. 34, no. 9, pp. 1113–1124, Sep. 1986.

- [21] N. Herscovici, Z. Sipus, and D. Bonefacic, “Circularly polarized single-fed wide-band microstrip patch,” *IEEE Trans. Antennas Propagat*, vol. 51, no. 6, pp. 1277–1280, June 2003.
- [22] D.M. Pozar, “The active element pattern,” *Antennas and Propagation, IEEE Transactions on*, vol. 42, no. 8, pp. 1176–1178, aug. 1994.
- [23] CST (Computer Simulation Technology), “www.cst.com/,” 2010.
- [24] R. Guinvarc’h and N. Ribiere-Tharaud, “A wideband antenna for p-band airborne sar applications,” *IEEE Antennas and Propagation Society International Symposium*, pp. 1–4, 5–11 July 2008.
- [25] B.A. Kramer, Ming Lee, Chi-Chih Chen, and J.L. Volakis, “Design and performance of an ultrawide-band ceramic-loaded slot spiral,” *IEEE Transactions on Antennas and Propagation*, vol. 53, no. 7, pp. 2193 – 2199, july 2005.
- [26] B.A. Kramer, C.-C. Chen, and J.L. Volakis, “Size reduction of a low-profile spiral antenna using inductive and dielectric loading,” *IEEE Antennas and Wireless Propagation Letters*, vol. 7, pp. 22 –25, 2008.

Abstract

HAA (High Altitude Airship) belongs to the family of the lighter-than-air craft that could operate at more than 20 kilometers of altitude above the ground. In this study, HAA is considered to be used as a spiral antenna array platform for radar applications. Spiral antennas are usually fed in the center by a balanced signal. However, in some configurations, like antenna mounted on airship, the center is not accessible. To overcome this issue, studies have been undertaken to move the feeding to the outermost arms. The aim is to obtain radiation characteristics similar to that of a classical center fed spiral antenna with an external feeding. Several solutions of externally fed spiral antennas have been developed. For each case, prototypes have been manufactured and measured to be compared with the modeled antennas. Good agreement is shown between measurement and simulation results. Therefore, the behaviors of the new designs have been validated and they can be used on various shapes that do not allow to feed the spiral in its center.

Keywords: spiral antenna, wideband, circular polarization, airship, multi-ports antenna, external feeding

Résumé

Un dirigeable haute altitude (HAA: High Altitude Airship) évoluant à plus de 20 km au-dessus du sol est envisagé en tant que plate-forme d'accueil pour un réseau d'antennes spirales pour des applications radar. L'antenne spirale d'Archimède est un excellent élément rayonnant pour des applications nécessitant une large bande de fréquences ainsi qu'une polarisation circulaire. Dans la plupart des cas, l'alimentation se fait au centre de l'antenne spirale. Cependant, certains environnements interdisent un accès au centre de l'antenne. Cela est notamment le cas des plateformes aéroportées tels que les dirigeables. Celles-ci ne permettent pas de conformer un réseau d'antennes spirales tout en accédant à leur centre. Il est donc indispensable, dans ces cas, d'alimenter l'antenne autrement. Une solution est d'exciter l'antenne spirale par l'extérieur avec plusieurs sources. L'objectif de cette étude est d'obtenir des caractéristiques de rayonnement similaires à celles de l'antenne spirale d'Archimède tout en libérant le centre. Plusieurs solutions d'alimentation dans le plan de l'antenne sont étudiées. Pour chaque antenne, un prototype a été réalisé et mesuré dans une chambre anéchoïque. Les résultats obtenus correspondent à de ceux de la simulation, ce qui nous permet de valider le fonctionnement des différents prototypes.

Mots clés: Antenne spirale, large bande, polarisation circulaire, dirigeable, antenne multi-ports, alimentation externe